Title
Studies in the role of microRNAs in class switch recombination, and the role of TLR9 complex antigens in shaping the germinal center response

Author
Wigton, Eric J

Publication Date
2020

Peer reviewed|Thesis/dissertation

Studies in the role of microRNAs in class switch recombination, and the role of TLR9 complex antigens in shaping the germinal center response

by
Eric Wigton

DISSERTATION
Submitted in partial satisfaction of the requirements for degree of
DOCTOR OF PHILOSOPHY

in

Biomedical Sciences

in the

GRADUATE DIVISION
of the
UNIVERSITY OF CALIFORNIA, SAN FRANCISCO

Approved:

DocuSigned by:
Jason Cyster
5FFFC327038A40D...

Jason Cyster
Chair

DocuSigned by:
K. Mark Ansel

K. Mark Ansel

DocuSigned by:
Anthony DeFranco
48907F75DC6D4A6...

Anthony DeFranco

Committee Members

Dedications/Acknowledgements

I have to thank all of my friends outside of the program that provided adventure and perspective, especially Robert Mora, John Christie and the Ugly Pickle Posse David Murphy and Kayla Abe who have been here for so many years of good times. Rest in peace Jack Fields, your free spirit is always an inspiration. I must thank my friends, roommates and compatriots in the program including Adair Borges, Elze Rackaityte, Andrew Mancini, Yvanka De'Soysa, Tim Marsh, and Roman Camarda. Through good and bad times in lab and outside, I truly grew as a person from my time spent with each of you. Thanks especially to John Gagnon who was an incredible friend and insightful lab mate

I want to thank all my mentors in science, beginning with Brian Cox back high school who first exposed me to GFP and the wonders of biomedical science. Thanks to Dr. Rongson Pongdee for my first research experience in organic chemistry, and all other teachers and mentors from Colorado College including Dr. Phoebe Lostroh and Dr. Neena Grover. A huge amount of gratitude goes to Dr. Rachel Friedman and Dr. Jordan Jacobelli for igniting my interest in the field of immunology, you were both great mentors. Finally I owe so much to mentors at UCSF, including Mark Anderson, Dr. Corey Miller, and Dr. Chris Allen. Much thanks to Dr. Tony DeFranco for providing meticulous guidance on paper writing and mentorship on projects, Dr. Jason Cyster for exceptional insight and guidance as the chair of my thesis committee, and Dr. Mark Ansel who was an incredible mentor day in and day out. Mark's immunological and scientific intellect is rivaled by his empathy and kindness, and I have so much respect for him as a scientist and a person.

I also have so much gratitude for all the Ansel lab members both past and present: Robin Kageyama for laying the Ago-HITSCLIP groundwork and Adam Litterman for the coding

wizardry; Kristina Johansson and Marlys Fassett for being rocks of positivity and burning the late night oil on experiments; Heather Pua for providing scientific guidance and wisdom; lab mangers Priti Singh, Darryl Mar, and Simon Zhou for keeping the lab running; fellow graduate students Misty Montoya, Didi Zhu, Ben Wheeler and Priscilla Munoz Sandoval for all making the lab a fun place to be. All the BMS coordinators: Demian Sainz, Lisa Magargal, Ned Molyneuax, Monique Piazza, and all others.

I dedicate this thesis to my family and friends that helped me out along the way. I must thank my partner Eliza Kingsley-Ma for supporting me in so many ways through the five years of graduate school; you are a truly incredible human being, and the support I got from you and your family was indispensable for me to complete this journey. I must thank Kathryn Ma, Sanford Kingsley, Emily Kingsley-Ma for treating me like family - and Hannah Kingsley-Ma for being (a) patient and understanding of me as a third roommate. My sister Jenny, your artistic prowess is inspiring, you are definitely the coolest. All my aunts, uncles and cousins in Colorado and beyond who are crushing it. Rest in peace Grandpa Brown and Grandma Jones I often think fondly to the simple things we did together. Thanks to my Grandpa Chet for being an OG doctor inspiration. And finally my Mother and Father, I love you so much.

Contributions and Acknowledgment of Previously Published Materials

The text of chapter 2 comes from a manuscript in preparation, and the work could not have been done without our collaborators: Yohei Mikami, Ryan McGonigle, Robin Kageyama, Adam Litterman, Carlos Castellanos, Suparna Roy, Emily Dykhuizen, Christopher D.C. Allen, Hui Hu, John J. O'Shea, K. Mark Ansel for mouse generation, chemical generation, experimental expertise and guidance.

The text of this thesis/dissertation/manuscript in Chapter 3 is a reprint of the material as it appears in (Wigton, 2019). Anthony Defranco, and K. Mark Ansel listed in this publication directed and supervised the research that forms the basis for this chapter of the dissertation.

Studies in the role of microRNAs in class switch recombination, and the role of TLR9 complex antigens in shaping the germinal center response

Eric Wigton

Abstract

The studies in this work are centered around two projects. The first two chapters are composed of background and primary research on the role of microRNAs (miRNAs) in B cell class switch recombination. MiRNAs regulate cell fate decisions by post-transcriptionally tuning networks of mRNA targets. We utilized miRNA-directed pathway discovery to reveal a regulatory circuit that influences B cell activation and immunoglobulin class switch recombination (CSR). We developed a system to deplete mature, activated B cells of miRNAs, and performed a rescue screen that identified the miR-221/222 family as a positive regulator of CSR. Endogenous miR-221/222 regulated B cell proliferation and CSR to IgE and IgG1 in vitro, and miR-221/222-deficient mice exhibited defective IgE production in allergic airway challenge and polyclonal B cell activation models in vivo. We combined comparative Ago2-HITS-CLIP and gene expression analyses to identify mRNAs bound and regulated by miR-221/222 in primary B cells. Interrogation of these putative direct targets uncovered functionally relevant downstream genes. Genetic depletion or pharmacological inhibition of *Foxp1* and *Arid1a* confirmed their roles as key modulators of CSR to IgE and IgG1. The third chapter is in the study of TLR9 co-signaling in the germinal center (GC) B cell response. It was previously unknown how co-signaling events through innate immune system receptors in B cells positively influenced the generation of GC B cells. In this chapter we addressed this question through transcriptomics to find that signaling and activation from TLR9-containing antigen increased Myc and mTORC signatures that bolstered the GC B cell response.

Table of contents

List of Figures

List of Tables

List of Abbreviations

αIgM-CpG, αIgM antibody complexed to CpG oligo with streptavidin

αIgM-Non, αIgM antibody complexed to non-CpG control oligo

Δ, miR-221/222 germline deleted mice.

AID, Activation-induced cytidine deaminase

CSR, class switch recombination

B-MyD88^{-} , Mb1-cre^{+} MyD88$^{fl/fl}$ genotype

B-MYD88^{-}Myc-GFP, Mb1-cre^{+} MyD88$^{fl/fl}$ Myc-GFP$^{+/+}$ mouse

DOTAP, Dioleoyl-3-trimethylammonium propane

FDR, false discovery rate

Flox, miR-221/222 germline flanked by loxP sites mice

GC, germinal center

GSEA, gene set enrichment analysis

MFI, mean fluorescent intensity

miRNA, microRNA

mTORC, mammalian target of rapamycin complex

NES, normalized enrichment score;

NP-CGG-CpG, NP-CGG complexed to CpG oligo with streptavidin

NP-CGG-Non, NP-CGG complexed to non-CpG control oligo with streptavidin

PC, plasma cell

pS6(ser235/236), protein S6 phosphorylated at serine 235/236

pS6(ser240/244), protein S6 phosphorylated at serine 240/244

Tfh, T follicular helper

TLR9, Toll like receptor 9

VLP, virus-like particle

WT, Mb1-cre^{+} MyD88$^{fl/+}$ or Mb1-cre^{+} MyD88$^{+/+}$

WT- Myc-GFP, Mb1-cre^{+} MyD88$^{fl/+}$ or Mb1-cre^{+} MyD88$^{+/+}$ Myc-GFP$^{+/+}$ mouse

Chapter One: Non-coding RNAs in B cell biology

The purpose of this chapter is to outline recent work in the field of non-coding RNAs (ncRNAs) as it pertains to B cell biology. A majority of the chapter is focused on how microRNAs (miRNAs) and long ncRNAs (lncRNAs), play pivotal roles in B cell activation and terminal effector functions. While extensive reviews exist for individual aspects of miRNA's role in B cell development and lymphomagenesis (Coffre and Koralov, 2017; Zheng et al., 2018), B cell responses (Cyster and Allen, 2019), and the molecular regulation of class switch recombination (CSR) (Yewdell and Chaudhuri, 2017; Yu and Lieber, 2019). This chapter highlights some of the key recent findings from primary studies and refers the reader to current in-depth reviews on these individual topics. The focus of this review is on B cell activation and CSR regulation by ncRNAs. The role of ncRNAs on B cell biology is extensive and the thousands of work hours that has gone into elucidating these processes is both breathtaking and inspiring.

Introduction to B cells

B cells form the humoral branch of the adaptive immune system and are key drivers in defending the host through immunological memory and antibody production. The complex life span of B cells requires distinct developmental checkpoints beginning with early development and lineage commitment in the bone marrow followed by migration to and maturity in secondary lymphoid organs like the spleen and peripheral lymph nodes (Ramirez et al., 2010). The entire process requires strict transcriptional and migratory cues. These mature cells are poised to respond directly to pathogens through engagement of their antigen B cell receptor (BCR) as well as pattern recognition receptors (PRRs) such as the Toll like receptors (TLRs) to a broad range of pathogenic stimuli. Antigen receptor stimulated responses can be in a T-independent (TI) fashion, where B cells expand rapidly and generate low affinity pathogen specific IgM (Cyster and Allen, 2019). The responses can also be T-dependent (TD), whereby activated cells enter the microanatomical

space of the germinal center (GC), and iteratively cycle between antigen receptor mutating and proliferating centroblasts in the dark zone (DZ), that then migrate to the light zone (LZ) as centrocytes where they are selected through pro-survival cues from T follicular helper (Tfh) cell stimulus (Cyster and Allen, 2019; Mesin et al., 2016). Through this process long-term immunological memory is established, and high affinity antibodies are produced against a specific pathogen or antigen.

Introduction to miRNAs

Initially discovered in *C. elegans,* miRNAs are small 18-22nt RNAs that destabilize protein coding mRNAs (Lee et al., 1993). Canonical miRNAs are transcribed as long pri-miRNA hairpins that require processing by Drosha/Dgcr8 in the nucleus to short hairpin pre-miRNAs that are exported from the nucleus, and further processed by Dicer to miRNA duplexes which are loaded into Argonaute proteins (O'Brien et al., 2018). MiRNAs guide the Argonaute (Ago) protein-containing miRNA-induced silencing complex (RISC) to the 3'UTR of target mRNAs via complementary base pairing (Bartel, 2004). Families of miRNAs with shared target repertoires are defined by their 'seed sequence' (nucleotides 2-8 from the 5' end of the mature miRNA), which is the major determinant of target recognition, while 3' ends of the miRNAs may contribute partially to target recognition (Bartel, 2004; Broughton et al., 2016). The miRISC mediates translational inhibition and destabilization of bound mRNAs (Jonas and Izaurralde, 2015). Individual miRNAs and their family members can target hundreds of unique transcripts and thereby regulate large gene networks in a manner specific to cellular context and gene expression program.

MiRNAs in early B cell development.

MiRNAs are indispensable for early B cell programming from the pro-B to pre-B stage, as ablation of miRNA processing machinery leads to complete block at this developmental stage (Brandl et al., 2016; Coffre and Koralov, 2017; Koralov et al., 2008). During this stage of development, B cells undergo VDJ recombination, a form of combinatorial DNA mutation to produce a unique antigen receptor in each developing B cell. Dysregulation of miRNA biogenesis at this stage leads to increased apoptosis, and an inability to form functional BCRs. Furthermore studies have implicated individual miRNAs that are necessary for key developmental checkpoints in the B cell lineage commitment and their dysregulation can lead to transformation and leukemia/lymphomagenesis phenotypes (Coffre and Koralov, 2017; de Yebenes et al., 2013; Zheng et al., 2018).

Endogenous miRNA biogenesis is also important for B cell maturation. CD19-cre mediated Dicer ablation leads to dysfunctional B cell selection and the generation of autoimmunity with lupus like disease and a skewing of the Ig repertoire towards a multitude of self-antigens (Belver et al., 2010). The developmental fate decision for mature B cells to commit to the marginal zone compartment over the follicular compartment is also mediated by control of miR146a (King et al., 2016).

MiRNAs in B cell activation, GC and PC development

In the context of acute activation, naive B cells undergo profound metabolic restructuring (Akkaya et al., 2018; Waters et al., 2018), poising these cells to rapidly proliferate, and undergo transcriptional changes. The miRNA landscape of activated B cells drastically changes from their naïve counterparts, as miRNAs are dynamically regulated to modulate the gene expression changes

necessary for such rapid cellular responses (Fowler et al., 2015; Kuchen et al., 2010). Deletion of Dicer at the GC/PC commitment stage (utilizing *Aicda*-Cre) leads to a profound defect in humoral immunity through decreased GC cells and PCs and isotype switched antibodies in response to immunization (Xu et al., 2012).

Multiple miRNAs regulate the activation of B cells, with miR-155 as a keystone regulator of B cell activation and terminal cell differentiation and transformation (Figure 1.1). Originally discovered as B cell integration cluster or (bic), the primary transcript from which miR-155 is processed is one of the most highly upregulated transcripts upon B cell activation (Clurman and Hayward, 1989). This miRNA has been shown to directly regulate GC and PC differentiation (Rodriguez et al., 2007; Thai et al., 2007; Vigorito et al., 2007), including promoting cell cycle (Arbore et al., 2019), regulating apoptosis (Nakagawa et al., 2016), and directly targeting AID and DNA mutation associated with CSR (Dorsett et al., 2008; Teng et al., 2008). Additionally, these studies are some of the only to mutate seed binding sites in 3'UTRs of target genes to test if single miRNA:target downregulation confers intermediate phenotypes to miRNA ablation, and in the case of miR-155 both AID seed match site (Dorsett et al., 2008; Teng et al., 2008) and PU.1 (Lu et al., 2014) seed match site mutation conferred an intermediate effect of miR-155 KO mice. The multitude of processes and mRNA targets regulated by miR-155 provide direct evidence for gene network mechanism of action and demonstrate the promiscuity with which a single miRNA can target multiple genes simultaneously in a cell fate dependent fashion.

In terms of B cell activation, recent studies have demonstrated a novel interplay of miRNA mediated regulation of metabolism (Jiang et al., 2018), and the converse of metabolite regulation of miRNA expression (Sanchez et al., 2020). The Let-7adf miRNA cluster represses T-independent B cell responses through metabolic regulation (Jiang et al., 2018). This miRNA

cluster directly targeted *hexokinase-2* and glutamine transporter *Slc1a5* to limit glycolysis and glutamine uptake, ultimately repressing c-Myc protein expression in response to both antigen and lipopolysaccharide stimulation of B cells. Mice with a B cell specific deficiency in this miRNA cluster showed increased antibody responses to T-independent immunizations, linking this metabolic control to the T-independent PC fate decision. Further evidence has directly linked metabolites as regulators of miRNA expression in B cells (Sanchez et al., 2020). Epigenetic changes elicited by short chain fatty acid metabolites butyrate and propionate in B cells upregulated miRNAs which in turn modulate *Aicda* and *Prdm1* and affect PC fate decisions and auto-antibody production. B cell activation has been shown to induce rapid metabolic changes (Waters et al., 2018) and recently GC B cells have been shown to utilize fatty acid oxidation over glycolysis (Weisel et al., 2020). Dynamic inter-regulation of miRNAs and metabolism in B cells in the context of fate decisions require further study.

The miRNA cluster miR-17~92 plays a key role in regulating PC development, migration to the bone marrow and isotype specific antibody production (Xu et al., 2015). Mice with germline deficiency in this miRNA have a profound pro-B to pre-B development block (Koralov et al., 2008; Ventura et al., 2008) . However, utilizing CD19-cre to ablate this cluster later in development leads to dysregulated B cell selection, central tolerance and autoimmunity (Lai et al., 2016). Deletion at this stage also leads to defects in IgG2c antibody titers and enhanced PC migration to the bone marrow, related to targeting of *Ikaros* and *S1pr1,* respectively (Xu et al., 2015). Further studies have implicated this miRNA as being necessary for immune responses driving graft vs host disease in both a T and B cell intrinsic fashions (Wu et al., 2018), and its overexpression can lead to lymphoproliferative disease (Dal Bo et al., 2015).

Direct intercellular transfer of miRNAs has been recently implicated as positively regulating the GC B cell response (Fernandez-Messina et al., 2020). Rab27-dependent extracellular micro-vesicle miRNA transfer of miR20a-5p, miR-25-3p, and miR-155-3p from Tfh cells to GC B cells was necessary for optimal GC B cell responses *in vivo*. Extracellular micro-vesicle transfer was relayed through the immune synapse formed between activated GC:Tfh cells during positive selection in the LZ and altered the LZ/DZ phenotype of the GC. Given that there are diverse cargos of other ncRNAs beyond miRNAs in the extracellular vesicles generated from activated T cells (Chiou et al., 2018), other non-miRNA species' transfer could influence these GC:Tfh cellular interactions and dynamics and require further study.

The role of ncRNAs in class switch recombination

miRNAs

The process of CSR, whereby B cells mutate constant regions of the heavy chain locus *Igh*, confers specific isotype-specific biological activity to the BCR and corresponding antibodies. This process requires active transcription in the *Igh* locus and the deaminase AID (Yewdell and Chaudhuri, 2017; Yu and Lieber, 2019). Several miRNAs directly regulate AID including miR-181b in mouse (de Yebenes et al., 2008), miR-29b in human (Recaldin et al., 2018), and miR-155-3p (Dorsett et al., 2008; Teng et al., 2008; Vigorito et al., 2007) in both (Figure 1.1). Our recent study further implicated miR-221/222 as regulators of CSR to IgG1 and IgE by a gene network regulation including *Arid1a* and *Foxp1*.

Germline Igh *transcripts*

Beyond miRNAs that directly regulate cellular functions necessary for CSR, ncRNA from active germline transcription (GLT) at switch (S) regions in the *Igh* locus have been shown to form

stable RNA:DNA hybrids known as R loops and further DNA and RNA G quadraplexes (G4) (Pavri, 2017; Roy et al., 2008; Yewdell and Chaudhuri, 2017; Yu and Lieber, 2019). The role of these R loops has been implicated as a mode of structural conformation stability allowing the targeting of the AID enzyme to single stranded DNA exposed during transcription (Yu and Lieber, 2019) (Figure 1.2). It had been postulated that R loops were necessary for AID recruitment as inversion of Sγ1 region in mice that profoundly reduced R loop formation concordantly reduced B cell CSR to IgG1 (Shinkura et al., 2003). However a recent study demonstrated that R loops are not required for AID mediated mutagenesis, as a transgenic mouse in which the *Igv* region was replaced with a core S region in either physiological or reverse orientation showed equivalent AID mutation rates in both cases (Yeap et al., 2015). These two studies together implicate that the frequency of R loops in the *Igh* region are correlated to CSR but not necessarily to AID recruitment, hinting that R loops could be a transient structural phenomenon. These studies were complemented by the finding that RNAse H overexpression in B cells, which rapidly digests R loops, led to an increase in AID mutations in the *Igh* locus and minimally decreased the frequency of CSR (Maul et al., 2017). Taken together, these studies showed that the physiological orientation of transcription in the *Igh* locus is necessary for R loop initiation, while prolonged R loop formation in this region is not necessary.

Recent protein crystallization studies have shown that AID binds directly to DNA G4 structures as a substrate (Qiao et al., 2017) , a motif that results in guanine rich regions of the non-template ssDNA during transcription in the *Igh* S regions. Thus it appears that DNA G4 structures are the main substrate for AID recruitment, and R loops are only necessary in that they facilitate DNA G4 structures on non-template DNA strands. However, RNA G4 structures arising from GLT processing and intronic lariat debranching can serve as an AID substrate as well (Zheng et

al., 2015). Whereby, limiting the production of these RNA G4 substrates by ablating the lariat debranching enzyme, Dbr1 to heterozygous levels in mice reduced CSR. Furthermore, it has recently been supported that these RNA G4 AID substrates must be processed by RNA helicase DDX1 to facilitate AID localization (Ribeiro de Almeida et al., 2018). While genetic ablation of mediators of these processing events diminished CSR frequency, they did not completely abolish it, indicating redundancy with other mechanism of AID recruitment like interactions with RNA polymerase II and other parts of the core transcriptional machinery (Nambu et al., 2003; Pavri et al., 2010). DNA G4 structures arising from R loop formation also serve as replication origin binding sites, plausibly facilitating CSR beyond an AID directing mechanism and through promotion of DNA replication events (Wiedemann et al., 2016). Without physiologically oriented GLT, CSR is fundamentally impaired, however the full extent to which these GLTs are processed and the mechanistic action they have on recruiting AID and other proteins to S regions to facilitate DNA breaks requires further study.

Long noncoding RNAs

Additional lncRNAs have also been implicated in controlling isotype specific CSR (Pefanis et al., 2014; Pefanis et al., 2015; Rothschild et al., 2020). It is well established that lncRNAs can modulate chromatin and act as enhancers for other genes (Nair et al., 2020). In a recent study, a newfound lncRNA-CSR^{IgA} and 2 other RNA expressing elements were elucidated megabases downstream of the *Igh* coding region (Rothschild et al., 2020). B cells isolated from a mouse model lacking transcription of lncRNA-CSR^{IgA} fail to undergo normal levels of CSR to IgA and IgG2b *in vitro* and to IgA in Peyer's patches. lncRNA-CSR^{IgA} was necessary for coordination of regulatory proteins to nearby CTCF sites that orchestrated long range chromatin changes and interactions with the 3' region of the *Igh* locus. Chromatin loop extrusion by a CTCF

and cohesin-dependent mechanism is necessary for the physical orientation and organization of S sites and efficient CSR (Zhang et al., 2019). It could be that regulation of CTCF/cohesin binding in the *lncRNA* locus also modulates chromatin loop extrusion in the neighboring *Igh* locus as well. The epigenetic regulation of multiple topologically associated domains of chromatin interacting through active transcription of a lncRNA is an interesting mechanism of gene regulation, and the influence of this process on other sites of the genome will require further study.

Concluding remarks

The role of ncRNAs can be broken into three main groups of action - miRNA mediated gene network control and regulation of cell state specific gene targets in B cell maturation and activation, R-loop mediated regulation of CSR, and lncRNA mediate topological associated domain regulation in chromatin epigenetics. While miRNAs have been extensively studied, there is more to glean from studying cell type and state-specific miRNA:target networks as a means of discovering novel genes and pathways that control their unique biology. Furthermore the improvement of RNA-Cross-linking-Immunoprecipitation techniques will further provide global maps of miRNA binding. The multivariate roles of lncRNAs as miRNA sponges (Karreth et al., 2015), protein interacting substrates (such as RNA G4 substrates for AID), and epigenetic regulators (as in the case of lncRNA^{IgA}) are a new horizon by which these ncRNAs dictate cellular function.

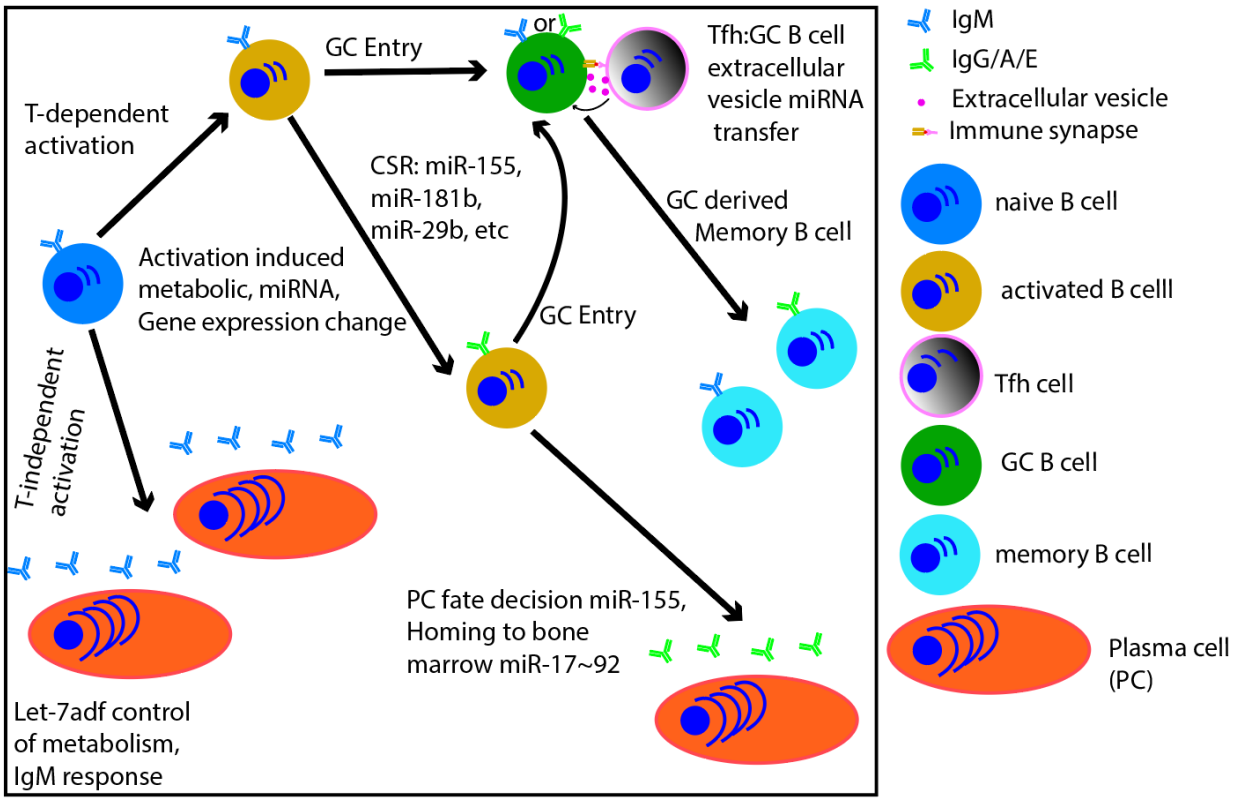

Figure 1.1: Schematic of B cell activation, fate decisions, and miRNAs that influence these processes.

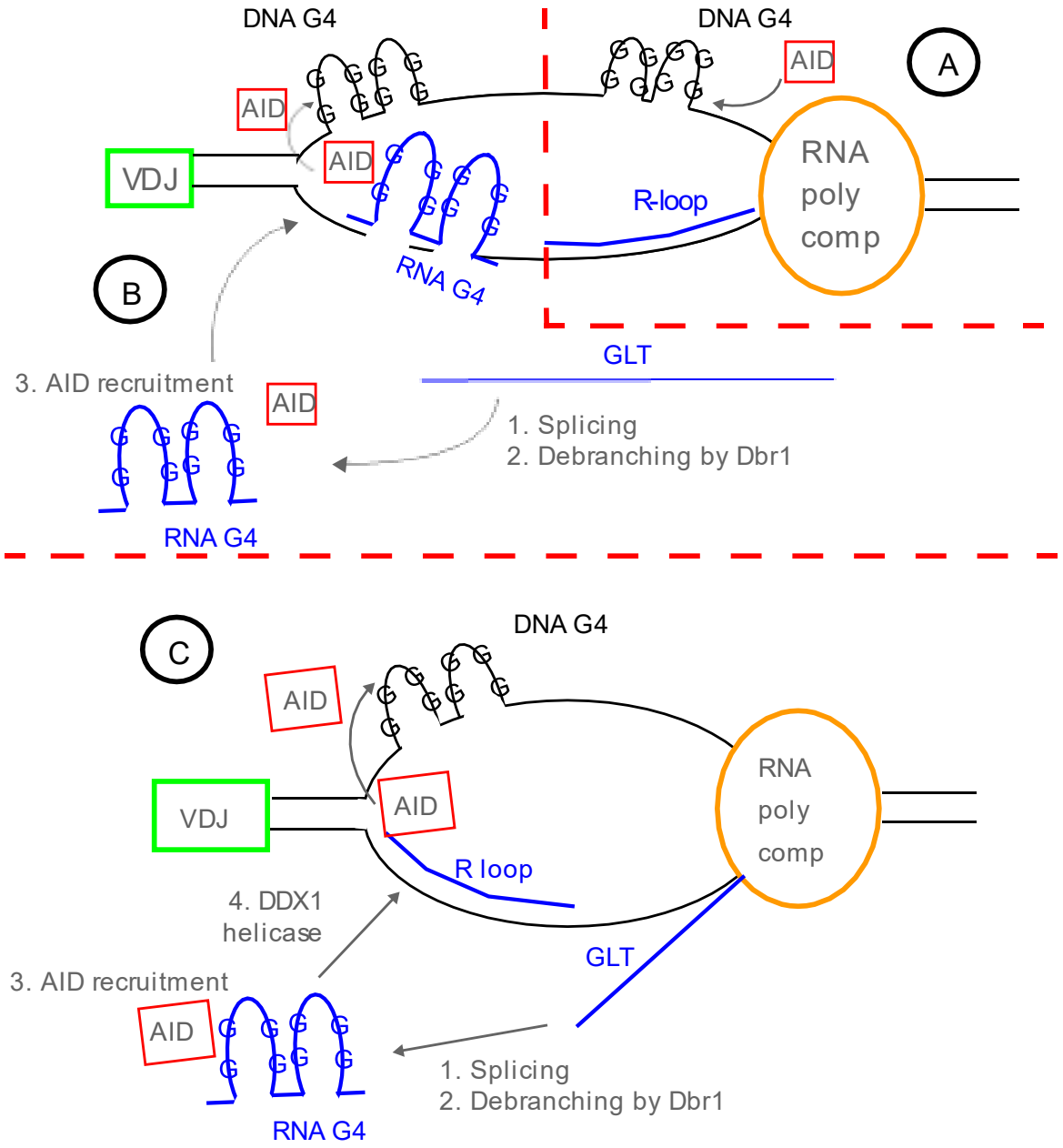

Figure 1.2: Schematic of R-loop mediated mechanisms of Switch region chromatin remodeling and AID recruitment.
A. Model by which active transcription complex guides AID directly to G4 DNA duplexes created from R-loop stabilization of the Switch region. **B.** Model by which the germline transcript (GLT) of the Switch region is processed to form RNA G4 complexes, which bind AID and provide sequence homology to Switch region sites whereby AID can bind G4 DNA duplexes. **C.** Model where in addition to GLT processing from B, DDX1 helicase activity is necessary for converting RNA G4 substrates into R-loops that releases AID to bind to DNA G4 substrates.

References

Akkaya, M., J. Traba, A.S. Roesler, P. Miozzo, B. Akkaya, B.P. Theall, H. Sohn, M. Pena, M. Smelkinson, J. Kabat, E. Dahlstrom, D.W. Dorward, J. Skinner, M.N. Sack, and S.K. Pierce. 2018. Second signals rescue B cells from activation-induced mitochondrial dysfunction and death. *Nat Immunol* 19:871-884.

Arbore, G., T. Henley, L. Biggins, S. Andrews, E. Vigorito, M. Turner, and R. Leyland. 2019. MicroRNA-155 is essential for the optimal proliferation and survival of plasmablast B cells. *Life Sci Alliance* 2:

Bartel, D.P. 2004. MicroRNAs: genomics, biogenesis, mechanism, and function. *Cell* 116:281-297.

Belver, L., V.G. de Yebenes, and A.R. Ramiro. 2010. MicroRNAs prevent the generation of autoreactive antibodies. *Immunity* 33:713-722.

Brandl, A., P. Daum, S. Brenner, S.R. Schulz, D.Y. Yap, M.R. Bosl, J. Wittmann, W. Schuh, and H.M. Jack. 2016. The microprocessor component, DGCR8, is essential for early B-cell development in mice. *Eur J Immunol* 46:2710-2718.

Broughton, J.P., M.T. Lovci, J.L. Huang, G.W. Yeo, and A.E. Pasquinelli. 2016. Pairing beyond the Seed Supports MicroRNA Targeting Specificity. *Mol Cell* 64:320-333.

Chiou, N.T., R. Kageyama, and K.M. Ansel. 2018. Selective Export into Extracellular Vesicles and Function of tRNA Fragments during T Cell Activation. *Cell Rep* 25:3356-3370 e3354.

Clurman, B.E., and W.S. Hayward. 1989. Multiple proto-oncogene activations in avian leukosis virus-induced lymphomas: evidence for stage-specific events. *Mol Cell Biol* 9:2657-2664.

Coffre, M., and S.B. Koralov. 2017. miRNAs in B Cell Development and Lymphomagenesis. *Trends Mol Med* 23:721-736.

Cyster, J.G., and C.D.C. Allen. 2019. B Cell Responses: Cell Interaction Dynamics and Decisions. *Cell* 177:524-540.

Dal Bo, M., R. Bomben, L. Hernandez, and V. Gattei. 2015. The MYC/miR-17-92 axis in lymphoproliferative disorders: A common pathway with therapeutic potential. *Oncotarget* 6:19381-19392.

de Yebenes, V.G., N. Bartolome-Izquierdo, and A.R. Ramiro. 2013. Regulation of B-cell development and function by microRNAs. *Immunol Rev* 253:25-39.

de Yebenes, V.G., L. Belver, D.G. Pisano, S. Gonzalez, A. Villasante, C. Croce, L. He, and A.R. Ramiro. 2008. miR-181b negatively regulates activation-induced cytidine deaminase in B cells. *J Exp Med* 205:2199-2206.

Dorsett, Y., K.M. McBride, M. Jankovic, A. Gazumyan, T.H. Thai, D.F. Robbiani, M. Di Virgilio, B. Reina San-Martin, G. Heidkamp, T.A. Schwickert, T. Eisenreich, K. Rajewsky, and M.C. Nussenzweig. 2008. MicroRNA-155 suppresses activation-induced cytidine deaminase-mediated Myc-Igh translocation. *Immunity* 28:630-638.

Fernandez-Messina, L., A. Rodriguez-Galan, V.G. de Yebenes, C. Gutierrez-Vazquez, S. Tenreiro, M.C. Seabra, A.R. Ramiro, and F. Sanchez-Madrid. 2020. Transfer of extracellular vesicle-microRNA controls germinal center reaction and antibody production. *EMBO Rep* 21:e48925.

Fowler, T., A.S. Garruss, A. Ghosh, S. De, K.G. Becker, W.H. Wood, M.T. Weirauch, S.T. Smale, B. Aronow, R. Sen, and A.L. Roy. 2015. Divergence of transcriptional landscape occurs early in B cell activation. *Epigenetics Chromatin* 8:20.

Jiang, S., W. Yan, S.E. Wang, and D. Baltimore. 2018. Let-7 Suppresses B Cell Activation through Restricting the Availability of Necessary Nutrients. *Cell Metab* 27:393-403 e394.

Jonas, S., and E. Izaurralde. 2015. Towards a molecular understanding of microRNA-mediated gene silencing. *Nat Rev Genet* 16:421-433.

Karreth, F.A., M. Reschke, A. Ruocco, C. Ng, B. Chapuy, V. Leopold, M. Sjoberg, T.M. Keane, A. Verma, U. Ala, Y. Tay, D. Wu, N. Seitzer, C. Velasco-Herrera Mdel, A. Bothmer, J. Fung, F. Langellotto, S.J. Rodig, O. Elemento, M.A. Shipp, D.J. Adams, R. Chiarle, and P.P. Pandolfi. 2015. The BRAF pseudogene functions as a competitive endogenous RNA and induces lymphoma in vivo. *Cell* 161:319-332.

King, J.K., N.M. Ung, M.H. Paing, J.R. Contreras, M.O. Alberti, T.R. Fernando, K. Zhang, M. Pellegrini, and D.S. Rao. 2016. Regulation of Marginal Zone B-Cell Differentiation by MicroRNA-146a. *Front Immunol* 7:670.

Koralov, S.B., S.A. Muljo, G.R. Galler, A. Krek, T. Chakraborty, C. Kanellopoulou, K. Jensen, B.S. Cobb, M. Merkenschlager, N. Rajewsky, and K. Rajewsky. 2008. Dicer ablation affects antibody diversity and cell survival in the B lymphocyte lineage. *Cell* 132:860-874.

Kuchen, S., W. Resch, A. Yamane, N. Kuo, Z. Li, T. Chakraborty, L. Wei, A. Laurence, T. Yasuda, S. Peng, J. Hu-Li, K. Lu, W. Dubois, Y. Kitamura, N. Charles, H.W. Sun, S. Muljo, P.L. Schwartzberg, W.E. Paul, J. O'Shea, K. Rajewsky, and R. Casellas. 2010. Regulation of microRNA expression and abundance during lymphopoiesis. *Immunity* 32:828-839.

Lai, M., A. Gonzalez-Martin, A.B. Cooper, H. Oda, H.Y. Jin, J. Shepherd, L. He, J. Zhu, D. Nemazee, and C. Xiao. 2016. Regulation of B-cell development and tolerance by different members of the miR-17 approximately 92 family microRNAs. *Nat Commun* 7:12207.

Lee, R.C., R.L. Feinbaum, and V. Ambros. 1993. The C. elegans heterochronic gene lin-4 encodes small RNAs with antisense complementarity to lin-14. *Cell* 75:843-854.

Lu, D., R. Nakagawa, S. Lazzaro, P. Staudacher, C. Abreu-Goodger, T. Henley, S. Boiani, R. Leyland, A. Galloway, S. Andrews, G. Butcher, S.L. Nutt, M. Turner, and E. Vigorito. 2014. The miR-155-PU.1 axis acts on Pax5 to enable efficient terminal B cell differentiation. *J Exp Med* 211:2183-2198.

Maul, R.W., H. Chon, K. Sakhuja, S.M. Cerritelli, L.A. Gugliotti, P.J. Gearhart, and R.J. Crouch. 2017. R-Loop Depletion by Over-expressed RNase H1 in Mouse B Cells Increases Activation-Induced Deaminase Access to the Transcribed Strand without Altering Frequency of Isotype Switching. *J Mol Biol* 429:3255-3263.

Mesin, L., J. Ersching, and G.D. Victora. 2016. Germinal Center B Cell Dynamics. *Immunity* 45:471-482.

Nair, L., H. Chung, and U. Basu. 2020. Regulation of long non-coding RNAs and genome dynamics by the RNA surveillance machinery. *Nat Rev Mol Cell Biol* 21:123-136.

Nakagawa, R., R. Leyland, M. Meyer-Hermann, D. Lu, M. Turner, G. Arbore, T.G. Phan, R. Brink, and E. Vigorito. 2016. MicroRNA-155 controls affinity-based selection by protecting c-MYC+ B cells from apoptosis. *J Clin Invest* 126:377-388.

Nambu, Y., M. Sugai, H. Gonda, C.G. Lee, T. Katakai, Y. Agata, Y. Yokota, and A. Shimizu. 2003. Transcription-coupled events associating with immunoglobulin switch region chromatin. *Science* 302:2137-2140.

O'Brien, J., H. Hayder, Y. Zayed, and C. Peng. 2018. Overview of MicroRNA Biogenesis, Mechanisms of Actions, and Circulation. *Front Endocrinol (Lausanne)* 9:402.

Pavri, R. 2017. R Loops in the Regulation of Antibody Gene Diversification. *Genes (Basel)* 8:

Pavri, R., A. Gazumyan, M. Jankovic, M. Di Virgilio, I. Klein, C. Ansarah-Sobrinho, W. Resch, A. Yamane, B. Reina San-Martin, V. Barreto, T.J. Nieland, D.E. Root, R. Casellas, and

M.C. Nussenzweig. 2010. Activation-induced cytidine deaminase targets DNA at sites of RNA polymerase II stalling by interaction with Spt5. *Cell* 143:122-133.

Pefanis, E., J. Wang, G. Rothschild, J. Lim, J. Chao, R. Rabadan, A.N. Economides, and U. Basu. 2014. Noncoding RNA transcription targets AID to divergently transcribed loci in B cells. *Nature* 514:389-393.

Pefanis, E., J. Wang, G. Rothschild, J. Lim, D. Kazadi, J. Sun, A. Federation, J. Chao, O. Elliott, Z.P. Liu, A.N. Economides, J.E. Bradner, R. Rabadan, and U. Basu. 2015. RNA exosome-regulated long non-coding RNA transcription controls super-enhancer activity. *Cell* 161:774-789.

Qiao, Q., L. Wang, F.L. Meng, J.K. Hwang, F.W. Alt, and H. Wu. 2017. AID Recognizes Structured DNA for Class Switch Recombination. *Mol Cell* 67:361-373 e364.

Ramirez, J., K. Lukin, and J. Hagman. 2010. From hematopoietic progenitors to B cells: mechanisms of lineage restriction and commitment. *Curr Opin Immunol* 22:177-184.

Recaldin, T., P.S. Hobson, E.H. Mann, F. Ramadani, D.J. Cousins, P. Lavender, and D.J. Fear. 2018. miR-29b directly targets activation-induced cytidine deaminase in human B cells and can limit its inappropriate expression in naive B cells. *Mol Immunol* 101:419-428.

Ribeiro de Almeida, C., S. Dhir, A. Dhir, A.E. Moghaddam, Q. Sattentau, A. Meinhart, and N.J. Proudfoot. 2018. RNA Helicase DDX1 Converts RNA G-Quadruplex Structures into R-Loops to Promote IgH Class Switch Recombination. *Mol Cell* 70:650-662 e658.

Rodriguez, A., E. Vigorito, S. Clare, M.V. Warren, P. Couttet, D.R. Soond, S. van Dongen, R.J. Grocock, P.P. Das, E.A. Miska, D. Vetrie, K. Okkenhaug, A.J. Enright, G. Dougan, M. Turner, and A. Bradley. 2007. Requirement of bic/microRNA-155 for normal immune function. *Science* 316:608-611.

Rothschild, G., W. Zhang, J. Lim, P.K. Giri, B. Laffleur, Y. Chen, M. Fang, Y. Chen, L. Nair, Z.P. Liu, H. Deng, L. Hammarstrom, J. Wang, and U. Basu. 2020. Noncoding RNA transcription alters chromosomal topology to promote isotype-specific class switch recombination. *Sci Immunol* 5:

Roy, D., K. Yu, and M.R. Lieber. 2008. Mechanism of R-loop formation at immunoglobulin class switch sequences. *Mol Cell Biol* 28:50-60.

Sanchez, H.N., J.B. Moroney, H. Gan, T. Shen, J.L. Im, T. Li, J.R. Taylor, H. Zan, and P. Casali. 2020. B cell-intrinsic epigenetic modulation of antibody responses by dietary fiber-derived short-chain fatty acids. *Nat Commun* 11:60.

Shinkura, R., M. Tian, M. Smith, K. Chua, Y. Fujiwara, and F.W. Alt. 2003. The influence of transcriptional orientation on endogenous switch region function. *Nat Immunol* 4:435-441.

Teng, G., P. Hakimpour, P. Landgraf, A. Rice, T. Tuschl, R. Casellas, and F.N. Papavasiliou. 2008. MicroRNA-155 is a negative regulator of activation-induced cytidine deaminase. *Immunity* 28:621-629.

Thai, T.H., D.P. Calado, S. Casola, K.M. Ansel, C. Xiao, Y. Xue, A. Murphy, D. Frendewey, D. Valenzuela, J.L. Kutok, M. Schmidt-Supprian, N. Rajewsky, G. Yancopoulos, A. Rao, and K. Rajewsky. 2007. Regulation of the germinal center response by microRNA-155. *Science* 316:604-608.

Ventura, A., A.G. Young, M.M. Winslow, L. Lintault, A. Meissner, S.J. Erkeland, J. Newman, R.T. Bronson, D. Crowley, J.R. Stone, R. Jaenisch, P.A. Sharp, and T. Jacks. 2008. Targeted deletion reveals essential and overlapping functions of the miR-17 through 92 family of miRNA clusters. *Cell* 132:875-886.

Vigorito, E., K.L. Perks, C. Abreu-Goodger, S. Bunting, Z. Xiang, S. Kohlhaas, P.P. Das, E.A. Miska, A. Rodriguez, A. Bradley, K.G. Smith, C. Rada, A.J. Enright, K.M. Toellner, I.C. Maclennan, and M. Turner. 2007. microRNA-155 regulates the generation of immunoglobulin class-switched plasma cells. *Immunity* 27:847-859.

Waters, L.R., F.M. Ahsan, D.M. Wolf, O. Shirihai, and M.A. Teitell. 2018. Initial B Cell Activation Induces Metabolic Reprogramming and Mitochondrial Remodeling. *iScience* 5:99-109.

Weisel, F.J., S.J. Mullett, R.A. Elsner, A.V. Menk, N. Trivedi, W. Luo, D. Wikenheiser, W.F. Hawse, M. Chikina, S. Smita, L.J. Conter, S.M. Joachim, S.G. Wendell, M.J. Jurczak, T.H. Winkler, G.M. Delgoffe, and M.J. Shlomchik. 2020. Germinal center B cells selectively oxidize fatty acids for energy while conducting minimal glycolysis. *Nat Immunol* 21:331-342.

Wiedemann, E.M., M. Peycheva, and R. Pavri. 2016. DNA Replication Origins in Immunoglobulin Switch Regions Regulate Class Switch Recombination in an R-Loop-Dependent Manner. *Cell Rep* 17:2927-2942.

Wu, Y., S. Schutt, K. Paz, M. Zhang, R.P. Flynn, D. Bastian, M.H. Sofi, H. Nguyen, M. Dai, C. Liu, Y.J. Chang, B.R. Blazar, and X.Z. Yu. 2018. MicroRNA-17-92 is required for T-cell and B-cell pathogenicity in chronic graft-versus-host disease in mice. *Blood* 131:1974-1986.

Xu, S., K. Guo, Q. Zeng, J. Huo, and K.P. Lam. 2012. The RNase III enzyme Dicer is essential for germinal center B-cell formation. *Blood* 119:767-776.

Xu, S., X. Ou, J. Huo, K. Lim, Y. Huang, S. Chee, and K.P. Lam. 2015. Mir-17-92 regulates bone marrow homing of plasma cells and production of immunoglobulin G2c. *Nat Commun* 6:6764.

Yeap, L.S., J.K. Hwang, Z. Du, R.M. Meyers, F.L. Meng, A. Jakubauskaite, M. Liu, V. Mani, D. Neuberg, T.B. Kepler, J.H. Wang, and F.W. Alt. 2015. Sequence-Intrinsic Mechanisms that Target AID Mutational Outcomes on Antibody Genes. *Cell* 163:1124-1137.

Yewdell, W.T., and J. Chaudhuri. 2017. A transcriptional serenAID: the role of noncoding RNAs in class switch recombination. *Int Immunol* 29:183-196.

Yu, K., and M.R. Lieber. 2019. Current insights into the mechanism of mammalian immunoglobulin class switch recombination. *Crit Rev Biochem Mol Biol* 54:333-351.

Zhang, X., Y. Zhang, Z. Ba, N. Kyritsis, R. Casellas, and F.W. Alt. 2019. Fundamental roles of chromatin loop extrusion in antibody class switching. *Nature* 575:385-389.

Zheng, B., Z. Xi, R. Liu, W. Yin, Z. Sui, B. Ren, H. Miller, Q. Gong, and C. Liu. 2018. The Function of MicroRNAs in B-Cell Development, Lymphoma, and Their Potential in Clinical Practice. *Front Immunol* 9:936.

Zheng, S., B.Q. Vuong, B. Vaidyanathan, J.Y. Lin, F.T. Huang, and J. Chaudhuri. 2015. Non-coding RNA Generated following Lariat Debranching Mediates Targeting of AID to DNA. *Cell* 161:762-773.

Chapter 2: Micro-RNA directed pathway discovery in B cells elucidates a miR-221/222 mediated *Foxp1, Arid1a* regulatory circuit in class switch recombination.

Adapted from a manuscript in progress:

Eric J. Wigton, Yohei Mikami, Ryan McGonigle, Robin Kageyama, Adam Litterman, Carlos Castellanos, Suparna Roy, Emily Dykhuizen, Christopher D.C. Allen, Hui Hu, John J. O'Shea, K. Mark Ansel

Introduction

MicroRNAs have been leveraged as discovery tools to elucidate genes and pathways that regulate lymphocyte fate and function in immunity. Rescue screens in miRNA-deficient T cells uncovered specific miRNAs that influence cytokine production (Pua et al., 2016; Steiner et al., 2011). Algorithms that use seed sequence matching and other 3' UTR sequence features are used to predict target gene networks (Agarwal et al., 2015), and these networks can be further filtered for miRNA effects on gene expression in the appropriate cellular context (Pua et al., 2016). Ago-2 high-throughput sequencing of RNA isolated by crosslinking immunoprecipitation (Ago2-HITS-CLIP) provides context-specific biochemical evidence for miRISC occupancy of potential target sites, and comparing Ago2-HITS-CLIP in miRNA-deficient and -sufficient cells facilitates mapping of specific miRNA:target interactions (Chi et al., 2009; Gagnon et al., 2019; Loeb et al., 2012). Functional interrogation of these targets can unearth regulatory genes and pathways previously unknown to be important to biological processes of interest and direct researchers to novel therapeutic targets.

Hyper-production of antibodies of the IgE isotype is a hallmark of allergy (Hu et al., 2018). IgE is directly involved in the pathogenesis of asthma and other allergic diseases, as it arms mast cells and basophils for rapid allergen-specific inflammatory responses (Galli and Tsai, 2012). Omalizumab, an approved therapeutic antibody that targets IgE, reduces asthma exacerbations in a subset of patients (Busse et al., 2001). It has been suggested that therapies that target or reduce the generation of IgE-producing B cells may provide better protection against symptoms of allergic diseases (Hu et al., 2018). The generation of IgE producing B cells from naïve B cells requires the induction of Immunoglobulin class switch recombination (CSR), a process of somatic DNA

mutation and recombination that preserves the B cell's antibody specificity while switching the isotype of its heavy chain (Yewdell and Chaudhuri, 2017; Yu and Lieber, 2019).

CSR requires multiple coordinated processes starting with active transcription driven by cytokine signaling (Stavnezer and Schrader, 2014), expression and regulation of the activation induced deaminase enzyme AID, DNA repair, (Yu and Lieber, 2019), and distinct regulation of cell cycle and proliferation (Hodgkin et al., 1996). AID is directly regulated by miRNAs, specifically miR-155 (Dorsett et al., 2008; Teng et al., 2008; Vigorito et al., 2007). CSR to IgG1 and IgE isotypes require IL-4 signaling (Finkelman et al., 1990; Kopf et al., 1993; Kuhn et al., 1991). Signaling from T follicular helper cells through CD40, and other cytokines also influence this process.

In this study, we developed a mouse model system to ablate miRNA processing in mature B cells, and then performed a rescue screen for miRNAs that regulate CSR. This screen identified miR-221/222, a miRNA family previously unstudied in mature, nonmalignant B cells, as a positive regulator of this process (Knoll et al., 2013; Lupini et al., 2013; Petkau et al., 2018). We characterized miR221/222-deficient B cells from gene-targeted mice *in vitro* and *in vivo*, and empirically defined direct targets of these miRNAs in B cells through a combination of bioinformatic, biochemical and gene expression analyses. MiR-221/222 promoted CSR and B cell proliferation in vitro, IgE production in an allergic airway hypersensitivity model, and IgE^+ plasmablast generation in a model of global B cell activation. Among the plausible direct targets of miR-221/222, we uncovered *Foxp1*, *Arid1a*, and *Cd164* as novel regulators of CSR. Together, these findings establish miR-221/222 as a regulator of B cell production of antibodies associated with allergy and asthma and provide insight into new regulators of CSR.

Materials and Methods

Mice

Mice used in this work included Cγ1-cre, B6.129P2(Cg)-Ighg1$^{tm1(cre)Cgn}$/J (Casola et al., 2006); CD21-cre, (Kraus et al., 2004); Dgcr8$^{fl/fl}$, B6.Cg-Dgcr8$^{tm1.1Blel}$/J (Rao et al., 2009); R26-LSL-YFP, B6.Gt(ROSA)26$^{Sortm1(EYFP)Cos}$/J (Srinivas et al., 2001), Cre^{ERT2}, B6.Cg-Ndor1Tg$^{(UBC-cre/ERT2)1Ejb}$/1J (Ruzankina et al., 2007); *Foxp1*$^{fl/fl}$, Foxp1$^{tm1.1Pwt}$/J (Feng et al., 2010); Arid1a$^{fl/fl}$, 129.Arid1a$^{tm1.1Zhwa}$/J (Gao et al., 2008); and flox: mirc50$^{fl/y}$ or Δ: micr50$^{-/y}$ generated in this study. Only male mice were used for miR-221/222 deletion experiments, except some female mice were used for creating the Ago2-HITS-CLIP libraries. For Foxp1 deletion, Cre^{ERT2}Foxp1$^{fl/fl}$ R26-LSL-YFP mice have been previously described (Feng et al., 2011). For CD21-cre mediated Arid1a$^{fl/fl}$ genetic deletion experiments, B6.129 N1 Arid1a-Het and Arid1a-WT mice were used, and B6.129 N2 Het and Cre+WT mice were used. All mice were used between 6-16 weeks for all strains, and all were age/sex matched for all other strains. All mice were cared for and experimented on under the guidance/compliance of UCSF and UAB Laboratory Animal Research Centers and IACUC guidelines.

B cell isolation, transfection and stimulation

Splenic naive B cells were isolated using Dynabead untouched B cell (CD43 negative selection kit, Thermo Fisher) and stimulated in RPMI 1640 supplemented with 10% FCS, HEPES, 2-mercaptoethanol, and L-glutamine. Pre-transfection stimulation consisted of 250 ng/mL anti-CD180 (RP105) (Biolegend) and 1 ng/ml IL-4 (recombinant mouse, Peprotech) at 10^6 cells/mL in 12 well plates (Costar) for transfection conditions. After 48hrs cells were washed 2x PBS and resuspended at 10^5 cells/10 µl in Neon transfection buffer R (Invitrogen) and mixed with siRNA (Dharmacon/GE), miRNA mimic (Dharmacon/GE), and/or luciferase plasmid before being immediately electroporated 3 x 10 ms at 1550 V on a Neon transfection instrument. The 10 µl

transfection was then transferred directly into 200 µl of CSR media in a round bottom 96 well plate (Costar). For CSR conditions cells were stimulated with 3µg/ml LPS (from Salmonella, Sigma) and 25 ng/ml IL-4 for miRNA and siRNA screens, or in 500 ng/ml-1µg/ml anti-CD40 (FGK45.1.1, Miltenyi), 25ng/ml IL-4 and 10-12.5 ng/ml IL-21 (eBioscience) at 10^5 cells/200 µl/ well in a 96 well round bottom plate for Ago-2-HITS-CLIP library generation or flow cytometry. For the ARID1A-BAF complex chemical inhibitor assay, cells were stimulated with BRD-K80443127 dissolved in DMSO at reported concentration or vehicle alone.

Foxp1 deletion and CD40LB feeder cell stimulation

For Foxp1 deletion, $Cre^{ERT2}Foxp1^{fl/fl}$ R26-LSL-YFP (Foxp1-KO), $Cre^{ERT2}Foxp1^{wt/wt}$ R26-LSL-YFP (Foxp1-WT) mice were immunized 4 days consecutively (Day 0-3) with 3 mg/day tamoxifen (Sigma) i.p. dissolved in corn oil (20 mg/mL), rested for one day (Day 4). CD40L-Baff 3T3 feeder cells (Nojima et al., 2011) that were plated $2x10^5$ in 24 well culture treated plates on Day 4. Spleens were harvested on Day 5 and follicular B cells that underwent cre-mediated recombination were FACS sorted (CD3-, CD19+, CD21/35 low, CD23+, YFP+) and co-cultured at 2 $x10^5$ B cells/well with pre-coated CD40L-Baff 3T3 feeder cells with and without IL-4 for 4 days (Day 9).

RNA isolation, qPCR, and RNA-sequencing

Stimulated B cells were pelleted, and RNA was extracted using TRIZOL reagent (Thermo Fisher). RNA was extracted using a RNeasy micro kit (Qiagen). cDNA was generated with one step miRX (Takara) for miRNA quantification or with super script III reverse transcription (SSIII) poly-dT first strand synthesis (Thermo Fisher) for *Dgcr8* quantification. miRNA primers for the miRX qPCR consisted of the full, mature miRNA sequence. Primers for *Dgcr8* were previously reported (Bronevetsky et al., 2013). qPCR cycle was a two-step cycle at 95C for 10 secs 60C for 15 secs for 40 cycles and amplification was read out by SYBRgreen advantage (Takara).

RNAseq Library preparation and sequencing was performed through the UCSF Functional Genomics Core and aligned to Ensembl Mouse GRCh38.78 (mm10) genome using STAR software and analyzed using DESeq2 as previously reported. Transcripts with at least a mean normalized count of 12.3 were used in the analysis, resulting in 12,074 annotated ENSEMBL transcripts.

Ago2-HITSCLIP library preparation

Libraries were prepared as previously described(Chi et al., 2009; Gagnon et al., 2019; Loeb et al., 2012). Briefly, 10^8 activated B cells/ml (5 mice per library) were UV crosslinked 1x 400mJ and 2x 200mJ and pelleted. Ago2 immunoprecipitation with 2D4 (Dako) was performed and protein/RNA complexes were digested with RNAse1, 3' and 5' adapters were ligated, and cDNA created from SSIII. Library was amplified with Phusion taq polymerase (NEB) to the peak exponential by qPCR with SYBRgold (Thermo Fisher) before being purified of adapter dimer on a 10% TBE (Bio-Rad) gel and analyzed by a Bioanalyzer micro DNA kit (Agilent). Libraries were combined and sequenced on an Illumina HISEQ-2500. Reads were binned based on individual barcode and aligned to the genome using Bowtie (John Hopkins University). Annotations were made using an in-house aligning algorithm for each library. Libraries were combined by genotype and combined libraries were used to run dCLIP (Wang et al., 2014) with default settings. All regions more bound in flox libraries or Δ libraries were intersected with miR-221/222-3p seed sequence reference BED file (generated in house), and those regions were further binned based on dCLIP internal score >1 or >10 to increase confidence of true binding regions.

In vivo house dust mite challenge and Goat anti-IgD serum immunization

Mice were primed with 25ug in 50 µl PBS HDM (Stallergenes Greer) by oropharyngeal aspiration, and 7 days later the mice were challenged similarly for 5 consecutive days before being

bled at D14 for serum analysis. Mice were immunized i.p. with 300 µl goat anti-IgD serum and spleen and inguinal lymph nodes analyzed 7 days later by flow cytometry. Flow cytometry plots and analysis are of lymph node samples.

ELISA

Serum was collected by submandibular bleed and micro-centrifugation at >18,000g for 30 mins. Half area high-binding 96 well plates (Costar) plates were used for all assays. For total Ig at steady state µplates were coated with Goat anti-Ig (2 µg/ml, Southern Biotech) overnight in coating buffer bicarbonate/carbonate coating buffer (100 mM, pH 9.6). Diluted serum was added over night at 4 C or at room temperature for 2 hours, and detected with biotinylated goat anti-IgG1, IgG3, IgG2b, or IgM (2 µg/ml, Southern Biotech) followed by HRP-avidin (1:5000, Southern Biotech) and developed with Super AquaBlue ELISA Substrate (Thermo Fisher) all with standard curves and read out a 405 nm absorbance. For total IgE the process was the same except for plates were coated with anti-IgE (2 µg/ml, R35-72) and detected with biotinylated anti-IgE (2µg/ml, R35-118). HDM specific IgE ELISA the coating process was the same as total IgE, however instead of detection with biotinylated anti-IgE, biotinylated HDM was used at 2 µg/ml followed by avidin-HRP and TMB substrate stopped with 0.16M sulfuric acid and read at 405 nm. For HDM specific IgG1 plates were coated with HDM (10 µg/ml) overnight and serum overnight at 4C or 2hr room temperature and then detected with biotinylated anti-IgG1 followed by avidin-HRP and TMB substrate (Thermo Fisher) stopped with 0.16M sulfuric acid M sulfuric acid.

Flow cytometry

For in vivo experiments single cell suspensions were prepared from spleen or lymphnode by gently passing them through 70 µm nylon mesh filters in complete RPMI. For Bone marrow,

long bones were cut at base and a 26 G needle was used to expel bone marrow, into complete RPMI. Single cell suspension was created by resuspending the BM with an 18 G needle and suspension was filtered through a 70 um filter. Fc receptors were blocked with anti-CD16/CD32 (2.4G2) and 2% normal rat serum in FACS buffer (PBS + 2% Fetal Bovine Serum + 2 µm EDTA + .01% NaN_3) before staining with antibodies for surface markers. Conjugated antibodies used included BV605 anti-CD4 (RM4-5), BV605 and PE-Cy7 anti-CD19 (6D5), PerCP-Cy5.5 anti-CD43 (1B11), AF647 anti-B220 (RA3-6B2), AF488 anti-IgM (RMM-1), ef450 and PE anti-IgD (11-26c), PE and APC anti-IgG1 (A85), biotin anti-IgE (R35-118), unconjugated and PE anti-IgE (RME-1), APC anti-CD138 (281-2), PE-Cy7 anti-CD45.2 (104), PerCP-Cy5.5 anti-CD45.1 (A20), PacBlue anti-CD21/35 (7E9), PE-Cy7 anti-CD23 (B3B4), PE anti-CD93 (AA4.1), BV711 anti-CD24 (M1/69). Biotin conjugates were detected using BV711 Streptavidin (BioLegend). Intracellular IgE staining was performed as previously described (Yang et al., 2018; Yang et al., 2012), where live cells were stained with surface antibody stain + 1:50 purified anti-IgE (RME-1) before fixing with BD cytofix/cytoperm and staining intracellularly with PE anti-IgE (RME-1). Dead cells were detected using efluor780 fixable viability dyes (Thermo Fisher). Flow cytometry analysis was performed on an LSRii cytometer or a FACSAria for sorting (BD).

Dual luciferase assay

Dual luciferase constructs were generated, and assay performed as previously reported (Gagnon et al., 2019; Pua et al., 2016). Cells were stimulated and transfect as outlined and luciferase activity was measured 24 h after transfection with the Dual Luciferase Reporter Assay System (Promega) and a FLUOstar Optima plate-reader (BMG Labtech). At least 1 kb of the 3'UTR of *Cd164, Foxp1* and *Arid1a* including the putative miR-221/222-3p seed match sequence(s) were cloned into the psiCHECK-2 luciferase reporter construct (Promega). Primers

used are as follows: *Foxp1* for: TAAGCAGCTCGAGAGCATGGTGACAGGGCTAAG; Foxp1 rev: TGCTTAGGCGGCCGC CTCCCCCGCAAAAGACAAAG; Cd164 for: TAAGCAGCTCGAGAGATGCCACACAG GGCAATC; Cd164 rev: TGCTTAGGCGGCCGCTGCTTGTGCAGCAAGTATGG; Arid1a for: TAAGCAGCTCGAG CCTCAGGACCCCACCCTAT Arid1a rev: TGCTTAGGCGGCCGC CACGTGGAACATATAGTATAAAG.

Software and Statistics

Data visualization and statistical calculations were performed using Prism GraphPad. Statistical tests and p values for each experiment are specified in figure legends for a single comparison between two groups, a student's t-test was used (paired or unpaired where mentioned); for multiple comparisons between pre-selected control and all other groups, a one way ANOVA with Dunnet's square test; and for multiple comparisons where all groups were compared, a one way ANOVA test with a Tukey correction for multiple comparisons was used. Flow cytometry data were analyzed with Flowjo version 10.2. Gene ontology was run using the Metascape analysis software (Zhou et al., 2019). CDF plots were generated using ggplot2, and MA plot was generated from DESeq2 results on miRNA captured reads in R version 3.3.4. Figures made in Adobe Illustrator.

Results

Development of a system to systematically interrogate miRNA regulation of class switch recombination

In prior work, we devised an arrayed screening approach to identify miRNAs that regulate helper T cell differentiation and effector function (Pua et al., 2016; Steiner et al., 2011). This approach allowed us to isolate the function of individual miRNAs by transfecting each one into T cells that lack endogenous miRNAs due to induced genetic deficiency for the miRNA biogenesis factor Dgcr8. For this study, we extended this approach to interrogate miRNA function in B cells. *Dgcr8* can be deleted with high penetrance during late stages of T cell development, but B cells exhibit a developmental defect at the pro to pre-B cell transition in the absence of miRNA biogenesis machinery (Koralov et al., 2008). To study the role of miRNAs in regulating class switch recombination (CSR), we bred Cγ1-cre Dgcr8$^{fl/fl}$ Rosa26-LSL-YFP mice to allow inducible *Dgcr8* inactivation in B cells upon activation of the Ighg1 germline transcript promoter. Splenic B cells from these mice were stimulated with mitogenic anti-CD180 crosslinking antibody and low dose IL-4 (1 ng/ml) for 48 hours (Day -2 to 0) to force expression of cre recombinase and inactivate *Dgcr8* without inducing CSR, then transferred to classical CSR conditions of LPS and high dose IL-4 (25 ng/ml) for an additional 48-96 hours (Day 0 to 4) (Fig. 2.1A). Thereafter, we analyzed viability, YFP as a reporter cre activity, and surface IgD and IgG1 expression by flow cytometry. In these cultures, 95% of viable cells expressed YFP at Day 2, indicating nearly uniform induction of cre recombinase activity (Fig. 2.1B, left panel). Importantly, these cells remained capable of undergoing CSR (Fig. 2.1B, right panel).

To validate *Dgcr8* ablation, we isolated RNA from Cγ1-cre Rosa26-LSL-YFP B cells that were also Dgcr8 $^{fl/fl}$ (D8-KO), Dgcr8$^{fl/+}$ (D8-HET) or Dgcr8$^{+/+}$ (D8-WT) to measure *Dgcr8* transcript and mature miRNAs throughout the stimulation timeline. *Dgcr8* mRNA abundance was

decreased by 8-fold in the D8-KO cells compared to D8-HET and D8-WT cells after the initial 48 hour stimulation and continued to decrease through day 4 (Fig. 2.1C). Furthermore, the activation-induced miRNAs mmu-miR-155-5p and mmu-miR-21-5p had 2 to 16-fold decreased expression in D8-KO compared to D8-HET and D8-WT cells, consistent with loss of Dgcr8-dependent miRNA processing activity (Fig. 2.1C). In contrast, mmu-miR-484-5p was unaffected throughout the stimulation and increased at Day 4 (Fig. S2.1A), consistent with previous reports that Dgcr8-independent miRNAs increase in abundance in the absence of Dgcr8-dependent miRNA biogenesis (Babiarz et al., 2008).

Utilizing these stimulation conditions, we tested the role of 85 miRNAs that are expressed in naïve, activated, and/or germinal center B cells (Fowler et al., 2015; Kuchen et al., 2010; Zhang et al., 2009). We transfected B cells using the Neon next generation transfection system (Pua et al., 2016; Steiner et al., 2011) to introduce individual miRNA mimics into D8-KO activated B cells at D0 and measured CSR to IgG1 at D2. These optimized conditions achieved close to 100% transfection efficiency with small RNAs, as indicated by uniform down-regulation of CD45 in cells transfected with an siRNA against its transcript, *Ptprc* (Fig. S2.1B). Surface IgG1 expression implicated miR-155-5p as a negative regulator of CSR to IgG1 (Fig. 2.1D), consistent with previous studies demonstrating that mutation of the miR-155 binding site in the Aicda 3'UTR led to an increase in transcript, protein and double stranded break induction in activated B cells (Dorsett et al., 2008; Teng et al., 2008). Similarly, congruent with a previous study, miR-18a positively regulated CSR (Xu et al., 2015). Interestingly, miR-222-3p was the most potent positive regulator of IgG1 surface expression (Fig. 2.1D). This miRNA and its family member miR-221-3p have been implicated in early B cell development and homing to the bone marrow (Knoll et al., 2013; Petkau et al., 2018), but not in CSR or B cell activation. In a re-screen of the top 10 and

bottom 10 regulating miRNAs and their family members, both miR222-3p and miR-221-3p increased CSR compared to control mimic (Fig. S2.1C). Given this consistent and robust effect, we decided to further investigate the role of the miR-221/222 family in CSR.

Germline deletion of the miR-221/222 cluster on the X chromosome does not alter B cell development.

In both mice and humans, miR-221 and miR-222 are processed from a single primary miRNA transcribed from the *Mirc50* locus on chromosome X. We generated mmu-miR221/222 deficient mice. We inserted loxP sites flanking miR-221 and miR-222 by gene targeting to create a conditional mutant allele (flox) that can be irreversibly converted to a deleted allele (Δ) upon introduction of cre recombinase. B cells from wildtype and flox mice expressed equivalent amounts of miR-221-3p and miR-222-3p, and these miRNAs were undetectable in B cells from Δ mice generated by cre expression in the germline (data not shown, see also Fig. 2.5C). In all further experiments, we compared mice with these two targeted alleles to determine the effect of miR-221 and miR-222 in B cells. Mice bearing either flox or Δ allele(s) exhibited normal B cell development in the bone marrow, with similar numbers and frequencies of pro-B, pre-B, immature and mature B cells (Fig. 2.2A-B). There was a subtle decrease in the frequency of transitional B cell subsets T2 and T3 in the spleen of Δ mice, but no difference in the numbers of transitional and mature B cells in the spleen (Fig. 2.2C-D). The abundance of serum IgM, IgG1, IgG2b and IgG3 were unchanged in flox and Δ mice (Fig. 2.2E), while IgE was undetectable in these unimmunized animals (data not shown). We conclude that the absence of miR-221 and miR-222 does not grossly perturb B cell development in the bone marrow or maturation in the periphery.

miR-221/222 regulate CSR to IgG1 and IgE in vitro

To test whether endogenous miR-221/222 regulate CSR, we compared flox and Δ B cells cultured under the same conditions used to screen for functional miRNAs in *Dgcr8*-deficient B cells. Compared to flox B cells, Δ B cells transfected with a control miRNA mimic (CM) showed a two-fold reduction in CSR to IgG1 (Fig. 2.3A, compare grey and black bars labeled CM). Transfecting Δ B cells with either miR-221-3p or miR-222-3p mimic restored IgG1 CSR to the frequency seen in CM-transfected flox B cells (Fig. 2.3A, compare grey bars). These data indicate that the CSR defect in Δ B cells is due to the absence of mature miR-221/222 and demonstrate that this defect can be reversed by restoring miRNA expression in mature B cells. Furthermore, miR-221-3p or miR-222-3p mimic transfection further increased IgG1 CSR in flox B cells (Fig. 2.3A, compare black bars), indicating that endogenous miR-221/222 is a dose-limited factor that enhances CSR to IgG1.

To determine the expression profile of these miRNAs, we performed qPCR for miR-221-3p and miR-222-3p on RNA from B cells stimulated under various conditions known to induce CSR to IgG1 and IgE. Compared to naïve B cells, stimulation with LPS + IL-4 for 4 days increased expression of miR221-3p and miR-222-3p by 3.7 and 2.5 fold, respectively (Fig. 2.3B). Stimulation with anti-CD40 + IL-4 increased miR-221-3p and miR-222-3p expression 8.1 and 3.1 fold, respectively, and the further addition of IL-21 in these conditions increased miR-221-3p induction to 12.5-fold and miR-222-3p to 4.7 fold that of naïve cells (Fig. 2.3B). Stimulating flox and Δ B cells with anti-CD40 + IL-4 + IL-21 revealed a requirement for miR-221/222 for optimal CSR to IgG1 and IgE (Fig. 2.3C-D). The frequency of IgE^+ cells was significantly reduced in Δ B cells compared to flox B cells in three independent experiments. The frequency of $IgG1^+$ cells was consistently reduced in two of these experiments, with the third showing the highest frequency

of IgE^+ cells. This could be due to depletion of $IgG1^+$ cells by consecutive CSR to IgE (Cameron et al., 2003; Mandler et al., 1993; Yoshida et al., 1990), or a higher rate of direct CSR to IgE in this experiment. In any case, comparing the combined frequency of IgE^+ and $IgG1^+$ cells revealed a clear and statistically significant CSR defect in Δ B cells compared to flox B cells (Fig. 2.3D). Given that CSR correlates with proliferation capacity (Hodgkin et al., 1996), CTV staining was performed on congenically labeled co-cultured Δ and flox cells in anti-CD40 + IL-4 + IL-21 conditions to determine if there was a proliferation defect in the absence of these miRNAs. Interestingly we found that Δ B cells showed a defect in the frequency of cells dividing 6 or more times compared to flox (Fig. 2.3E), indicating a subtle proliferation defect.

miR221-222 regulates IgE production in vivo

Having confirmed an *in vitro* CSR defect in the Δ B cells, we went on to test whether the defect in CSR would translate to a physiological *in vivo* model of allergy and asthma, specifically house dust mite challenge. Examining total and HDM specific IgE titers in mice challenged with HDM by ELISA, showed that the Δ mice had a statistically significant defect in total IgE production, and a trending defect in high affinity HDM specific IgE production (Fig. 2.3F). No difference was seen in *in vivo* IgG1 production in this model, limiting the *in vivo* effect of this miRNA cluster to IgE production, specifically.

To determine if the *in vivo* effect was due to IgE cell number and the plasma cell fate decision, we utilized a goat anti-IgD polyclonal B cell activation model (Finkelman et al., 1987). Seven days post immunization with goat anti-IgD serum showed a massive B cell response, where around half of the total lymph node cells were composed of CD138+, CD19int B cell plasma-blast cells (Fig. 2.4A). While the frequency of total plasma cells was not different between flox and Δ animals (Fig. 2.4B), the frequency of IgE+ plasma cells was decreased in Δ animals compared to

flox (Fig. 2.4C), as were the numbers of total plasma cells and IgE+ plasma cells (Fig. 2.4D-4E). This decrease in frequency and number of IgE producers in the Δ animals is congruent with the findings of increased IgE serum levels in HDM challenged flox animals compared to Δ animals and provides two independent *in vivo* systems where IgE production is diminished in the absence of miR-221/222-3p.

Combination of Ago-2-HITS-CLIP and mRNA-seq reveal 70 plausible miR221/222 targets

Having determined a clear *in vitro* and *in vivo* phenotype, of miR-221/222-3p in CSR to IgG1 and IgE, we wanted to determine the direct targets of this miRNA family in activated B cells. To determine direct targets of miR-221-3p and miR-222-3p we performed Ago-2-HITS-CLIP on Δ and flox B cells stimulated for 4 days with anti-CD40 + IL-4 + IL-21. Libraries were generated and sequenced as previously described (Gagnon et al., 2019). Four independent libraries were generated for Δ and flox genotypes. Analysis of the target transcript space identified the 3'UTR as the most abundant RNA species target as would be expected, although binding was seen in exon, intron, and 5'UTR space as well (Fig. 2.5A). Furthermore a 2:1 miRNA: non-miRNA ratio of reads was captured from the library, indicating either preferential cross linking of miRNA in Ago2-miRNA-targetRNA complexes, or an abundance of AGO2-miRNA complexes not yet bound to target RNA sequences in our activated B cells (Fig. 2.5B). Furthermore analysis of the differentially bound miRNAs by DESeq2 analysis showed that both miR-221-3p and miR-222-3p (as well as their star sequence 5p counterparts) were differentially captured in flox libraries and absent in Δ libraries, indicating a complete deletion of the miRNAs as well as confirming that global miRNA expression and loading into Ago2 is not altered in the absence of this cluster (Fig. 2.5C).

The 4 Ago2-HITSCLIP libraries for each genotype were combined for a single comparison of differential peak binding, utilizing dCLIP (Wang et al., 2014). Utilizing sequence homology identity of all miR-221/222-3p target sites within the mouse genome identified 10,638 possible binding sites in the annotated 3'UTRs of the mouse genome. To validate the efficacy in which dCLIP positively identified miR-221/222-3p peaks, differential peaks containing at least a 6-mer target site were binned, and those more bound in the flox than Δ and vice versa were analyzed at increasing differentials determined by the program. Using the internal dCLIP-differential ranking metric of at least 1 yielded a total of 652 peaks in 534 gene transcript 3'UTRs that were more bound in the flox than Δ library. However, using the same parameters of a differential of at least 1 yielded a total of 636 peaks in 547 gene transcript 3'UTRs that were more bound in the Δ than flox library, of which 80 of those transcripts overlapped with those in the flox (Fig. S2.2A). To improve confidence of the truly differential targets and limit the amount of seed sites that were more occupied in Δ and flox due to spurious read differences from adjacent miRNA binding, a differential of 10 was used, and in this case at least 6-mer containing peaks more bound in the flox lead to a total of 412 peaks in 343 gene transcript 3'UTRs. When the analysis was performed with the differential of 10 on sites more bound in Δ libraries compared to flox only 61 peaks were found in 57 gene transcript 3'UTRs, and of these only 8 gene transcripts overlapped with those of flox (Fig. S2.2B).

RNA sequencing was performed on flox and Δ B cells stimulated similarly to the Ago-2-HITSCLIP libraries to determine differentially expressed genes between Δ and flox activated B cells. A total of 12,074 ENSEMBL transcripts were found to be expressed under these conditions, of which 429 were differentially expressed by an FDR <0.1. Of these differentially expressed transcripts, 286 were upregulated in the KO compared to the flox libraries. The 12,074 transcripts

were binned into subsets containing no miR-221/222-3p seed match, only 6mer match, at least 7mer match (+ 6mer), or at least 8mer match (+ 7mer + 6mer) binding sites in annotated 3'UTRs. Cumulative distribution function (CDF) plots were generated and each seed-containing bin was compared to the no seed bin generating a Differential D= 0.132 for 6-mer, D= 0.126 for 7mer, and D= 0.171 for 8-mer, indicating increased differential expression of 8-mer seed match containing transcripts in the Δ compared to flox B cells (Fig. 2.6A). The absence of miR221/222 leads to a subtle increase in expression of all genes containing a putative seed sequence by sequence match alone. Using these 343 dCLIP putative target genes to create a CDF plot compared to all other expressed genes led to a differential of D= 0.19 (Fig. 2.6B). Indicating an increased confidence of these genes being direct targets and providing more confidence of direct targeted regulation by miR-221/222-3p than that of putative seed sequence match alone.

To compare our dCLIP analysis with predicted targets from the sequence homology, we analyzed the predicted target genes from the Bartel lab's Targetscan 7.1 program (Agarwal et al., 2015). Targetscan 7.1 predicts 404 gene targets for the miR-221/222-3p family, of which 290 were expressed in our B cell cultures by RNA-seq. Generating CDF plots of the 290 Targetscan predicted genes compared to all others produced a differential D=0.193 (Fig. 2.6C), further increasing the confidence of these genes being directly targeted by miR-221/222-3p. Of these 290 Targetscan predicted gene targets, 70 of them overlapped with those 343 gene targets predicted from our differential HITS-CLIP analysis (Fig. S2.2C). Creating a further CDF plot comparing these 70 putative targets to all other genes further increased the differential D=0.293, providing strong confidence for these genes being directly regulated by this miRNA family (Fig. 2.6D). The union of both cell specific dCLIP and the predictive capabilities of Targetscan7.1 provided a subset of genes we could directly test through small inhibitory RNA screening. Running Metascape

(Zhou et al., 2019) on the 70 genes, provided a gene ontology profile enriched in a cell cycle profile, among others (Fig. 2.6E), congruent with our finding of this miRNA regulating proliferation in mature B cells, and findings in other cell types (Galardi et al., 2007; Mayoral et al., 2009).

siRNA screen of the 70 direct gene targets implicates Foxp1, cd164 and Arid1a as regulators of CSR to IgG1/IgE.

To validate the putative targets as regulators of CSR, we performed and siRNA screen similar to that of the miRNA screen performed in Fig. 2.1. In this case B6 mice were used with the same timing schematic as the miRNA screen, where cells were first activated in anti-CD180 + IL4 low dose conditions and then transferred to canonical CSR conditions of LPS + IL4 high dose conditions. Four siRNAs were used per gene target, and surface IgG1+ and viability were analyzed by flow cytometry. Of the 85 targets, siRNA KD of the pro-apoptotic factor *Bcl2l11* (Bim protein) increased viability of transfected cells to 65%, a 15% increase from control siRNA (Fig. 2.7A). Furthermore, siRNA KD of *Rnps1*, an enzyme necessary for pre-mRNA splice junction formation (Mayeda et al., 1999), negatively regulated both CSR to IgG1 as well as viability. SiRNA KD of three candidate miR-221/222 targets: *Foxp1*, *Cd164*, and *Arid1a* - resulted in the highest increase of surface IgG1 frequency compared to control mimics (Fig. 2.7A). This KD correlated increase of surface IgG1 was confirmed in an siRNA rescreen where these were the three most positive regulators of CSR to IgG1 (Fig. 2.7B). Analysis of our RNA sequencing found that expression of *Foxp1*and *Arid1a* were statistically higher in Δ mice compared to flox mice (1.45 and 1.40 fold increased, respectively), whereas *Cd164* expression was only moderately different between the two genotypes at 1.06 fold higher in Δ vs flox mice (Fig. 2.7C). Furthermore, dual luciferase constructs were made to confirm that these transcripts' 3'UTRs were targeted directly by

miR221/222. We found that both *Cd164* and *Foxp1* 3'UTR fragments containing the Targetscan 7.1 predicted sites (as well as an additional 6-mer sequence in the 3'UTR of *Foxp1*) showed destabilization and direct targeting of that 3'UTR. This in conjunction with the differential binding implicated from our dCLIP expression supports that *Cd164* and *Foxp1* are direct gene targets, whereas *Arid1a* may be an indirect target of this miRNA cluster.

Genetic Ablation of Foxp1 increases B cell propensity to Switch to IgG1 and IgE

To confirm that Foxp1 is itself a regulator of CSR to IgG1 and IgE, we utilized a tamoxifen inducible cre deletion model of *Foxp1* and then cultured the cells under IgG1/IgE class switching conditions (Fig. 2.8A). Cre^{ERT2} mediated $Foxp1^{fl/fl}$ deletion (Foxp1-KO) B cells cultured on BAFF/CD40L expressing cells in the presence of IL4 showed a threefold increase in the frequency of IgG1 and IgE surface expression compared to $Foxp1^{fl/fl}$ or Cre^{ERT2} (Foxp1-WT) cells (Fig. 2.8B). Induction of CSR to IgG1 ranged from 10% to 60% from experiment to experiment, while that of IgE ranged from 3% to 20%, however the 2.5-3 fold further induction of either isotype in Foxp1-cKO compared to WT cells was robust. Interestingly the CSR to both IgE and IgG1 required IL-4 indicating that the activated B cells were not switching during deletion of pre-immunized mice in the *in vivo* setting. This confirmation of the siRNA KD, implicates miR-221/222 mediated Foxp1 regulation as a modulator that controls CSR to IgG1 and IgE in B cells.

Genetic Ablation and Chemical inhibition of Arid1a affects IgG1 and IgE CSR.

We utilized another genetic approach to target Arid1a deletion in mature mice by utilizing $CD21^{cre}$ (Cre+WT) and $Arid1a^{fl/wt}$ (Arid1a-WT) mice to make heterozygous animals $CD21^{cre}$ $Arid1a^{fl/wt}$ (Arid1a-HET). Deletion of Arid1a in the hematopoietic system causes profound defects in development (Han et al., 2019). Using the same *in vitro* stimulation conditions of anti-CD40,

IL-4, IL-21 we found that Arid1a-HET mice showed a defect in the frequency of IgE CSR compared to Cre+WT and Arid1a-WT control mice (Fig. 2.9A right panel), and this was concordant with an increase in the frequency of IgG1+ B cells (Fig. 2.9A, left panel). Indicating that partial loss of this BAF complex member alters CSR fate in these conditions.

We also used a specific Arid1a-BAF complex chemical inhibitor, BRD-K80443127 a macrolactam (Marian et al., 2018), to test the effect of BAF complex dysregulation on CSR to IgG1/IgE. Interestingly, cells cultured in anti-CD40, IL-4, IL-21 conditions showed no decrease in viability in the presence of BRK-K8-4431327 (Fig. 2.9B top left panel), and even a slight increase at the 20-40 uM range, indicating that dysregulation of these complexes is not vital for mature B cell homeostasis under this stimulus. Similarly, plasma cell differentiation showed a defect only at the highest concentration of 40 uM (Fig. 2.9B top right panel), while both IgG1 and IgE showed a dose dependent decrease (Fig. 2.9B bottom left and bottom right, respectively). Interestingly, the frequency of IgE switching was more sensitive to Arid1a-BAF inhibition beginning at 5 uM compared to IgG1 at 10uM. Furthermore IgG1 frequency remained 80% of vehicle control up to 40uM inhibitor concentration, thereafter falling off sharply to 10%. Targeting Arid1a through both genetic and chemical means shows that this miR-221/222-3p regulated gene has a direct effect in modulating CSR to IgG1 and IgE.

Discussion

MicroRNA rescue screens have been used to study embryonic stem cell pluripotency and self-renewal (Froidure et al., 2016; Wang et al., 2008), and in miRNA-depleted lymphocytes to study T cell proliferation, differentiation and cytokine production (Pua et al., 2016; Steiner et al., 2011). In this study, we developed and executed a rescue screen in primary mouse B cells to reveal that miR-221/222 can positively regulate CSR to IgG1, and leveraged this finding to elucidate a previously unknown miRNA regulated gene network that modulates CSR to IgG1 and IgE. These rescue screens measure the effects of individual miRNAs introduced at potentially supraphysiological quantities in the absence of other miRNAs. However, analysis of miR-221/222-deficient B cells demonstrated that endogenous miR-221/222 regulate CSR *in vitro* and *in vivo*. Extending this screen for miRNA influence with biochemical elucidation of direct targets of miR-221/222, we uncovered evidence for a network of downstream regulators of CSR including *Foxp1* *Arid1a*, and *Cd164*.

Foxp1 is essential for B cell development (Hu et al., 2006) and its down regulation in activated mature B cells is necessary for germinal center entry and plasma cell differentiation (Sagardoy et al., 2013; van Keimpema et al., 2015). Through the investigation of miR-221/222 targets, we uncovered an additional role for this transcription factor as a negative regulator of CSR to IgG1 and IgE. *Foxp1* deletion in mature B cells also hinders T-independent B cell response, production of IgG3, and B1 cell development (Patzelt et al., 2018). A previous study of T-dependent antibody responses showed no clear difference in IgG1 serum titers in B cell lineage-specific *Foxp1*-deficient mice, but this finding is complicated by developmental defects that result in fewer mature B cells in these mice (Dekker et al., 2019; Patzelt et al., 2018). As previously reported (Dekker et al., 2019), B cells lacking FOXP1 exhibited increased proliferation in response

to CD40 and IL4 stimulation. This accelerated cycling likely contributes to their dramatically increased CSR to IgG1 and IgE *in vitro*. However, whether FOXP1 acts as a transcriptional repressor to dampen activation signals, cell cycle regulators or other factors remains to be determined. Further studies are needed to fully elucidate the transcriptional targets and downstream mechanisms through which FOXP1 controls CSR in conjunction with its effects on B cell fate decisions.

The role of chromatin architecture and remodeling in the context of CSR has recently come into full appreciation as DNA orientation and chromatin regulation were shown to be critical for switch site orientation and stabilization for AID-mediated mutation (Yu and Lieber, 2019; Zhang et al., 2019). Interestingly, our analysis of regulated miR-221/222 interactors identified 3 predicted targets that play a role in chromatin remodeling: *Ctcf*, *Smarca5*, and *Arid1a*. CTCF is a central regulator of chromatin domain architecture and CSR (Perez-Garcia et al., 2017; Thomas-Claudepierre et al., 2013; Zhang et al., 2019). Human *Ctcf* is an established target of miR-221/222 (Lupini et al., 2013). *Arid1a* encodes a key component of the BAF nucleosome remodeling complexes, which are critical for chromatin remodeling during hematopoiesis (Han et al., 2019). We found that the action of these complexes is necessary for B cell activation as cells cultured with an ARID1A-containing BAF complex inhibitor (Marian et al., 2018) remained in a quiescent state, neither undergoing cell death nor proliferation. However, genetically or pharmacologically limiting (rather than eliminating) ARID1A-containing BAF complexes revealed a selective effect on CSR. Surprisingly, B cells with reduced ARID1A were more prone to IgG1 CSR but exhibited a strong defect in IgE CSR. Whether ARID1A-BAF complex nucleosome remodeling mediates access to critical regions of the *Igh* locus deserves further study. In any case, the selective

sensitivity of IgE CSR to BAF inhibition indicates the existence of isotype specific effects of regulating (or dysregulating) this machinery.

Previous studies of miR-221/222 in other immune cell types and cancer demonstrated direct regulation of *Cdkn1b*, which encodes p27-kip protein, a positive regulator of cell cycle progression from G1 to S (Fornari et al., 2008; Galardi et al., 2007; Mayoral et al., 2009). Our biochemical data also implicated *Cdkn1b* as a direct target. However, siRNAs against this gene decreased B cell proliferation without a discernible effect on CSR. While our data do not definitively prove that miR-221/222 directly target *Cdkn1b* in B cells, the fact that miR-221/222-deficient B cells exhibited a subtle proliferative defect implicates these miRNAs in regulation of B cell cycle progression, possibly through multiple targets including *Cdkn1b*.

miR-221/222 appears to regulate allergic responses through coordinate control of multiple cell types. Mast cells, basophils, and other granulocytes very strongly express miR-221/222 (Kuchen et al., 2010; Monticelli et al., 2005), and these miRNAs regulate mast cell proliferation and degranulation in response to IgE receptor crosslinking (Mayoral et al., 2011; Mayoral et al., 2009). In this study, we found that miR-221/222-deficiency also impaired B cell production of IgE in allergic airway sensitization and pan-B cell activation models. Further studies will be necessary to determine whether miR-221/222 absence in granulocyte populations further affects allergic responses *in vivo*. The control of complex immunological processes through regulation of distinct cell types by a common factor is an interesting regulatory phenomenon exemplified by the orchestration of humoral responses by the transcription factor BCL6 (Crotty, 2019; Okada et al., 2012) and the miRNA cluster miR-17~92 (Baumjohann et al., 2013; Jin et al., 2013; Kang et al., 2013) acting in both GC B cells and T follicular helper cells.

Other highly expressed miRNAs also regulate humoral immune responses, including miR-155 and miR181b, both of which directly target the critical CSR factor *Aicda* in B cells (Dorsett et al., 2008; Rodriguez et al., 2007; Teng et al., 2008; Thai et al., 2007; Vigorito et al., 2007) (de Yebenes et al., 2008). miRNA expression is dramatically modulated in activated B cells (Fowler et al., 2015; Kuchen et al., 2010). In our experiments, miR-221/222 were upregulated upon B cell activation, yet their abundance was still less than 1% that of the most highly expressed miRNAs. Nevertheless, comparing Ago2 binding, gene expression in the presence and absence of miR-221/222 singled out direct targets even for these modestly expressed miRNAs. We provide these data as a resource for mining the Ago2-bound transcript space in mouse B cells activated to mimic T cell-dependent stimulation, complementing previous experiments performed under different conditions (Hsin et al., 2018; Jin et al., 2013).

Unbiased investigation of miR-221/222 target genes identified by Ago2-HITS-CLIP and gene expression analysis revealed a functionally relevant downstream gene network actively regulated in B cells undergoing CSR. Our overall experimental approach, which we term miRNA-directed target pathway discovery, coopts the coevolution of miRNAs and their targets to reveal novel players in biological processes without requiring genome-wide functional screens. miRNA-directed pathway discovery can be adapted to interrogate cell-type specific miRNA and target networks operative in nearly any biological process.

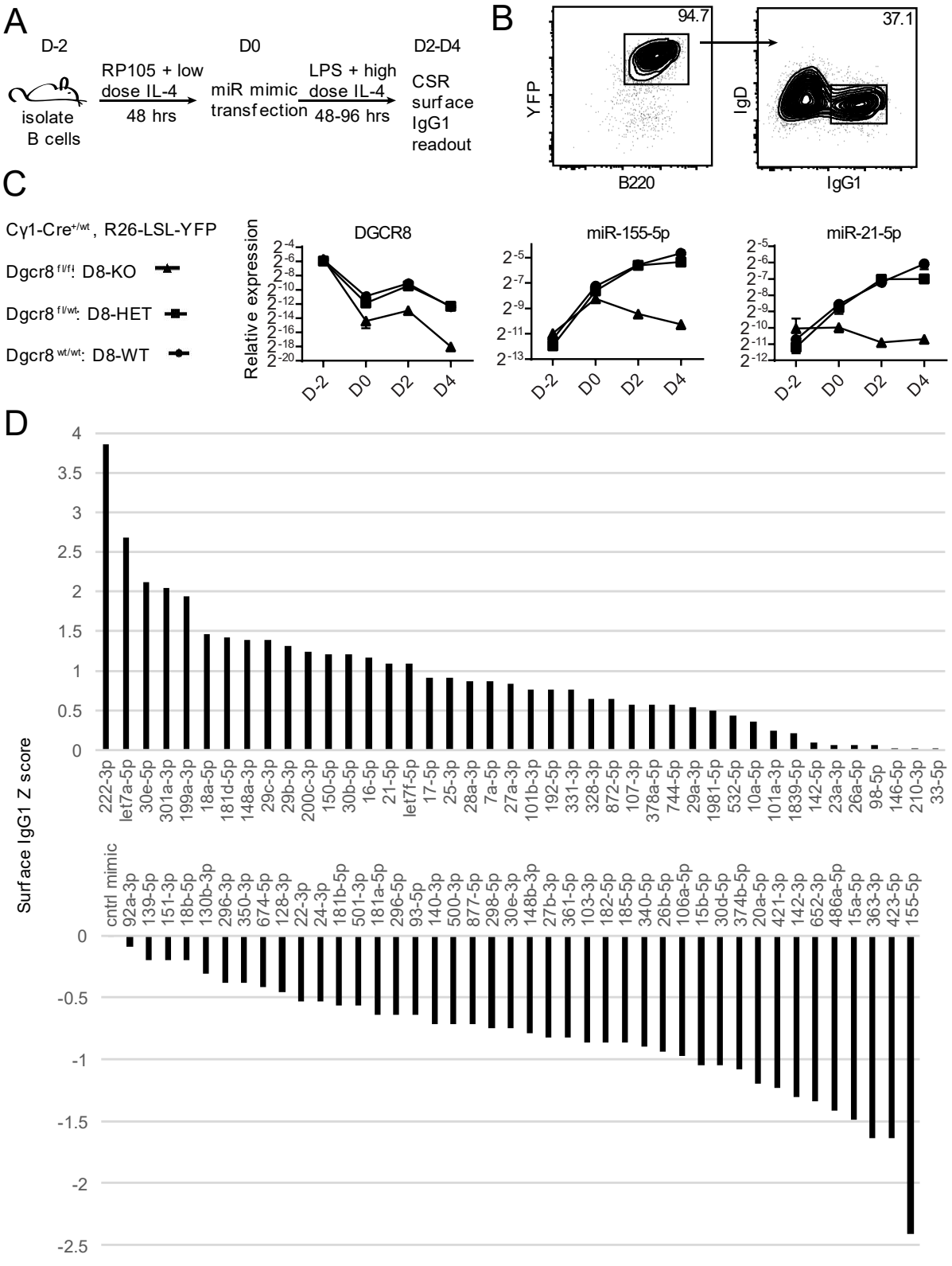
A
D-2
RP105 + low dose IL-4
48 hrs
isolate B cells
D0
miR mimic transfection
LPS + high dose IL-4
48-96 hrs
D2-D4
CSR surface IgG1 readout
B
94.7
37.1
YFP
B220
IgD
IgG1
C
Cγ1-Cre+/wt, R26-LSL-YFP
Dgcr8 fl/fl: D8-KO
Dgcr8 fl/wt: D8-HET
Dgcr8 wt/wt: D8-WT
DGCR8
miR-155-5p
miR-21-5p
Relative expression
D-2
D0
D2
D4
D
Surface IgG1 Z score
222-3p
let7a-5p
30e-5p
301a-3p
199a-3p
18a-5p
181d-5p
148a-3p
29c-3p
29b-3p
200c-3p
150-5p
30b-5p
16-5p
21-5p
let7f-5p
17-5p
25-3p
28a-3p
7a-5p
27a-3p
101b-3p
192-5p
331-3p
328-3p
872-5p
107-3p
378a-5p
744-5p
29a-3p
1981-5p
532-5p
10a-5p
101a-3p
1839-5p
142-5p
23a-3p
26a-5p
98-5p
146-5p
210-3p
33-5p
cntrl mimic
92a-3p
139-5p
151-3p
18b-5p
130b-3p
296-3p
350-3p
674-5p
128-3p
22-3p
24-3p
181b-5p
501-3p
181a-5p
296-5p
93-5p
140-3p
500-3p
877-5p
298-5p
30e-3p
148b-3p
27b-3p
361-5p
103-3p
182-5p
185-5p
340-5p
26b-5p
106a-5p
15b-5p
30d-5p
374b-5p
20a-5p
421-3p
142-3p
652-3p
486a-5p
15a-5p
363-3p
423-5p
155-5p

Figure 2.1: Development of miRNA rescue screen in mature B cells stimulated to CSR to IgG1 implicates miR-222 as a regulator.

A. Timing and stimulation conditions to induce Cγ1-cre deletion of *Dgcr8* and transfect miRNA and test CSR. **B.** Representative flow plot of gating strategy for YFP reporter and IgG1 surface expression. **C.** RT-qPCR of D8-WT, D8-HET, D8-KO B *Dgcr8* and miRNA expression throughout culturing (*Dgcr8* normalized to *Gapdh*, miRNAs normalized to snoRNA U6). **D.** Screen results from the individual miRNA rescue transfections at timepoint D2. Control bar is average of 6 transfections ranging from +1 to -1 z score averaged.

Figure 2

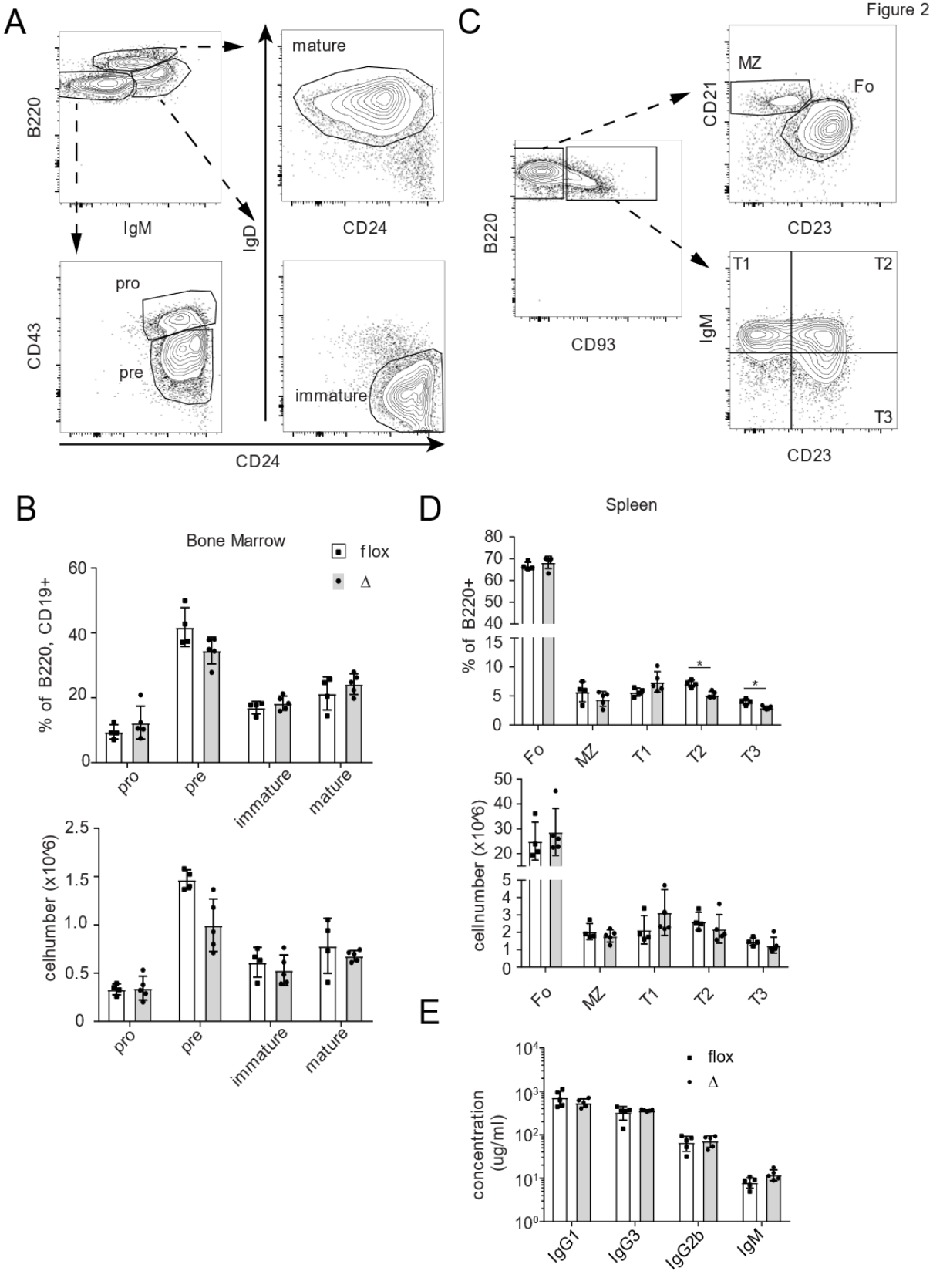
A
B220
IgM
IgD
mature
CD24
pro
pre
CD43
immature
CD24
C
MZ
Fo
CD21
CD23
B220
CD93
T1
T2
IgM
T3
CD23
B
Bone Marrow
flox
Δ
% of B220, CD19+
pro
pre
immature
mature
cellnumber (x10^6)
D
Spleen
% of B220+
Fo
MZ
T1
T2
T3
cellnumber (x10^6)
E
flox
Δ
concentration (ug/ml)
IgG1
IgG3
IgG2b
IgM

Figure 2.2: Loss of miR-221/222 does not alter B cell development in the bone marrow nor spleen and steady state serum antibody levels are unaffected.

A. Representative flow cytometry gating strategy for bone marrow analysis. Upper left gate is a subgate of live, singlet, CD19+, B220+ cells. Further sub-setting by B220int, CD43+,CD24+, IgM- pro-B cells; B220-int, CD43-int,CD24+, IgM- pre-B cells; B220-int, CD24+, IgM-hi, IgD- immature B cells; and B220-hi, IgM-int, IgD+, CD24-lo mature cells. **B.** Enumeration of percentage and number of each developmental bone marrow subset determined in A. **C.** Representative flow cytometry gating strategy for splenic analysis. Leftmost plot is pre gated on live, singlet, B220+, CD4- cells that are subdivided into transitional CD93+ subsets: CD23-, IgM-hi T1; CD23+, IgM-hi T2; and CD23+, IgM-lo T3. Or subset into mature CD93-: CD23+, CD21-int Follicular and CD23 lo, CD21-hi Marginal zone B cells. **D.** Enumeration of percentage and number of each developmental splenic subset determined in C. **E** Steady state serum concentrations for the labeled isotypes in flox and Δ mice. All p values from two-tailed student's t-test $p>.05$ for all unlabeled comparisons *= $p<0.05$.

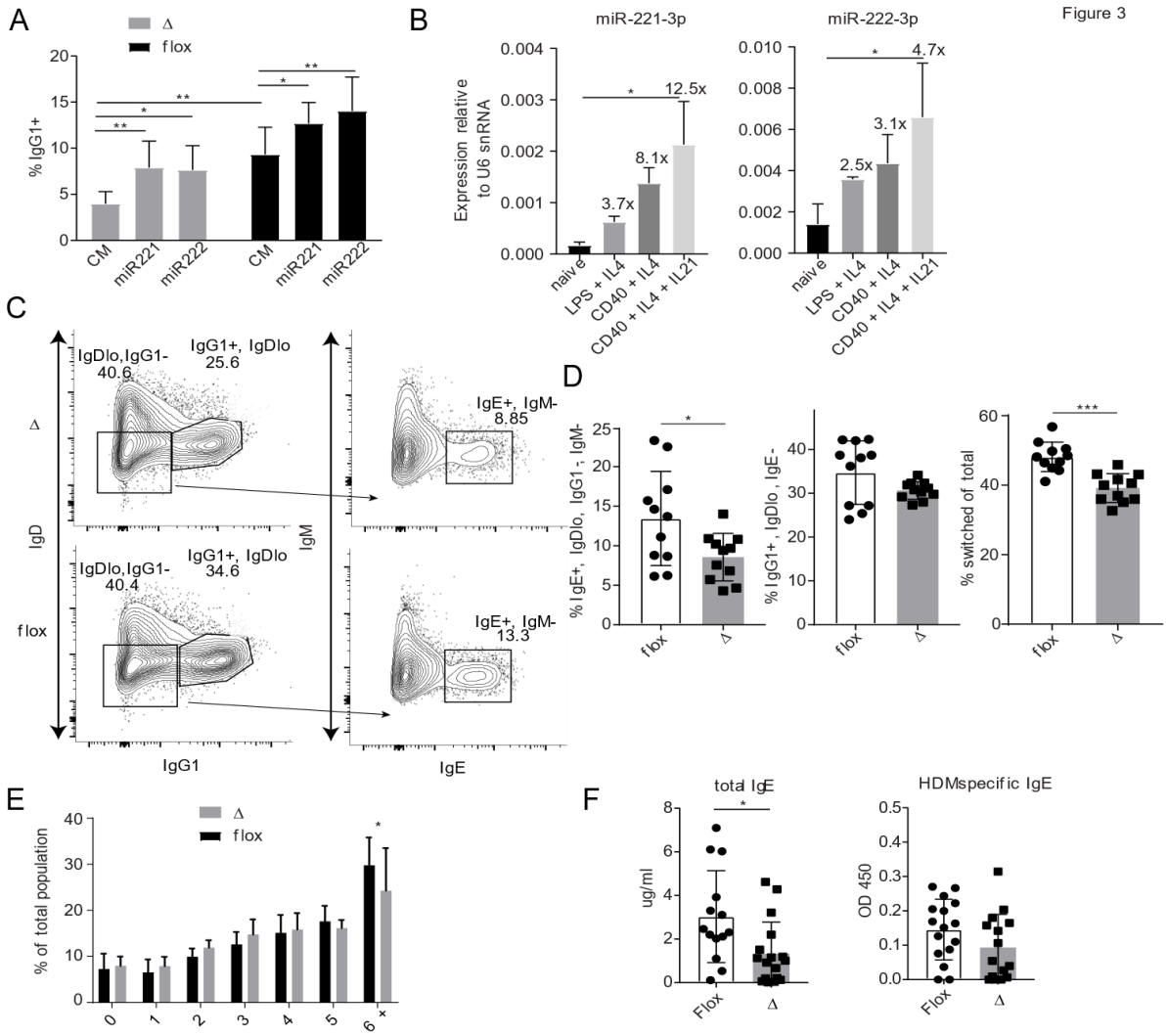

Figure 2.3: Loss of miR-221/222 leads to defects in B cell CSR to IgG1/IgE *in vitro* and IgE production *in vivo*.

A. Δ or flox B cells stimulated in screen conditions and transfected with miR-221-3p (miR221) or miR-222-3p (miR222), or control mimic (CM) at D0 and surface IgG1 read out at D2. 3 mice per genotype paired student's t test comparisons within genotype. Experiment is representative of 3 independent experiments. **B.** Expression of each miRNA in given IgG1/IgE CSR stimulation media for 96 hrs, relative to U6 snoRNA. **C.** Representative flow cytometry plots CSR phenotype of Δ or flox B cells stimulated in anti-CD40, IL4, IL21 media for 96 hours gated on live singlets to determine IgDlo, IgG1+ cells. IgE+ cells are IgM- and gated from IgDlo, IgG1- population **D.** Quantification of % surface IgE+, IgG1+, or either + from figure C. Combined 3 independent experiments with at least 3 mice per genotype. **E.** Quantification of Division number from co-cultured Δ and flox B cells stimulated in anti-CD40, IL-4, IL-21 media for 96 hours. Paired t test for each co-cultured well. Combined from 3 independent experiments with at least 2 independent co-cultures per experiment. **F.** ELISA data for total IgE and HDM specific IgE in mouse challenged with HDM for a 2 week protocol (see materials and methods from 4 independent experiments with 4 mice per group. *= $p<0.05$; **=$p<0.01$; ***= $p<0.001$.

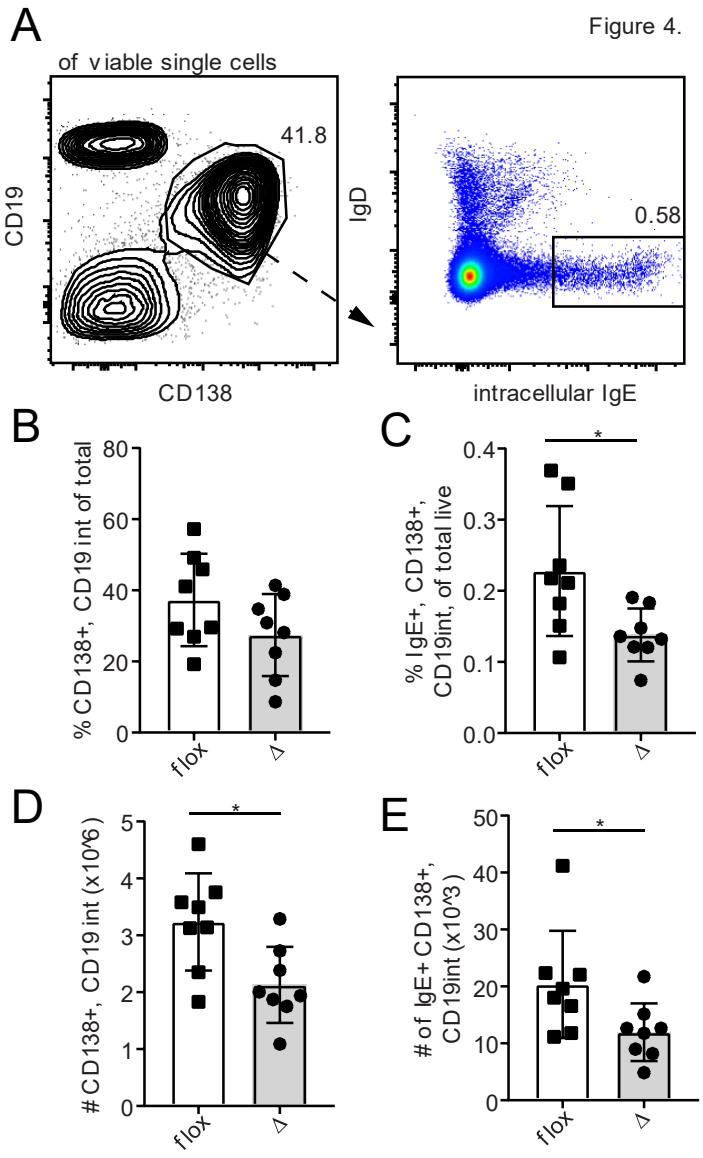

Figure 2.4: Loss of miR-221/222 decreases the number of PCs and IgE+ PCs in a pan-B cell activation model of Goat anti-IgD immunization.

A. Representative flow plot of the lymph node cell environment showing PC CD19 int, CD138+ cells gated on intra-cellular IgE+ fraction. **B.** Frequency and **D.** Numbers of PC of total lymph node cells. **C.** Frequency and **D.** numbers of IgE+ PCs. Each data point represents a mouse from 2 independent experiments. All statistics are from two-sided student's t-test. * $p < 0.05$.

Figure 5

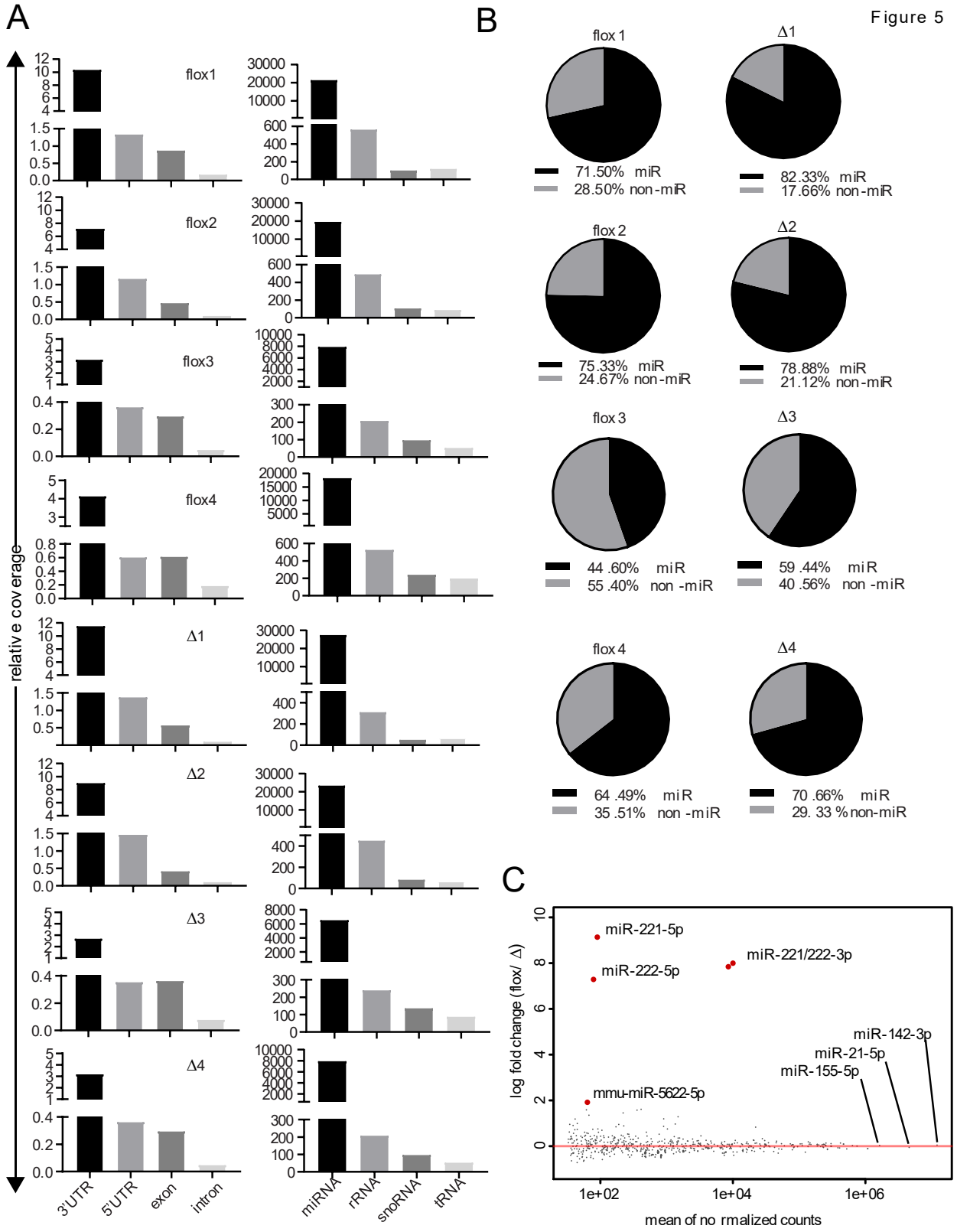
A
relative coverage
flox1
flox2
flox3
flox4
Δ1
Δ2
Δ3
Δ4
3'UTR
5'UTR
exon
intron
miRNA
rRNA
snoRNA
tRNA
B
flox 1
71.50% miR
28.50% non-miR
Δ1
82.33% miR
17.66% non-miR
flox 2
75.33% miR
24.67% non-miR
Δ2
78.88% miR
21.12% non-miR
flox 3
44 .60% miR
55 .40% non -miR
Δ3
59 .44% miR
40 .56% non -miR
flox 4
64 .49% miR
35 .51% non -miR
Δ4
70 .66% miR
29. 33 % non-miR
C
log fold change (flox/ Δ)
miR-221-5p
miR-222-5p
miR-221/222-3p
miR-142-3p
miR-21-5p
miR-155-5p
mmu-miR-5622-5p
1e+02
1e+04
1e+06
mean of normalized counts

Figure 2.5: Characterization of Ago-2 binding in Δ or flox B cells stimulated with anti-CD40, IL-4, IL-21.

A. Annotations and relative coverage of reads from each of the Δ and flox B cell libraries aligning to annotated mRNA sequences (left) and non-coding RNA sequences (right). **B.** Distribution of miRNA and non-miRNA reads in each library. **C.** Mean Analysis plot for miRNA reads only. Mean miRNA read count vs log10 miRNA read count per million of flox vs Δ reads. Red dots are Differentially captured miRNAs by DESeq2 with FDR< 0.05.

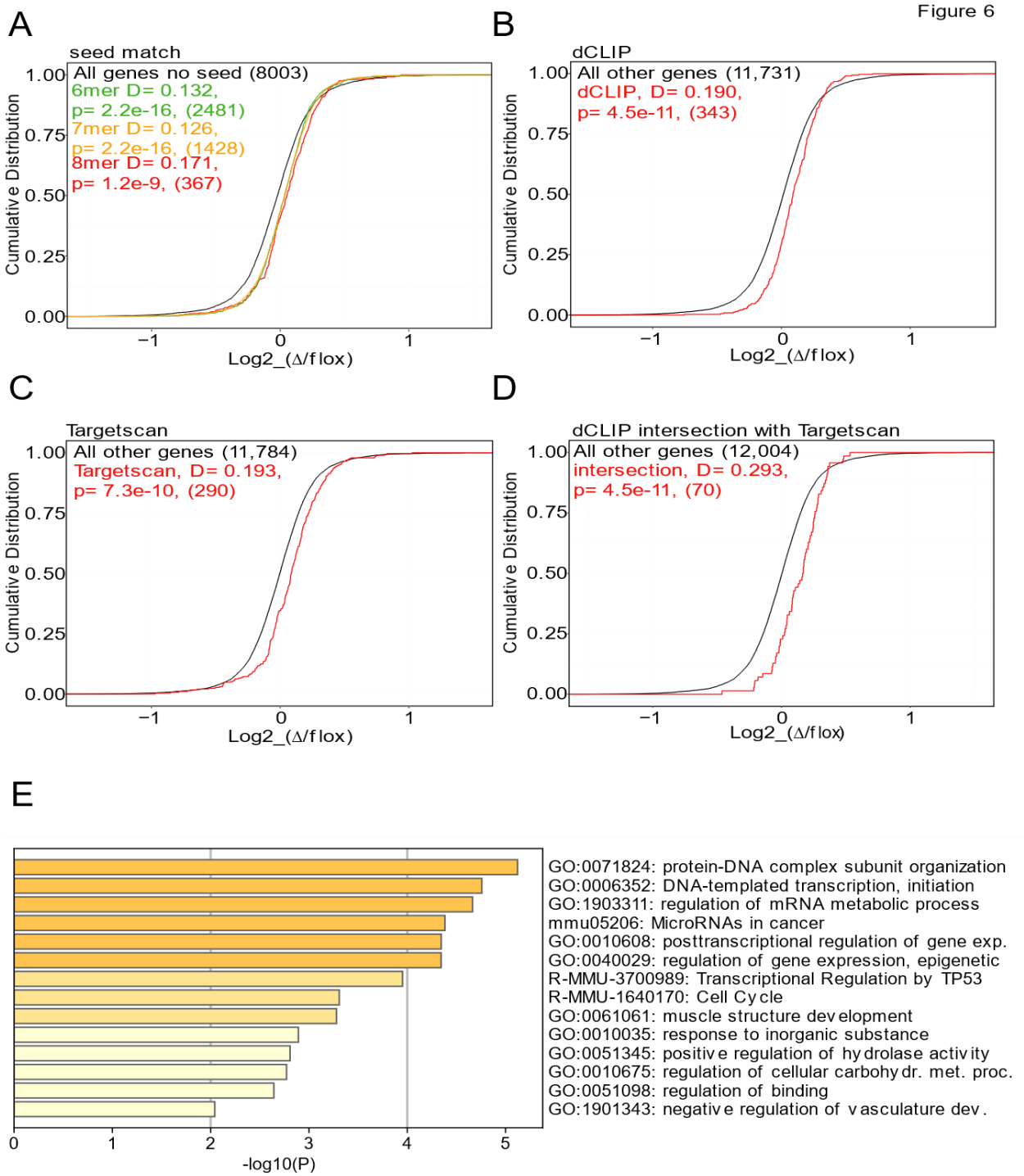

Figure 2.6: Intersection of dCLIP, RNA-seq, and Targetscan indicate 70 possible gene targets of miR-221/222 in B cells.

A-D. CDF plots comparing RNA-seq gene expression on x axis vs cumulative distribution on y axis **A.** genes with at least one 6-mer (green), at least one 7-mer (orange), or at least one 8-mer (red) to those lacking a miR-221/222-3p seed site (black). **B.** dCLIP predicted genes (red) to all others (black). **C.** Targetscan predicted genes (red) to all others (black). **D.** dCLIP and Targetscan predicted genes (red) to all others black. **E.** Ranked GO terms and kegg pathways enriched in the dCLIP and Targetscan gene subset.

Figure 7

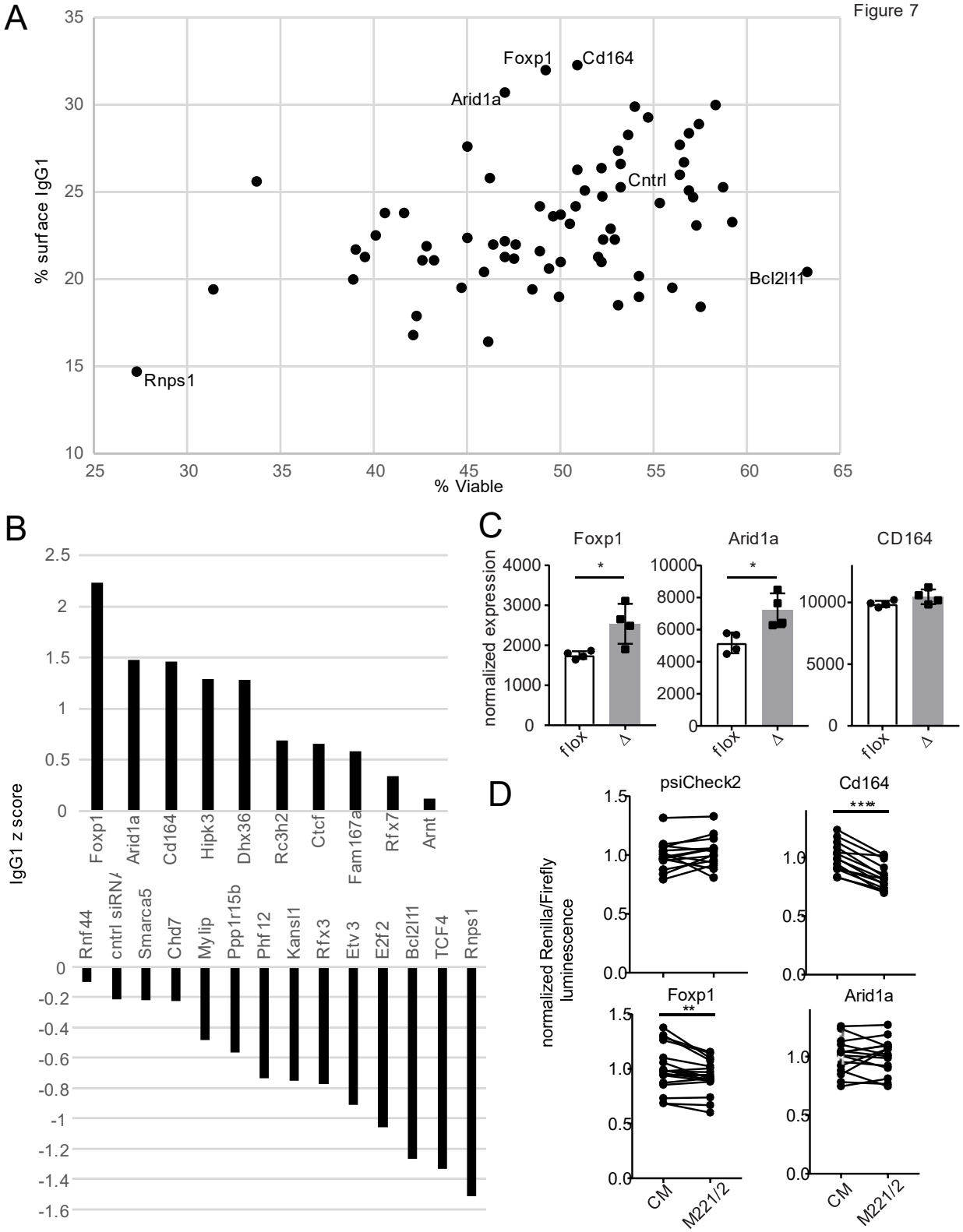
A
% surface IgG1
% Viable
Foxp1
Cd164
Arid1a
Cntrl
Bcl2l11
Rnps1
B
IgG1 z score
Foxp1
Arid1a
Cd164
Hipk3
Dhx36
Rc3h2
Ctcf
Fam167a
Rfx7
Arnt
Rnf44
cntrl siRNA
Smarca5
Chd7
Mylip
Ppp1r15b
Phf12
Kansl1
Rfx3
Etv3
E2f2
Bcl2l11
TCF4
Rnps1
C
Foxp1
Arid1a
CD164
normalized expression
flox
Δ
D
psiCheck2
Cd164
Foxp1
Arid1a
normalized Renilla/Firefly luminescence
CM
M221/2

Figure 2.7: SiRNA knockdown screen on dCLIP and Targetscan predicted miR-221/222-3p gene targets identifies Foxp1, Arid1a, and CD164 as regulators of CSR.
A. Frequency of Viable vs frequency of surface IgG1+ for the 70 gene targets predicted by dCLIP and Targetscan. **B.** Z-score plot for surface IgG1 for a rescreen of the top ten and bottom 10 genes from A. **C.** Gene expression data for *Foxp1, Arid1a, and Cd164* from RNA-seq data. **D.** Dual-luciferase reporter assay results for B cells transfected with either CM or miR221/222-3p mimic and labeled psicheck-2 constructs containing >1kb of each annotated 3'UTR containing miR-221/222 target sequence. *= $p<0.05$; **=$p<0.01$; ****= $p<0.0001$

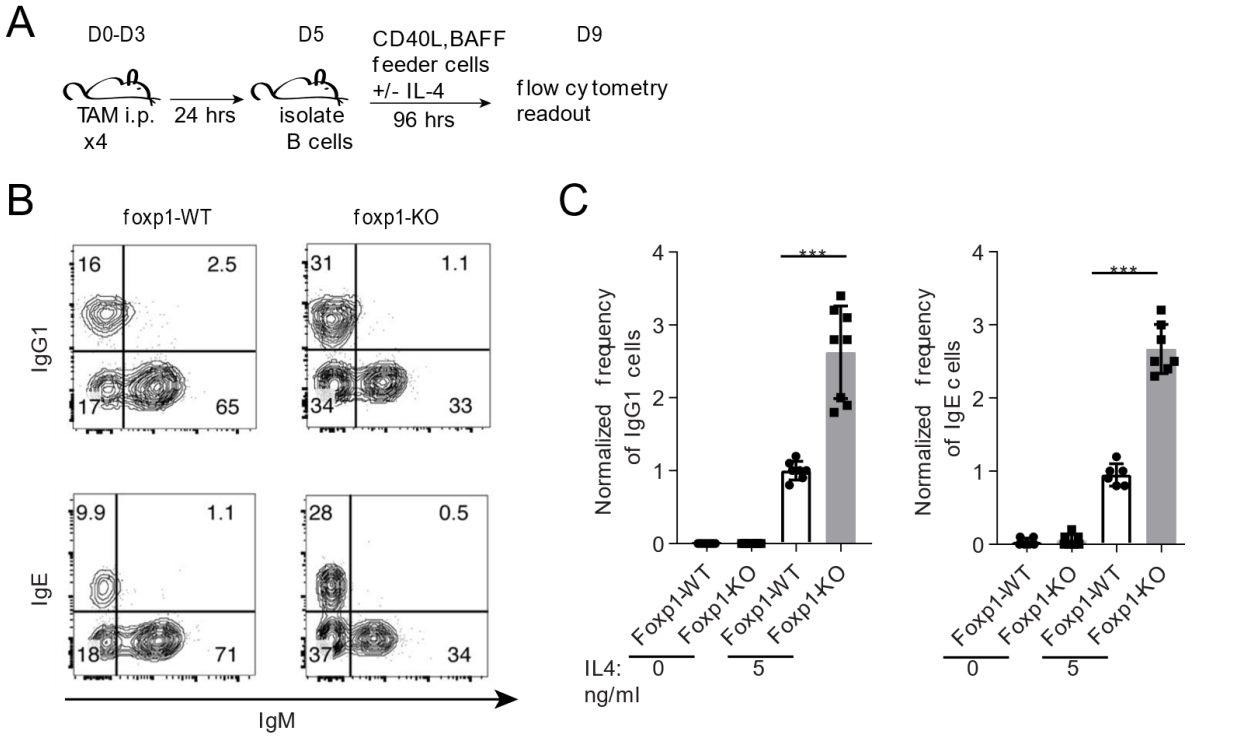

Figure 2.8: Genetic ablation of *Foxp1* increases the propensity for activated B cells to switch to IgG1 and IgE.

A. Schematic for tamoxifen induced deletion and culturing of Foxp1-wt and Foxp1-KO B cells. **B.** Representative flow cytometry plots of B cells from Foxp1-wt and Foxp1-KO mice post stimulation with and without supplemental IL-4. **C.** Normalized frequency of IgG1 and IgE surface expression. Each data point represents an individual biological replicate normalized to mean WT Ig frequency (og 1) within each experiment. Statistics generated by two-tailed student's t-test.*** $p<0.001$

Figure 9

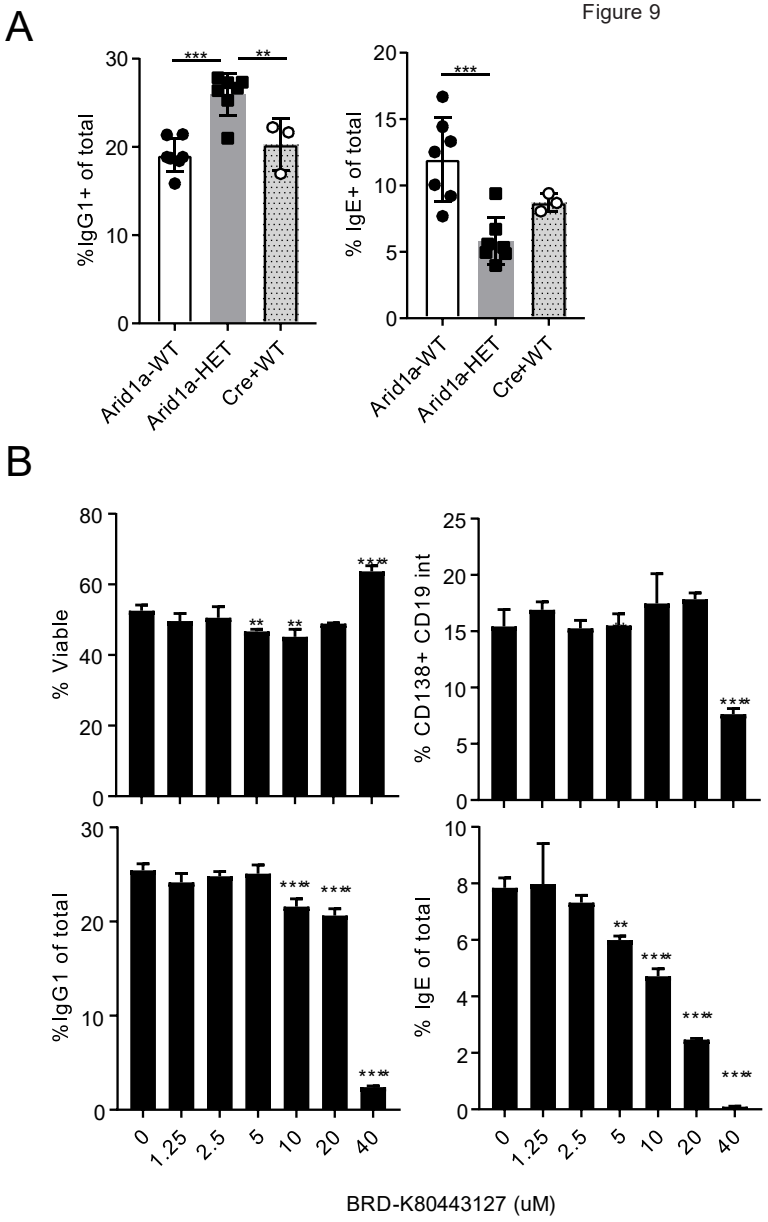

Figure 2.9: Genetic ablation of *Arid1a* and chemical inhibition of Arid1a-BAF complexes alters B cell IgG1 and IgE CSR frequency.

A. Quantification of Arid1a-WT, Arid1a-HET, and Cre+WT B cells stimulated with anti-CD40, IL-4, IL-21 frequency to switch to IgG1 and IgE each point is a single mouse, representative of 2 independent experiments. **B.** Quantification of viability, frequency plasma cell (CD138+, CD19int) and frequency of IgG1 or IgE surface expression throughout dilution series of chemical lactam. Statistics generated by ordinary one-way ANOVA with for A. Dunnet's multiple comparison test for B all comparisons to vehicle alone leftmost column. ** $p<0.01$, *** $p<0.001$ ****$p<0.0001$

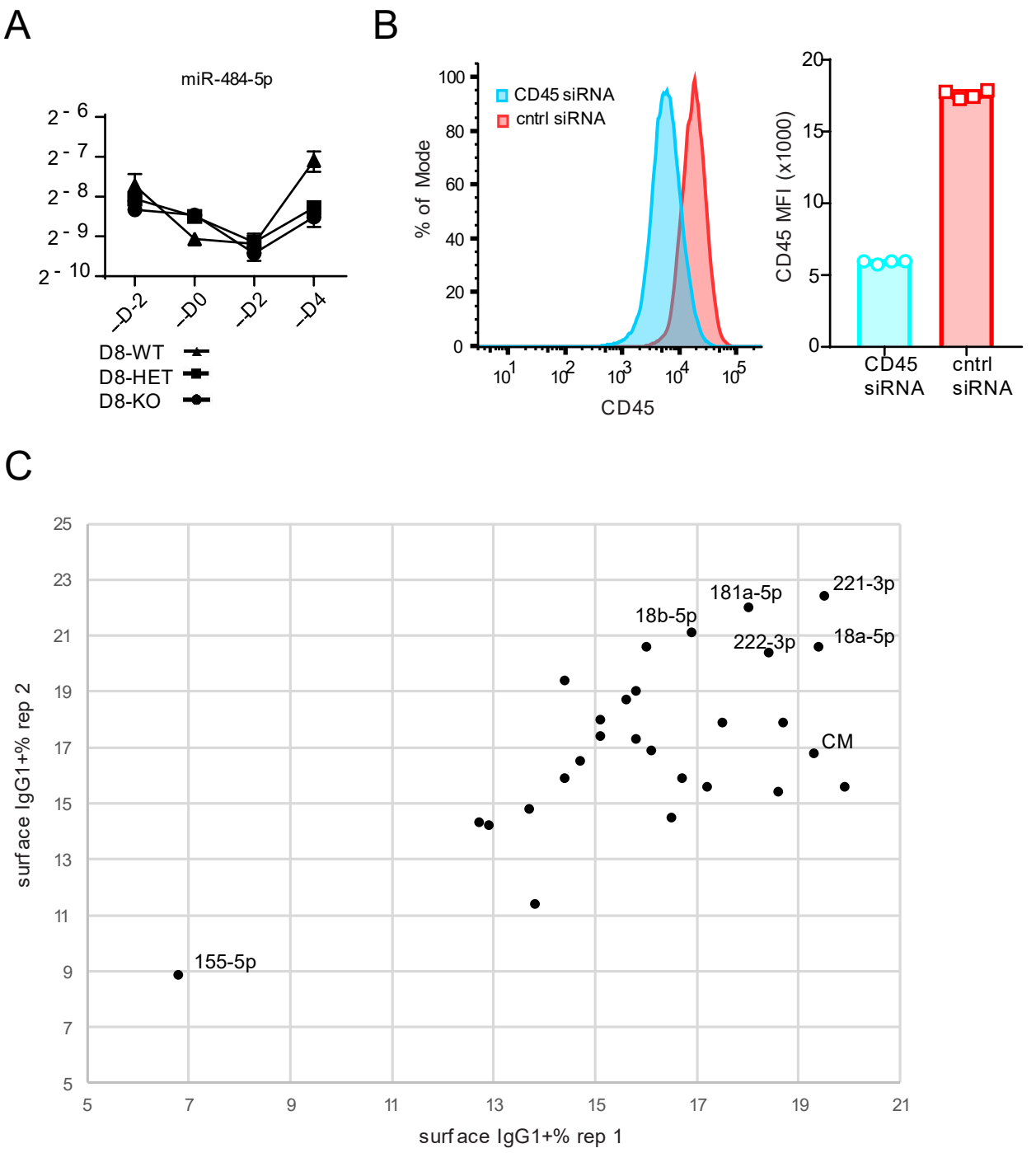

Supplemental Figure 2.1: Extended Validation of model, transfection method, and miRNA candidates

A. qPCR timecourse for miR-484-5p a DGCR8 independent miRNA. **B.** Flow cytometry histograms and quantification of CD45 expression on B cells stimulated in conditions outlined in Fig. 2.1A, and transfected with CD45 siRNA or Control siRNA **C.** Follow-up re-screen of top 10 and bottom 10 z-score miRNAs from original screen, transfected in duplicate over two replicates plotted on individual axes.

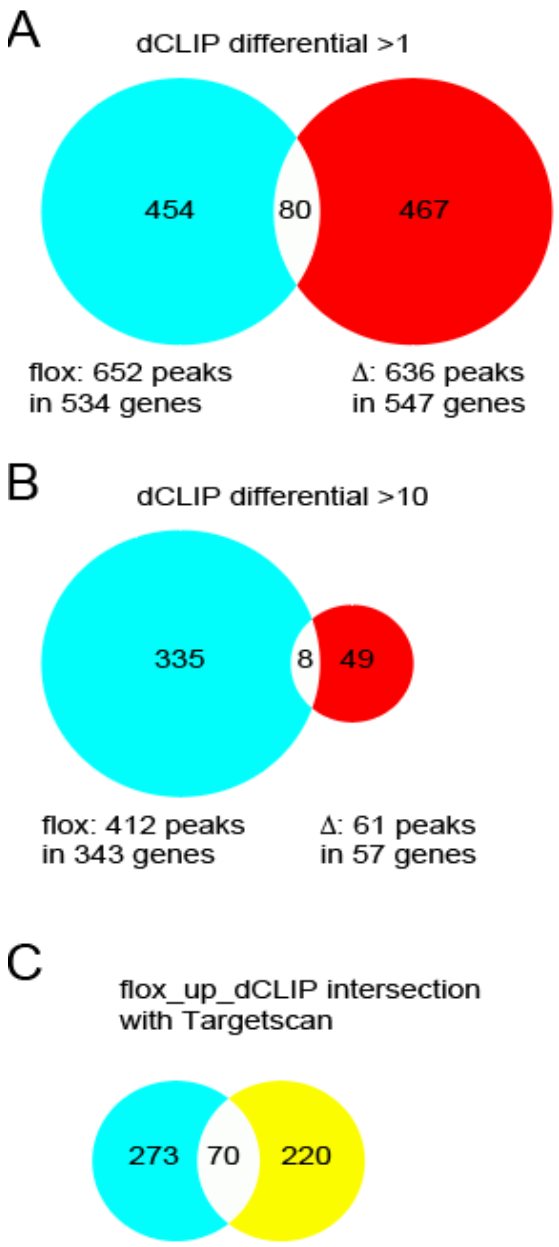

Supplemental Figure 2.2: Validation scheme for dCLIP analysis cutoff and selection of targets based on intersection of dCLIP and Targetscan.

A/B. Total number of genes containing a miR221/222 seed sequence (6-mer or better) in a region with more binding for flox library (aqua) or Δ library (red) or genes having a region for both genotypes (white) when filtering on a dCLIP internal parameter of **A.** 1. **B.** 10. **C** Of the 343 genes from B (aqua + white), those that intersect with the 290 genes predicted to be miR221/222-3p targets by Targetscan (yellow) were selected as siRNA screen candidates (white).

References

Agarwal, V., G.W. Bell, J.W. Nam, and D.P. Bartel. 2015. Predicting effective microRNA target sites in mammalian mRNAs. *Elife* 4:

Babiarz, J.E., J.G. Ruby, Y. Wang, D.P. Bartel, and R. Blelloch. 2008. Mouse ES cells express endogenous shRNAs, siRNAs, and other Microprocessor-independent, Dicer-dependent small RNAs. *Genes Dev* 22:2773-2785.

Baumjohann, D., R. Kageyama, J.M. Clingan, M.M. Morar, S. Patel, D. de Kouchkovsky, O. Bannard, J.A. Bluestone, M. Matloubian, K.M. Ansel, and L.T. Jeker. 2013. The microRNA cluster miR-17 approximately 92 promotes TFH cell differentiation and represses subset-inappropriate gene expression. *Nat Immunol* 14:840-848.

Bronevetsky, Y., A.V. Villarino, C.J. Eisley, R. Barbeau, A.J. Barczak, G.A. Heinz, E. Kremmer, V. Heissmeyer, M.T. McManus, D.J. Erle, A. Rao, and K.M. Ansel. 2013. T cell activation induces proteasomal degradation of Argonaute and rapid remodeling of the microRNA repertoire. *J Exp Med* 210:417-432.

Busse, W., J. Corren, B.Q. Lanier, M. McAlary, A. Fowler-Taylor, G.D. Cioppa, A. van As, and N. Gupta. 2001. Omalizumab, anti-IgE recombinant humanized monoclonal antibody, for the treatment of severe allergic asthma. *J Allergy Clin Immunol* 108:184-190.

Cameron, L., A.S. Gounni, S. Frenkiel, F. Lavigne, D. Vercelli, and Q. Hamid. 2003. S epsilon S mu and S epsilon S gamma switch circles in human nasal mucosa following ex vivo allergen challenge: evidence for direct as well as sequential class switch recombination. *J Immunol* 171:3816-3822.

Casola, S., G. Cattoretti, N. Uyttersprot, S.B. Koralov, J. Seagal, Z. Hao, A. Waisman, A. Egert, D. Ghitza, and K. Rajewsky. 2006. Tracking germinal center B cells expressing germ-line

immunoglobulin gamma1 transcripts by conditional gene targeting. *Proc Natl Acad Sci U S A* 103:7396-7401.

Chi, S.W., J.B. Zang, A. Mele, and R.B. Darnell. 2009. Argonaute HITS-CLIP decodes microRNA-mRNA interaction maps. *Nature* 460:479-486.

Crotty, S. 2019. T Follicular Helper Cell Biology: A Decade of Discovery and Diseases. *Immunity* 50:1132-1148.

de Yebenes, V.G., L. Belver, D.G. Pisano, S. Gonzalez, A. Villasante, C. Croce, L. He, and A.R. Ramiro. 2008. miR-181b negatively regulates activation-induced cytidine deaminase in B cells. *J Exp Med* 205:2199-2206.

Dekker, J.D., G.V. Baracho, Z. Zhu, G.C. Ippolito, R.J. Schmitz, R.C. Rickert, and H.O. Tucker. 2019. Loss of the FOXP1 Transcription Factor Leads to Deregulation of B Lymphocyte Development and Function at Multiple Stages. *Immunohorizons* 3:447-462.

Dorsett, Y., K.M. McBride, M. Jankovic, A. Gazumyan, T.H. Thai, D.F. Robbiani, M. Di Virgilio, B. Reina San-Martin, G. Heidkamp, T.A. Schwickert, T. Eisenreich, K. Rajewsky, and M.C. Nussenzweig. 2008. MicroRNA-155 suppresses activation-induced cytidine deaminase-mediated Myc-Igh translocation. *Immunity* 28:630-638.

Feng, X., G.C. Ippolito, L. Tian, K. Wiehagen, S. Oh, A. Sambandam, J. Willen, R.M. Bunte, S.D. Maika, J.V. Harriss, A.J. Caton, A. Bhandoola, P.W. Tucker, and H. Hu. 2010. Foxp1 is an essential transcriptional regulator for the generation of quiescent naive T cells during thymocyte development. *Blood* 115:510-518.

Feng, X., H. Wang, H. Takata, T.J. Day, J. Willen, and H. Hu. 2011. Transcription factor Foxp1 exerts essential cell-intrinsic regulation of the quiescence of naive T cells. *Nat Immunol* 12:544-550.

Finkelman, F.D., J. Holmes, I.M. Katona, J.F. Urban, Jr., M.P. Beckmann, L.S. Park, K.A. Schooley, R.L. Coffman, T.R. Mosmann, and W.E. Paul. 1990. Lymphokine control of in vivo immunoglobulin isotype selection. *Annu Rev Immunol* 8:303-333.

Finkelman, F.D., C.M. Snapper, J.D. Mountz, and I.M. Katona. 1987. Polyclonal activation of the murine immune system by a goat antibody to mouse IgD. IX. Induction of a polyclonal IgE response. *J Immunol* 138:2826-2830.

Fornari, F., L. Gramantieri, M. Ferracin, A. Veronese, S. Sabbioni, G.A. Calin, G.L. Grazi, C. Giovannini, C.M. Croce, L. Bolondi, and M. Negrini. 2008. MiR-221 controls CDKN1C/p57 and CDKN1B/p27 expression in human hepatocellular carcinoma. *Oncogene* 27:5651-5661.

Fowler, T., A.S. Garruss, A. Ghosh, S. De, K.G. Becker, W.H. Wood, M.T. Weirauch, S.T. Smale, B. Aronow, R. Sen, and A.L. Roy. 2015. Divergence of transcriptional landscape occurs early in B cell activation. *Epigenetics Chromatin* 8:20.

Froidure, A., J. Mouthuy, S.R. Durham, P. Chanez, Y. Sibille, and C. Pilette. 2016. Asthma phenotypes and IgE responses. *Eur Respir J* 47:304-319.

Gagnon, J.D., R. Kageyama, H.M. Shehata, M.S. Fassett, D.J. Mar, E.J. Wigton, K. Johansson, A.J. Litterman, P. Odorizzi, D. Simeonov, B.J. Laidlaw, M. Panduro, S. Patel, L.T. Jeker, M.E. Feeney, M.T. McManus, A. Marson, M. Matloubian, S. Sanjabi, and K.M. Ansel. 2019. miR-15/16 Restrain Memory T Cell Differentiation, Cell Cycle, and Survival. *Cell Rep* 28:2169-2181 e2164.

Galardi, S., N. Mercatelli, E. Giorda, S. Massalini, G.V. Frajese, S.A. Ciafre, and M.G. Farace. 2007. miR-221 and miR-222 expression affects the proliferation potential of human prostate carcinoma cell lines by targeting p27Kip1. *J Biol Chem* 282:23716-23724.

Galli, S.J., and M. Tsai. 2012. IgE and mast cells in allergic disease. *Nat Med* 18:693-704.

Gao, X., P. Tate, P. Hu, R. Tjian, W.C. Skarnes, and Z. Wang. 2008. ES cell pluripotency and germ-layer formation require the SWI/SNF chromatin remodeling component BAF250a. *Proc Natl Acad Sci U S A* 105:6656-6661.

Han, L., V. Madan, A. Mayakonda, P. Dakle, T.W. Woon, P. Shyamsunder, H.B.M. Nordin, Z. Cao, J. Sundaresan, I. Lei, Z. Wang, and H.P. Koeffler. 2019. Chromatin remodeling mediated by ARID1A is indispensable for normal hematopoiesis in mice. *Leukemia* 33:2291-2305.

Hodgkin, P.D., J.H. Lee, and A.B. Lyons. 1996. B cell differentiation and isotype switching is related to division cycle number. *J Exp Med* 184:277-281.

Hsin, J.P., Y. Lu, G.B. Loeb, C.S. Leslie, and A.Y. Rudensky. 2018. The effect of cellular context on miR-155-mediated gene regulation in four major immune cell types. *Nat Immunol* 19:1137-1145.

Hu, H., B. Wang, M. Borde, J. Nardone, S. Maika, L. Allred, P.W. Tucker, and A. Rao. 2006. Foxp1 is an essential transcriptional regulator of B cell development. *Nat Immunol* 7:819-826.

Hu, J., J. Chen, L. Ye, Z. Cai, J. Sun, and K. Ji. 2018. Anti-IgE therapy for IgE-mediated allergic diseases: from neutralizing IgE antibodies to eliminating IgE(+) B cells. *Clin Transl Allergy* 8:27.

Jin, H.Y., H. Oda, M. Lai, R.L. Skalsky, K. Bethel, J. Shepherd, S.G. Kang, W.H. Liu, M. Sabouri-Ghomi, B.R. Cullen, K. Rajewsky, and C. Xiao. 2013. MicroRNA-17~92 plays a causative role in lymphomagenesis by coordinating multiple oncogenic pathways. *EMBO J* 32:2377-2391.

Kang, S.G., W.H. Liu, P. Lu, H.Y. Jin, H.W. Lim, J. Shepherd, D. Fremgen, E. Verdin, M.B. Oldstone, H. Qi, J.R. Teijaro, and C. Xiao. 2013. MicroRNAs of the miR-17 approximately 92 family are critical regulators of T(FH) differentiation. *Nat Immunol* 14:849-857.

Knoll, M., S. Simmons, C. Bouquet, J.R. Grun, and F. Melchers. 2013. miR-221 redirects precursor B cells to the BM and regulates their residence. *Eur J Immunol* 43:2497-2506.

Kopf, M., G. Le Gros, M. Bachmann, M.C. Lamers, H. Bluethmann, and G. Kohler. 1993. Disruption of the murine IL-4 gene blocks Th2 cytokine responses. *Nature* 362:245-248.

Koralov, S.B., S.A. Muljo, G.R. Galler, A. Krek, T. Chakraborty, C. Kanellopoulou, K. Jensen, B.S. Cobb, M. Merkenschlager, N. Rajewsky, and K. Rajewsky. 2008. Dicer ablation affects antibody diversity and cell survival in the B lymphocyte lineage. *Cell* 132:860-874.

Kraus, M., M.B. Alimzhanov, N. Rajewsky, and K. Rajewsky. 2004. Survival of resting mature B lymphocytes depends on BCR signaling via the Igalpha/beta heterodimer. *Cell* 117:787-800.

Kuchen, S., W. Resch, A. Yamane, N. Kuo, Z. Li, T. Chakraborty, L. Wei, A. Laurence, T. Yasuda, S. Peng, J. Hu-Li, K. Lu, W. Dubois, Y. Kitamura, N. Charles, H.W. Sun, S. Muljo, P.L. Schwartzberg, W.E. Paul, J. O'Shea, K. Rajewsky, and R. Casellas. 2010. Regulation of microRNA expression and abundance during lymphopoiesis. *Immunity* 32:828-839.

Kuhn, R., K. Rajewsky, and W. Muller. 1991. Generation and analysis of interleukin-4 deficient mice. *Science* 254:707-710.

Loeb, G.B., A.A. Khan, D. Canner, J.B. Hiatt, J. Shendure, R.B. Darnell, C.S. Leslie, and A.Y. Rudensky. 2012. Transcriptome-wide miR-155 binding map reveals widespread noncanonical microRNA targeting. *Mol Cell* 48:760-770.

Lupini, L., C. Bassi, M. Ferracin, N. Bartonicek, L. D'Abundo, B. Zagatti, E. Callegari, G. Musa, F. Moshiri, L. Gramantieri, F.J. Corrales, A.J. Enright, S. Sabbioni, and M. Negrini. 2013. miR-221 affects multiple cancer pathways by modulating the level of hundreds messenger RNAs. *Front Genet* 4:64.

Mandler, R., F.D. Finkelman, A.D. Levine, and C.M. Snapper. 1993. IL-4 induction of IgE class switching by lipopolysaccharide-activated murine B cells occurs predominantly through sequential switching. *J Immunol* 150:407-418.

Marian, C.A., M. Stoszko, L. Wang, M.W. Leighty, E. de Crignis, C.A. Maschinot, J. Gatchalian, B.C. Carter, B. Chowdhury, D.C. Hargreaves, J.R. Duvall, G.R. Crabtree, T. Mahmoudi, and E.C. Dykhuizen. 2018. Small Molecule Targeting of Specific BAF (mSWI/SNF) Complexes for HIV Latency Reversal. *Cell Chem Biol* 25:1443-1455 e1414.

Mayeda, A., J. Badolato, R. Kobayashi, M.Q. Zhang, E.M. Gardiner, and A.R. Krainer. 1999. Purification and characterization of human RNPS1: a general activator of pre-mRNA splicing. *EMBO J* 18:4560-4570.

Mayoral, R.J., L. Deho, N. Rusca, N. Bartonicek, H.K. Saini, A.J. Enright, and S. Monticelli. 2011. MiR-221 influences effector functions and actin cytoskeleton in mast cells. *PLoS One* 6:e26133.

Mayoral, R.J., M.E. Pipkin, M. Pachkov, E. van Nimwegen, A. Rao, and S. Monticelli. 2009. MicroRNA-221-222 regulate the cell cycle in mast cells. *J Immunol* 182:433-445.

Monticelli, S., K.M. Ansel, C. Xiao, N.D. Socci, A.M. Krichevsky, T.H. Thai, N. Rajewsky, D.S. Marks, C. Sander, K. Rajewsky, A. Rao, and K.S. Kosik. 2005. MicroRNA profiling of the murine hematopoietic system. *Genome Biol* 6:R71.

Nojima, T., K. Haniuda, T. Moutai, M. Matsudaira, S. Mizokawa, I. Shiratori, T. Azuma, and D. Kitamura. 2011. In-vitro derived germinal centre B cells differentially generate memory B or plasma cells in vivo. *Nat Commun* 2:465.

Okada, T., S. Moriyama, and M. Kitano. 2012. Differentiation of germinal center B cells and follicular helper T cells as viewed by tracking Bcl6 expression dynamics. *Immunol Rev* 247:120-132.

Patzelt, T., S.J. Keppler, O. Gorka, S. Thoene, T. Wartewig, M. Reth, I. Forster, R. Lang, M. Buchner, and J. Ruland. 2018. Foxp1 controls mature B cell survival and the development of follicular and B-1 B cells. *Proc Natl Acad Sci U S A* 115:3120-3125.

Perez-Garcia, A., E. Marina-Zarate, A.F. Alvarez-Prado, J.M. Ligos, N. Galjart, and A.R. Ramiro. 2017. CTCF orchestrates the germinal centre transcriptional program and prevents premature plasma cell differentiation. *Nat Commun* 8:16067.

Petkau, G., Y. Kawano, I. Wolf, M. Knoll, and F. Melchers. 2018. MiR221 promotes precursor B-cell retention in the bone marrow by amplifying the PI3K-signaling pathway in mice. *Eur J Immunol* 48:975-989.

Pua, H.H., D.F. Steiner, S. Patel, J.R. Gonzalez, J.F. Ortiz-Carpena, R. Kageyama, N.T. Chiou, A. Gallman, D. de Kouchkovsky, L.T. Jeker, M.T. McManus, D.J. Erle, and K.M. Ansel. 2016. MicroRNAs 24 and 27 Suppress Allergic Inflammation and Target a Network of Regulators of T Helper 2 Cell-Associated Cytokine Production. *Immunity* 44:821-832.

Rao, P.K., Y. Toyama, H.R. Chiang, S. Gupta, M. Bauer, R. Medvid, F. Reinhardt, R. Liao, M. Krieger, R. Jaenisch, H.F. Lodish, and R. Blelloch. 2009. Loss of cardiac microRNA-mediated regulation leads to dilated cardiomyopathy and heart failure. *Circ Res* 105:585-594.

Rodriguez, A., E. Vigorito, S. Clare, M.V. Warren, P. Couttet, D.R. Soond, S. van Dongen, R.J. Grocock, P.P. Das, E.A. Miska, D. Vetrie, K. Okkenhaug, A.J. Enright, G. Dougan, M. Turner, and A. Bradley. 2007. Requirement of bic/microRNA-155 for normal immune function. *Science* 316:608-611.

Ruzankina, Y., C. Pinzon-Guzman, A. Asare, T. Ong, L. Pontano, G. Cotsarelis, V.P. Zediak, M. Velez, A. Bhandoola, and E.J. Brown. 2007. Deletion of the developmentally essential gene ATR in adult mice leads to age-related phenotypes and stem cell loss. *Cell Stem Cell* 1:113-126.

Sagardoy, A., J.I. Martinez-Ferrandis, S. Roa, K.L. Bunting, M.A. Aznar, O. Elemento, R. Shaknovich, L. Fontan, V. Fresquet, I. Perez-Roger, E.F. Robles, L. De Smedt, X. Sagaert, A. Melnick, and J.A. Martinez-Climent. 2013. Downregulation of FOXP1 is required during germinal center B-cell function. *Blood* 121:4311-4320.

Srinivas, S., T. Watanabe, C.S. Lin, C.M. William, Y. Tanabe, T.M. Jessell, and F. Costantini. 2001. Cre reporter strains produced by targeted insertion of EYFP and ECFP into the ROSA26 locus. *BMC Dev Biol* 1:4.

Stavnezer, J., and C.E. Schrader. 2014. IgH chain class switch recombination: mechanism and regulation. *J Immunol* 193:5370-5378.

Steiner, D.F., M.F. Thomas, J.K. Hu, Z. Yang, J.E. Babiarz, C.D. Allen, M. Matloubian, R. Blelloch, and K.M. Ansel. 2011. MicroRNA-29 regulates T-box transcription factors and interferon-gamma production in helper T cells. *Immunity* 35:169-181.

Teng, G., P. Hakimpour, P. Landgraf, A. Rice, T. Tuschl, R. Casellas, and F.N. Papavasiliou. 2008. MicroRNA-155 is a negative regulator of activation-induced cytidine deaminase. *Immunity* 28:621-629.

Thai, T.H., D.P. Calado, S. Casola, K.M. Ansel, C. Xiao, Y. Xue, A. Murphy, D. Frendewey, D. Valenzuela, J.L. Kutok, M. Schmidt-Supprian, N. Rajewsky, G. Yancopoulos, A. Rao, and K. Rajewsky. 2007. Regulation of the germinal center response by microRNA-155. *Science* 316:604-608.

Thomas-Claudepierre, A.S., E. Schiavo, V. Heyer, M. Fournier, A. Page, I. Robert, and B. Reina-San-Martin. 2013. The cohesin complex regulates immunoglobulin class switch recombination. *J Exp Med* 210:2495-2502.

van Keimpema, M., L.J. Gruneberg, M. Mokry, R. van Boxtel, M.C. van Zelm, P. Coffer, S.T. Pals, and M. Spaargaren. 2015. The forkhead transcription factor FOXP1 represses human plasma cell differentiation. *Blood* 126:2098-2109.

Vigorito, E., K.L. Perks, C. Abreu-Goodger, S. Bunting, Z. Xiang, S. Kohlhaas, P.P. Das, E.A. Miska, A. Rodriguez, A. Bradley, K.G. Smith, C. Rada, A.J. Enright, K.M. Toellner, I.C. Maclennan, and M. Turner. 2007. microRNA-155 regulates the generation of immunoglobulin class-switched plasma cells. *Immunity* 27:847-859.

Wang, T., Y. Xie, and G. Xiao. 2014. dCLIP: a computational approach for comparative CLIP-seq analyses. *Genome Biol* 15:R11.

Wang, Y., S. Baskerville, A. Shenoy, J.E. Babiarz, L. Baehner, and R. Blelloch. 2008. Embryonic stem cell-specific microRNAs regulate the G1-S transition and promote rapid proliferation. *Nat Genet* 40:1478-1483.

Xu, S., X. Ou, J. Huo, K. Lim, Y. Huang, S. Chee, and K.P. Lam. 2015. Mir-17-92 regulates bone marrow homing of plasma cells and production of immunoglobulin G2c. *Nat Commun* 6:6764.

Yang, Z., J.B. Jung, and C.D.C. Allen. 2018. Study of IgE-Producing B Cells Using the Verigem Fluorescent Reporter Mouse. *Methods Mol Biol* 1799:247-264.

Yang, Z., B.M. Sullivan, and C.D. Allen. 2012. Fluorescent in vivo detection reveals that IgE(+) B cells are restrained by an intrinsic cell fate predisposition. *Immunity* 36:857-872.

Yewdell, W.T., and J. Chaudhuri. 2017. A transcriptional serenAID: the role of noncoding RNAs in class switch recombination. *Int Immunol* 29:183-196.

Yoshida, K., M. Matsuoka, S. Usuda, A. Mori, K. Ishizaka, and H. Sakano. 1990. Immunoglobulin switch circular DNA in the mouse infected with Nippostrongylus brasiliensis: evidence for successive class switching from mu to epsilon via gamma 1. *Proc Natl Acad Sci U S A* 87:7829-7833.

Yu, K., and M.R. Lieber. 2019. Current insights into the mechanism of mammalian immunoglobulin class switch recombination. *Crit Rev Biochem Mol Biol* 54:333-351.

Zhang, J., D.D. Jima, C. Jacobs, R. Fischer, E. Gottwein, G. Huang, P.L. Lugar, A.S. Lagoo, D.A. Rizzieri, D.R. Friedman, J.B. Weinberg, P.E. Lipsky, and S.S. Dave. 2009. Patterns of microRNA expression characterize stages of human B-cell differentiation. *Blood* 113:4586-4594.

Zhang, X., Y. Zhang, Z. Ba, N. Kyritsis, R. Casellas, and F.W. Alt. 2019. Fundamental roles of chromatin loop extrusion in antibody class switching. *Nature* 575:385-389.

Zhou, Y., B. Zhou, L. Pache, M. Chang, A.H. Khodabakhshi, O. Tanaseichuk, C. Benner, and S.K. Chanda. 2019. Metascape provides a biologist-oriented resource for the analysis of systems-level datasets. *Nat Commun* 10:1523.

Chapter 3: Antigen Complexed with a TLR9 Agonist Bolsters c-Myc and mTORC1 Activity in Germinal Center B Lymphocytes

This chapter is adapted from the published work (Wigton et al., 2019):

Wigton, E. J., et al. (2019). "Antigen Complexed with a TLR9 Agonist Bolsters c-Myc and mTORC1 Activity in Germinal Center B Lymphocytes." Immunohorizons **3**(8): 389-401.

Abstract

The Germinal Center (GC) is the anatomical site where humoral immunity evolves. B cells undergo cycles of proliferation and selection to produce high affinity antibodies against antigen. Direct linkage of a TLR9 agonist (CpG) to a T-dependent antigen increases the number of GC B cells. We used a T-dependent antigen complexed with CpG and a genetic model for ablating the TLR9 signaling adaptor molecule MyD88 specifically in B cells (B-MyD88$^-$ mice) together with transcriptomics to determine how this innate pathway positively regulates the GC. GC B cells from complex antigen immunized B-MyD88$^-$ mice were defective in inducing gene expression signatures downstream of c-Myc and mTORC1. In agreement with the latter gene signature, ribosomal protein S6 phosphorylation was increased in GC B cells from wild type mice compared to B-MyD88$^-$ mice. However, GC B cell expression of a c-Myc protein reporter was enhanced by CpG attached to antigen in both WT and B-MyD88$^-$ mice, indicating a B cell-extrinsic effect on c-Myc protein expression combined with a B cell-intrinsic enhancement of gene expression downstream of c-Myc. Both mTORC1 activity and c-Myc are directly induced by T cell help, indicating that TLR9 signaling in GC B cells either enhances their access to T cell help or directly influences these pathways to further enhance the effect of T cell help. Taken together, these findings indicate that TLR9 signaling in the GC could provide a surrogate pro-survival stimulus, "TLR help", thus lowering the threshold for selection and increasing the magnitude of the GC response.

Introduction

Toll like receptors (TLRs) recognize pathogen associated molecular patterns (PAMPs) and serve as key mediators of the innate immune response against pathogens. However, TLRs are expressed on both adaptive and innate immune cells. Deficiency in these receptors or their key signaling molecules, such as MyD88, impair both innate and adaptive responses to pathogens (Akira and Takeda, 2004; Blasius and Beutler, 2010; Iwasaki and Medzhitov, 2004). The dual function of TLRs in initiating the early inflammatory response while at the same time directly shaping the slower antigen-specific adaptive response shows that these receptors act through multiple elements within the immune system. It has been appreciated for a number of years that several TLRs are expressed by B cells and these receptors regulate B cell activation and fate decisions (Gavin et al., 2006; Pasare and Medzhitov, 2005). Studies using mice in which the critical TLR-signaling component MyD88 is selectively ablated in B cells or mixed bone marrow chimeras in which B cells were selectively deficient in a particular TLR revealed that such mice also have substantial defects in germinal center (GC) and plasma cell (PC) generation, and in isotype switched antibody titers in response to multiple TLR agonists mixed with T-dependent and T-independent antigens (Eckl-Dorna and Batista, 2009; Hou et al., 2011; Jegerlehner et al., 2007).

This biological role for TLR signaling in B cells is important for making high quality antibodies to a number of viral infections of mice, in which case endosomal TLR7 and TLR9, which recognize nucleic acids, are critical. (Clingan and Matloubian, 2013; Eckl-Dorna and Batista, 2009). BCR-mediated endocytosis of the antigen and associated BCR signaling delivers TLR ligands to the endosomal location of these receptors (Chaturvedi et al., 2008; O'Neill et al., 2009). In addition, TLR7 and TLR9 function in B cells is required for production of anti-DNA and anti-ribonucleoprotein autoantibodies in several mouse models of systemic lupus erythematosus (Rawlings et al., 2017).

One experimental strategy for studying how BCR signaling and TLR9 signaling enhance the germinal center response is to immunize with a T-dependent antigen physically coupled to a synthetic TLR9 agonist - CpG deoxyoligonucleotides (CpG) (Rookhuizen and DeFranco, 2014). In order to activate the potential of TLR9 to enhance a GC response, the antigen must be oligovalent (as is the case for a haptenated protein) (Rookhuizen and DeFranco, 2014). The TLR9 ligand can be present in virus-like particles (VLPs) (Hou et al., 2011; Tian et al., 2018), or combined with DOTAP adjuvants (Akkaya et al., 2017) to form liposome-like oligovalent antigens. MyD88-deficiency in B cells compromises GC B cell number and antibody titers to such antigens (Hou et al., 2011; Rookhuizen and DeFranco, 2014), but how TLR signaling enhances the response that remains dependent upon T follicular helper (Tfh) cells is unclear. In a murine model of autoimmune lupus in which TLR7 and TLR9 are necessary for sustained autoreactive B cell responses, cognate autoreactive T-cells could partially rescue GC B cell activation defects in the absence of TLR7/9 (Giles et al., 2017). This suggests the overlap of pro-survival signals derived from T cell help and TLR7/9 signaling in supporting GC B cell survival and humoral immunity, but the molecular nature of the signals provided by TLRs were not defined.

Here, we explored the mechanistic basis by which a TLR9 ligand attached to an antigen signals within the antigen-specific B cell to promote the GC response. The wildtype GC B cells immunized with NP-haptenated T-dependent antigen complexed with a CpG oligonucleotide had increased oxidative phosphorylation, mTORC1, and c-Myc gene expression signatures compared to MyD88-deficient GC B cells. Remarkably, both c-Myc and mTORC1 are induced by Tfh cell mediated interactions with GC B cells through CD40L:CD40 signaling (Calado et al., 2012; Dominguez-Sola et al., 2012; Ersching et al., 2017). As such, MyD88-dependent TLR9 signaling induced gene expression signatures that were previously associated with Tfh cell help, suggesting

that TLR signaling in GC B cells enhanced the GC response by mimicking the effects of Tfh on the B cells, without replacing the requirement for Tfh. Together, these findings indicate that TLR9 signaling in GC B cells can provide a supplemental stimulus that allows more B cells to occupy the GC in an environment where Tfh cell help is limiting for survival.

Materials and Methods

Generation of Complex antigens and BCR stimulants

NP-CGG Complex antigen was generated similarly to as previously published with the following modifications: NP(14-30)CGG (Biosearch) was biotinylated using biotin(xx)-NHSS in DMF, as previously reported (Rookhuizen and DeFranco, 2014). The biotinylated NP(14-30)CGG was mixed (5mg/ml) with streptavidin (Thermofisher) (10mg/ml), and 5'biotinylated CpG oligo 1826 (CCATGACGTTCCTGACGTT) (IDT) or a 5'biotinylated Non-CpG oligo (TCCAGGACTTCTCTCAGGTT) (IDT) (5mg/ml), at a molar ratio of 1:4:48 in PBS, respectively for 24 hrs before being washed in 5mls PBS in an Amicon Ultra-15 Centrifugal Filter Unit 10kD (Millipore) 3 times, and resuspended at 100µgtotal mass per 50 µl. Similarly biotinylated αIgM (goat polyclonal, Jackson Immunoresearch) was mixed with Streptavidin and 5'biotinylated CpG oligo 1826 (IDT) or a 5'biotinylated Non-CpG oligo (5mg/ml), at a molar ratio of 2:1:2 in PBS for 24hours before being transferred to an Amicon Ultra-15 Centrifugal Filter Unit 10kD filter (Millipore) and washed 3 times with PBS and re-suspended at 1.5µg αIgM per µl.

Mice and Immunizations

Mice used in these experiments consisted of Mb1-cre (C(Cg)- Cd79a$^{tm1(cre)Reth}$/EhobJ), MyD88 flox (B6.129P2(SJL)-MyD88^{tm1Defr}/J), c-Myc-GFP reporter (B6;129-Myc^{tm1Slek}/J) (backcrossed 10 times to B6/J) and Eµ-Bcl2 transgenic (C.Cg-Tg(BCL2)22Wehi/J) (a gift from the Cyster laboratory) all of which were maintained in house according to all IACUC guidelines.

Mice were immunized subcutaneously in the scruff and flanks with a total of 100µg NP-CGG in complex antigen for cell sorting and in vivo phosphor-flow experiments, and with 25µg NP-CGG complex antigen in the footpad for c-Myc-GFP and general flow cytometry experiments. Draining

lymph nodes were analyzed. Eμ-BCL2 transgenic c-Myc-GFP mice were immunized with 100μg NP(14-30)-CGG (Biosearch) in alum Imject (ThermoFisher) intraperitoneally, and GC B cells were isolated from spleen 12-14 days later.

RNA isolation and mRNA-sequencing

10,000 NP+ GC B cells were collected by FACS sorting directly into the lysis buffer of the Dynabead direct mRNA extraction kit (Thermo Fisher). mRNA was isolated by use of poly-dT beads according to the manufacturer's instructions (Thermo Fisher). Library preparation and RNA sequencing was performed through the UCSF Functional Genomics Core and aligned to Ensembl Mouse GRCh38.78 (mm10) genome using STAR software and analyzed using DESeq2 as previously reported(Pua et al., 2016).

Flow cytometry,

Single cell suspensions were prepared from either popliteal or inguinal, axillary, and brachial LNs by gently passing them through 70μm nylon mesh filters. Cells were collected by centrifugation and incubated with anit-CD16/CD32 (2.4G2) in FACS buffer (PBS + 2% Fetal Bovine Serum + 2 μm EDTA + .01% NaN_3) to block antibody binding to Fc receptors before staining with antibodies for surface markers. For phospho-flow analysis of in vivo cells, mice were perfused with 10% Paraformaldehyde (PFA) directly after sacrifice (Sigma), and single cell suspensions from Lymph nodes were prepared directly in 2% PFA and incubated for 15 minutes on ice before permeabilizing the cell plasma membranes with ice cold methanol. Fixed cells were rehydrated with PBS, washed by centrifugation in FACS buffer and blocked and stained with antibodies as described above. Conjugated antibodies used included PE-Cy7 anti-CD95 (Jo2); FITC and PerCP-Cy5.5 anti-GL7, BV605 anti-CD19 (6D5), FITC anti-B220 (RA3-6B2), biotin

anti-CD11c, biotin anti-CD3ε (145-2C11), biotin anti-Ter119, biotin anti-Gr1, ef450 anti-IgD (11-26c), biotin anti-CXCR4 (2B11), APC anti-CD86 (GL-1), APC anti-CD83 (Michel-19), AF647 anti-pS6 ser240/244 (D68F8), AF647 anti-pS6-ser235/236 (D57.2.2E), AF647 anti-pAkt ser473 (D9E). Biotin conjugates were detected using BV711 or BV786 Streptavidin (BioLegend). NP(8-30)-PE (Biosearch) was used to detect NP-binding B cells. Dead cells were detected using efluor780 or UV Blue fixable viability dyes (Thermofisher). Flow cytometry analysis and sorting was performed on an LSR II and a FACS Aria II cytometers (BD), respectively.

In-vitro and Ex vivo naïve and GC B cell isolation and stimulation

WT, B-MyD88^{-}, WT-c-Myc-GFP and B-MYD88-c-Myc-GFP naive B cells were isolated using Dynabead negative CD43 selection kit (ThermoFisher) and stimulated in RPMI 1640 supplemented with 10% FCS, HEPES, 2-mercaptoethanol, and L-glutamine with αIgM-CpG and αIgM-Non for 24 hours then stained for viability before being analyzed by flow cytometry or fixed before staining for phospho-flow. Eμ-BCL2 MycGFP B cells were isolated by anti-CD11c, anti-CD43 and anti-IgD (GC) or anti-GL7 (naïve) biotin antibodies followed by an anti-biotin magnetic bead isolation (Miltenyi) according to a previously published protocol (Cato et al., 2011). Purity was confirmed at least 95% B220+ for naïve B cells and 90% Fas+, CD38- for GC B cells. Cells were stimulated with 10-20 μg αCD40 (FGK4.51, Miltenyi), 10-20 μg αIgM (Goat polyclonal μ chain, Jackson immunoresearch), 75 nM CpG 1826 oligo (IDT), or combinations of these reagents for 4 hours in complete RPMI1640 medium and processed for flow cytometry.

Software and Statistics

Data visualization and statistical calculations were performed using Prism GraphPad. Statistical tests and p values for each experiment are specified in figure legends for a single

comparison between two groups, a student's t-test was used; for multiple comparisons between preselected groups, a one way anova test with Holm-Sidek correction for multiple comparisons was used; and for multiple comparisons where all groups were compared, a one way anova test with a Tukey correction for multiple comparisons was used. Flow cytometry data were analyzed with Flowjo.

GSEA was run on the graphical user interface according to the manufacturers recommendations (https://software.broadinstitute.org/gsea/doc/GSEAUserGuideFrame.html) to compare the WT and MyD88^{-} RNA-seq data sets using all genes (Subramanian et al., 2005).

RNA-seq data are publicly available on Gene Expression Omnibus at GSE126849 https://www.ncbi.nlm.nih.gov/geo/query/acc.cgi?acc=GSE126849.

Results

TLR9 agonist complexed to T-dependent antigen increases the frequency and number of germinal center B cells in response to immunization.

Previous studies have demonstrated that attachment of a TLR7 or TLR9 ligand to an antigen can boost the germinal center antibody response (Hou et al., 2011; Rookhuizen and DeFranco, 2014). We created two complex antigens composed of biotinylated 4-nitro-3-phenylacetyl (NP) chicken gamma globulin (CGG) complexed with streptavidin and either biotinylated CpG deoxyoligonucleotide (CpG) or biotinylated control deoxyoligonucleotide (Non) yielding NP-CGG-CpG or NP-CGG-Non respectively (Rookhuizen and DeFranco, 2014). C57BL/6 mice were immunized subcutaneously with either NP-CGG-CpG or NP-CGG-Non and the GC response was analyzed at day 14 (D14) (Fig. S3.3.1A). As the high affinity anti-NP antibody response to NP-CGG is known to have a substantial contribution of λ light chain-containing antibodies, we also analyzed the frequency of NP-binding, λ^+ GC B cells. Mice immunized with the NP-CGG-CpG showed a 3.5 -fold increase in the number of total GC B cells ($CD19^+$, IgD^{lo}, Fas^+) as well as a 4-fold increase in the number of NP-binding λ^+ GC B cells (Fig. S3.3.1B/1C). These results agree with a previous study using a similar complex antigen (Rookhuizen and DeFranco, 2014).

To specifically test the role of TLR9 agonism in the B cell compartment, we immunized B cell lineage-specific MyD88-deficient *Mb1-cre$^+$MyD88$^{fl/fl}$* (B-MyD88$^-$) and control Mb1-cre$^+$ MyD88$^{fl/+}$ or Mb1-cre$^+$ MyD88$^{+/+}$ (WT) mice with NP-CGG-CpG antigen and analyzed the GC response at D14 (Fig. S3.3.1D/E). WT mice exhibited a 2.4-fold higher frequency and number of $GL7^{hi}$ GC B cells as compared to the B-MYD88$^-$ mice (Fig. 3.1A). Thus in agreement with

previous work, these results show that B cell TLR9 signaling enhances the GC response to a haptenated antigen attached to a TLR9 ligand. There was also likely to be some contribution of TLR signaling in another cell type, such as classical dendritic cells.

NP-CGG-CpG antigen induces MyD88-dependent c-Myc and mTORC1 signature gene expression

To determine the effect of TLR9 signaling on the GC response at a transcriptional level, we performed mRNA-sequencing on NP-binding WT and B-MYD88$^-$ GC B cells at D14 post immunization with NP-CGG-CpG using the gating strategy illustrated in Fig. S3.1E. This analysis uncovered 479 differentially expressed genes (FDR<0.05 by Fisher exact test, Table S3.1), of which 260 were increased in WT and 219 were increased in B-MYD88$^-$ cells. Among the genes with higher expression in WT GC B cells many corresponded to ribosomal proteins, NADH dehydrogenase, ATP synthase, and cytochrome oxidase machinery pointing towards increased oxidative phosphorylation activity (Fig. 3.3A). This metabolic phenotype is consistent with the recent finding that TLR9 signaling can rescue naïve B cells from apoptosis resulting from mitochondrial dysfunction elicited by BCR engagement in the absence of CD40 or TLR signals (Akkaya et al., 2018b). There was also increased *Ighg2c* gene expression in WT samples compared to B-MYD88$^-$ samples, as well as increased expression of *Aicda*, the gene encoding the activation-induced cytidine deaminase that is directly involved in somatic hypermutation and in class switch recombination (Table 3.1). These results are consistent with the strong effect of the TLR9 ligand in promoting class switch to IgG2a/IgG2c (Jegerlehner et al., 2007; Rookhuizen and DeFranco, 2014). Surprisingly, expression of the transcriptional regulator Bcl6, which directs the germinal center fate in B cells, was increased in B-MYD88$^-$ GC B cells (Table 3.1). Conversely, mRNA encoding the survival factor Bcl2 was higher in WT cells (Table 3.1) suggesting that increased

survival may contribute to the increased GC B cell frequency and number in the context of intact TLR9/MyD88 signaling.

To gain greater insight from the mRNA expression data sets, we applied Gene Set Enrichment Analysis (GSEA) to the Hallmark gene sets (Subramanian et al., 2005). Gene sets enriched in WT compared to B-MYD88$^-$ GC B cells included the Myc signature with a normalized enrichment score (NES)=2.38 FDR<10^{-5}; the E2F signature with a NES=1.60, FDR= 0.02; and the mTORC1 signature with a NES= 1.46, FDR= 0.057 (Table 3.2, Fig. 3.3B). We performed a leading-edge analysis on the Hallmark subsets from Table 3.2 and found that the genes driving the difference in the context of mTORC1 and c-Myc had very little overlap and thus these two gene signatures represented independent enrichments (Fig. S3.3.2). Similarly, independently curated mTORC1 (Bilanges et al., 2007) and c-Myc (Zeller et al., 2003) gene sets were also enriched in WT compared to B-MYD88$^-$ GC B cells (Fig. 3.1D, 1F, Table 3.2). Furthermore, the KEGG ribosomal pathway showed a large enrichment in WT GC B cells (Table 3.2). From our RNA-seq, *Aicda* was 2 fold increased in WT compared to B-MYD88$^-$ (FDR=0.088) concordant with this being positively regulated by mTORC1 signaling (Chiu et al., 2019; Raybuck et al., 2018). In contrast, no Hallmark gene sets were enriched in the antigen-specific B-MYD88$^-$ GC B cells compared to the antigen-specific WT GC B cells (FDR q values greater than 0.25 - data not shown). Interestingly both c-Myc and mTORC1 have been implicated as downstream effectors of Tfh cell help and their dysregulation negatively impacts the GC response(Calado et al., 2012; Dominguez-Sola et al., 2012; Ersching et al., 2017). These results suggest that TLR9-MyD88 signaling in the antigen-specific GC B cell increases the transcriptional outputs of the MYC and mTORC1 pathways, either via direct transcriptional effects or indirectly by enhancing the ability

of the GC B cells to interact with Tfh and receive CD40L and cytokine signals, which are known to promote these two programs

TLR9 signaling in naïve B cells increases c-Myc expression

To better understand how TLR9 signaling enhances the c-Myc pathway transcriptional response, we examined the effect of BCR signaling and TLR9 signaling on c-Myc protein expression. First naïve polyclonal B cells were stimulated through the BCR and TLR9 in a linked fashion by addition of αIgM bound to streptavidin and biotin-conjugated CpG or Non oligos to make the complex artificial antigens αIgM-CpG and αIgM-Non, respectively (Sindhava et al., 2017). To measure the c-Myc protein expression on a single cell level we crossed a knock-in c-Myc-GFP protein fusion reporter (Huang et al., 2008) to WT and B-MYD88^{-} mouse strains. We stimulated purified naïve Mb1-cre^{+} MyD88$^{fl/fl}$Myc-GFP$^{+/+}$ (B-MYD88^{-} Myc-GFP) or WT Mb1-cre^{+}, MyD88$^{+/+}$ c-Myc-GFP$^{+/+}$ (WT -Myc-GFP) splenic B cells with either αIgM-CpG or αIgM-Non for 24 hours and then analyzed the cells for c-Myc-GFP expression by flow cytometry (Fig. 3.2A). The presence of a TLR9 ligand attached to the αIgM antibodies greatly enhanced c-Myc expression in naïve B cells after 24 hours at which time 90% of WT-Myc-GFP cells stimulated with αIgM-CpG were c-Myc-GFP+ (Fig. 3.2B). In contrast, WT-Myc-GFP cells stimulated with αIgM-Non, and B-MyD88^{-}Myc-GFP cells stimulated with either αIgM-CpG or αIgM-Non exhibited much lower c-Myc induction at this time, with 5-10% c-Myc-GFP+ cells (Fig. 3.2B). Less than 2% of unstimulated naïve B cells of either genotype were c-Myc-GFP+. Per cell c-Myc-GFP abundance was also increased by TLR9/MyD88 signaling, with αIgM-CpG stimulated WT-Myc-GFP B cells displaying a 4-fold increase in GFP mean fluorescence intensity (MFI) compared to αIgM-Non stimulated WT-Myc-GFP and B-MyD88^{-}Myc-GFP cells under either stimulation

conditions (Fig. 3.2B). Thus, in naïve B cells, combined antigen receptor and TLR9 signals induced c-Myc levels much more strongly than antigen receptor signals alone.

Attachment of a TLR9 ligand to the antigen increased the frequency of GC B cells expressing c-Myc protein in a non-cell-intrinsic manner

We next used the c-Myc-GFP reporter to address the mechanism by which attachment of a TLR ligand to CGG increased the c-Myc transcriptional signature in GC B cells. Previous work established that CD40L delivered by Tfh cells strongly induces c-Myc expression in Light Zone (LZ) GC B cells, which consequently return to the Dark Zone (DZ) and undergo further clonal expansion (Calado et al., 2012; Dominguez-Sola et al., 2012). Therefore, we examined c-Myc-GFP expression in day 14 LZ and DZ phenotype GC B cells, identified by elevated CD86/CD83 or CXCR4 expression, respectively, from c-Myc-GFP$^{+/+}$ mice immunized with NP-CGG-CpG or NP-CGG-Non antigen (Fig. 3.2C, S3A) (Victora et al., 2012; Victora et al., 2010). Both immunization groups had similar distributions of DZ and LZ phenotype cells among GC B cells (NP-CGG-CpG: DZ= 51% ± 6% LZ = 41% ± 5%; NP-CGG-Non: DZ 52% ± 10%; = LZ= 44% ± 9%;) (Fig. S3.3A). In agreement with our sequencing data, the NP-CGG-CpG antigen group had a higher percentage (2.7% vs. 1.1%), and a greater mean number (3,000 vs. 1,700) of c-Myc-GFP^{+} GC B cells than did NP-CGG-Non immunized animals (Fig. 3.2D). A majority of c-Myc-GFP+ cells exhibited a LZ phenotype for both immunization conditions (NP-CGG-CpG: 66% ± 9%; NP-CGG-Non: 69.8% ± 13%)(Fig. S3.3B), consistent with previous studies showing enrichment of the LZ phenotype (Victora et al., 2010) and localization of c-Myc^{+} GC B cells to the LZ (Calado et al., 2012; Dominguez-Sola et al., 2012).

To test whether TLR9/MyD88 signaling in the GC B cells contributed to the increased frequency of c-Myc-expressing GC B cells seen upon immunization with NP-CGG-CpG we

immunized WT-Myc-GFP and B-MyD88^{-}Myc-GFP mice with either one allele or two alleles of the c-Myc-GFP fusion reporter and analyzed c-Myc-GFP expression at D14. Interestingly, neither the number nor percentage of c-Myc-GFP^{+} GC B cells were increased in the GC B cells from WT-Myc-GFP mice compared to the GC B cells from the B-MyD88^{-}Myc-GFP mice (Fig. 3.2E). The distribution of LZ and DZ phenotypes of bulk and c-Myc-GFP^{+} GC B cells were also unaltered by the inability of the B cells to signal via MyD88 (Fig. S3.3C). The per-cell c-Myc-GFP MFI was also similar in WT-Myc-GFP and B-MyD88^{-}Myc-GFP groups (Fig. S3.3D). Thus, there was a non-B cell-intrinsic effect of attaching a TLR9 ligand to NP-CGG on expression of c-Myc-GFP. Moreover, these results suggest that the increased c-Myc transcription signature resulting from TLR9/MyD88 signaling in GC B cells (Fig. 3.1) may have resulted from a regulatory change in c-Myc transcriptional activity, rather than an increase in c-Myc protein expression

Dual TLR9 and BCR signaling increases phosphorylation of ribosomal protein S6 in naïve B cells and in GC B cells.

Next, we examined whether TLR9/MyD88 signaling in purified naïve splenic B cells leads to enhanced Akt/mTOR signaling. Initially, purified naïve splenic B cells were stimulated *in vitro* with αIgM complex antigens as before, and phosphorylation of mTORC1 targets was assessed by intracellular staining of permeabilized cells with phospho-specific antibodies and flow cytometry. Remarkably, phosphorylation of ribosomal protein S6, at ser240/244 (pS6(ser240/244)) and at ser235/236 (pS6(ser235/236), known mTORC1 pathway targets, were almost entirely dependent on CpG stimulation in naïve B cells (Fig. 3.3A and S4A). αIgM-CpG stimulated WT cells were 90% positive for pS6(ser240/244) at 24 hours compared to the 5-15% range seen for WT B cells stimulated with αIgM-Non or for B-MyD88^{-} B cells treated with either stimulus (Fig. 3.3B). The αIgM-CpG stimulated WT B cells showed the highest pS6(ser240/44) MFI, which was 14 times

greater than any other group (Fig. 3.3B). Cell size is in part dependent upon protein content of the cell and WT B cells stimulated with αIgM-CpG also showed the largest increase in cell size (FSC-A) compared to the three other groups (Fig. 3.3B), which is consistent with a role of mTORC1 in enhancing global protein synthesis.

Next, we examined the effect of including a TLR9 ligand attached to NP-CGG on the size of GC B cells and on their pS6 phosphorylation status. GC B cells were substantially larger than naïve B cells as would be expected, but no differences in cell size were evident when comparing B-MyD88^{-} and WT GC at D14 post immunization with NP-CGG-CpG antigen (Fig. 3.3C). Additionally, no difference in cell size was evident when only NP-binding GC B cells of these two genotypes were compared (Fig. 3.3C). Utilizing phospho-flow cytometry we analyzed pS6(ser240/244) and pS6(ser235/236) in GC B cells. There was an increase in pS6(ser240/244) MFI of WT compared to B-MyD88^{-} GC B cells that was significant ($p=0.021$) (Fig. 3.3D). However, we found that WT and B-MyD88^{-} GC B cells exhibited similar MFI staining for pS6(ser235/236) (Fig. S3.4B). When mice were immunized with NP-CGG-CpG vs NP-CGG-Non, we found a 2 fold increase in both pS6(ser240/244) (Fig.3E) and pS6(ser235/236) in GC B cells (Fig. S3.4C). Interestingly we saw an increase in the pS6 level of non-GC B cells in the NP-CGG-CpG immunized mice compared to NP-CGG-Non, indicating that another CpG responsive cell type alters the metabolic and inflammatory environment of the lymph node increasing mTORC1 activity in non-GC B cells in a non-cell intrinsic manner. Thus, combined CpG-induced TLR signaling and BCR signaling positively regulated mTORC1 signaling robustly in naïve B cells, and while all GC B cells had evidence of active mTORC1 signaling, consistent with previous studies (Ersching et al., 2017; Jones et al., 2016; Zhang et al., 2013) TLR9/MyD88 signaling

appeared to further increase phosphorylation of the mTORC1 target pS6 by both B cell intrinsic and extrinsic mechanisms.

Ex vivo stimulation of GC B cells with CpG oligonucleotide increases mTORC1 phosphorylation targets and c-Myc induction similarly to CD40 stimulation

To test whether TLR signaling ex vivo in GC B cells would enhance mTORC1 signaling and c-Myc expression in the absence of continued Tfh cell interaction, GC B cells were isolated from immunized Eμ-BCL2 transgenic mice (to promote their survival during *in vitro* culture) and stimulated with αCD40, αIgM, αIgM + CpG oligo, or αCD40 + αIgM for 4 hours, and fixed before staining for pS6(ser240/244). It was previously reported that both αIgM and αCD40 signaling are necessary to increase mTORC1 activity and induce c-Myc expression in GC B cells, whereas naïve B cells respond to either stimulus individually (Luo et al., 2018). Similarly, we found that stimulation of naïve B cells with αIgM and/or αCD40 for 4 hours led to at least 90% of cells being pS6(ser240/244) positive (Fig. 3.4A-4B). Furthermore, CpG stimulation led to 75% of naïve cells being pS6(ser240/244) positive, and the addition of αIgM increased the response to >95% pS6(ser240/244) positive (Fig. 3.4A-4B). In contrast, ex-vivo stimulation of Eμ-BCL2 transgenic GC B cells with αIgM alone failed to induce increased phosphorylation of this residue compared to unstimulated GC B cells (Fig. 3.4A-B). Either αCD40 or CpG oligo stimulation conditions increased the percentage of pS6(ser240/244) positive Eμ-BCL2 GC B cells to comparable levels (50-60%) (Fig. 3.4A-4B). These results demonstrate that TLR9 stimulation and CD40 engagement can have similar effects on mTORC1 signaling in GC B cells. Furthermore, stimulation of the BCR via αIgM did not increase the response to αCD40 or CpG oligonucleotide in the Eμ-BCL2 GC B cells.

Next, we crossed the c-Myc-GFP$^{+/+}$ mice to the Eμ-BCL2 transgenic mice to facilitate examination of c-Myc expression in naïve and GC B cell stimulated ex vivo. Naïve c-Myc-GFP$^{+/WT}$ B cells and c-Myc-GFP$^{+/WT}$ Eμ-BCL2 GC B cells were stimulated with αIgM, αCD40 or CpG oligonucleotides or combinations thereof. All stimulation conditions increased the expression of c-Myc-GFP substantially in the naïve B cells (MFI increased by αIgM 2.4-fold, αCD40 2.0-fold, CpG 1.7-fold, αIgM + αCD40 3.7-fold, αIgM + CpG 3.8-fold, compared to no stimulation), which is congruent with previous studies demonstrating that CpG induces c-Myc expression in immature and naïve B cells (Arunkumar et al., 2013; Azulay-Debby et al., 2007). Thus, c-Myc induction in naïve cells was responsive to each stimulus individually and exhibited an additive response to multiple stimuli. For the Eμ-BCL2 GC B cells, ex vivo αIgM stimulation did not induce c-Myc expression above the unstimulated control (1.1 fold increase in MFI) (Fig. 3.4C, 4D), similarly to what was seen with phosphorylation sites on ribosomal protein S6. In contrast, stimulation with CpG oligonucleotide or αCD40 induced small but significant increases in c-Myc-GFP expression (MFI increased by 1.3-fold, p=.0007; and 1.2-fold p=0.0013, respectively, compared to no stimulation. Addition of αIgM may have further increased c-Myc-GFP expression, but it was not statistically significant compared to the individual stimulations. Thus we did not see a clear synergy between αIgM and αCD40 stimulation for the induction of c-Myc expression or mTORC1 signaling, in contrast to a previous report (Luo et al., 2018). As both c-Myc expression and phosphorylation of a key mTORC1 target were increased to similar levels upon stimulation of GC B cells with αCD40 or CpG oligonucleotide, it is possible that TLR9 signaling in GC B cells could be a partial surrogate for CD40 mediated Tfh cell help. According to this interpretation, more GC B cells would get pro-survival mTORC1 signaling and c-Myc induction in the context of TLR9 signaling in the GC, lowering the need for CD40 stimulation and Tfh cell help. This

would increase the number of cells that survive and the pool of GC B cells as a percentage of the B cell population.

Discussion

Previous work established that a TLR ligand attached to a haptenated-protein antigen or contained within a virus particle can promote the magnitude and quality of the GC reaction and moreover that TLR signaling within the antigen-specific B cell is an important contributor to that enhancement (Hou et al., 2011; Rookhuizen and DeFranco, 2014). Here, we used mRNA sequencing and GSEA to identify the intracellular transcriptional programs that were enhanced by coupled antigen and TLR9/MyD88 signaling in GC B cells. Especially enhanced were the transcriptional signatures associated with c-Myc transcriptional activity and mTORC1 signaling. Both of these pathways are central to the control of cell growth and proliferation in many cell types and are critical in B cells for the GC response (Calado et al., 2012; Jones et al., 2016; Zhang et al., 2013). Interestingly, Tfh cells recognizing antigen presented by GC B cells also stimulate these pathways in the antigen-presenting GC B cell, leading to positive selection of the GC B cells (Dominguez-Sola et al., 2012; Ersching et al., 2017; Mayer et al., 2017). Thus, one potential mechanism by which TLR9/MyD88 signaling may have enhanced c-Myc transcription and mTORC1 signaling is by enhancing interactions of GC B cells with Tfh cells. Alternatively, TLR9/MyD88 signaling in the antigen-specific B cells may have directly increased the transcriptional activities of one or both of these pathways. Consistent with the latter, direct mechanism, we found that ex vivo stimulation of Bcl2-transgenic GC B cells with a TLR9 ligand increased expression of a c-Myc-GFP protein reporter and increased phosphorylation of the mTORC1 target protein ribosomal protein S6, in both cases similarly to the response induced by anti-CD40, which mimics a key aspect of helper T cell action.

It is likely that several mechanisms contributed to the enhanced c-Myc transcriptional activity seen in antigen-specific GC B cells responding to NP-CGG-CpG immunization. Both

naïve B cells and Bcl2-transgenic GC B cells cultured ex vivo and stimulated with a TLR9 ligand oligonucleotide exhibited increased c-Myc-GFP protein reporter induction, indicating direct TLR9/MyD88 signaling can induce elevated levels of c-Myc protein. Moreover, MyD88 signaling has been shown to stabilize c-Myc protein in intestinal epithelial cells (Lee et al., 2010). However, the increase in c-Myc-GFP expression in vivo after immunization with the NP-CGG-CpG conjugate was seen not only in wild type mice but also in mice in which MyD88 was deleted selectively in B cells, indicating that the observed increase in c-Myc-GFP can also occur by an indirect mechanism, mostly likely by induction following cognate interactions with antigen-specific Tfh cells. This indirect mechanism of promoting c-Myc protein expression in GC B cells could result from TLR9 signaling in other cell types, such as conventional dendritic cells - or stromal cells such as follicular dendritic cells (FDCs). Indeed, previous studies showed that TLR9 signaling in dendritic cells enhanced the number of Tfh cells following immunization with NP-CGG-CpG (Rookhuizen and DeFranco, 2014), possibly indicating increased availability of Tfh cell help for GC B cells. Interestingly, c-Myc protein levels were similar in WT and MyD88^{-} GC B cells immunized with NP-CGG-CpG, whereas the c-Myc transcriptional program was stronger in the former mice. The lack of concordance between gene expression data in sorted GC B cells and c-Myc-GFP fluorescent reporter expression indicates that c-Myc-dependent transcription is not necessarily directly proportional to c-Myc protein levels in GC B cells. Therefore, differences in the c-Myc-driven transcriptional signature could be orchestrated through c-Myc phosphorylation, binding partners, or chromatin accessibility (Conacci-Sorrell et al., 2014; Wang et al., 2011) programmed in activated B cells by dual BCR/TLR9 signaling that persists into the GC fate. This GC B cell-intrinsic enhancement of c-Myc transcriptional activity would perhaps

enhance the effect of Tfh induction of c-Myc protein by making that c-Myc more active and driving higher levels of gene expression, accounting for the transcriptional profiling results.

The increased mTORC1 transcriptional signature identified by GSEA in GC B cells of mice immunized with NP-CGG-CpG was mirrored by increased phosphorylation of ribosomal protein S6, a downstream target of mTORC1. While the MyD88^{-} GC B cells showed a subtle defect in ribosomal protein S6 phosphorylation in vivo, the remaining observed response in these cells could have been due to CD40 stimulation resulting from cognate interactions with Tfh cells. In addition, we observed that ex vivo stimulation of GC B cells with a TLR9 ligand also induced an increase in phospho-S6 in the GC B cells, indicating that the NP-CGG-CpG likely also directly stimulated this pathway in wild type GC B cells. Previous studies have demonstrated MyD88-mediated mTORC1 activation and binding in innate immune cells, and a similar process could occur in GC B cells (Schmitz et al., 2008).

While TLR agonists can promote both T-independent and T-dependent antibody responses, the nature of the antigen and the presence of additional adjuvants can have a major impact on the contribution of TLR signaling to the response. Previous work has shown that the valency of the antigen and its propensity to cross-link the BCR dictates the impact of B cell intrinsic MyD88-mediated signaling in shaping the GC response. Immunization with monovalent T-dependent antigens (such as ovalbumin) fused to CpG oligo show no difference in GC B cell numbers or antibody titers between B-MyD88^{-} and WT mice (DeFranco et al., 2012; Hou et al., 2011), whereas B-MyD88^{-} mice immunized with multi-valent VLPs have a profound deficit in the GC response and antibody titers compared to WT mice (Hou et al., 2011; Tian et al., 2018). Furthermore, addition of the lipid adjuvant DOTAP in conjunction with CpG oligonucleotide and NP-CGG, forming a multivalent particulate antigen, increased GC B cell and Tfh numbers as well as both

high affinity and low affinity NP-specific antibody titers when compared to immunization with CpG oligonucleotide and NP-CGG in soluble form (Akkaya et al., 2017). However, when the same group performed experiments with CpG oligonucleotide and NP-CGG complexed with alum, they saw a decrease in high affinity antibody titers against NP in WT mice compared to B-MyD88^{-} mice (Akkaya et al., 2018a). Moreover, the inclusion of alum to complex a large murine self CpG DNA molecule with an amyloid conformed protein (chemically modified human serum albumin) also diminished total GC number and total anti-HSA titers (Sindhava et al., 2017). These differences demonstrate that the exact conformation of the protein CpG oligo complex and other adjuvants, specifically alum, can profoundly affect the quality and quantity of the humoral response. The inclusion of alum and its inflammasome-mediated adjuvant activity in monocytes (MacLeod et al., 2011; McKee and Marrack, 2017) could be a complicating factor in these two experimental settings in which a decrease in the GC response was observed.

While it is clear that TLR9 signaling in B cells can substantially promote the GC response (Akkaya et al., 2017; Rookhuizen and DeFranco, 2014; Tian et al., 2018), the exact timing of when TLR9-mediated MyD88 signaling influences the GC fate has not been well defined. This signaling event during early B cell activation could provide a selective advantage for initiating the GC or alternatively, TLR9/MyD88 signaling event in GC cells could directly enhance their ongoing participation in the GC reaction. The enhanced c-Myc and mTORC1 transcriptional programs seen in GC B cells on d14 are certainly consistent with the latter possibility, but these possibilities are not mutually exclusive. In our in vivo and ex vivo stimulation experiments, both naïve and GC B cells responded directly to TLR9 stimulation by upregulating mTORC1 signaling and c-Myc protein expression. However, recent studies have demonstrated that MyD88 signaling during the initial activation of naive B cells in the response to nucleic acid-containing VLPs also plays a key

role in activated B cell survival, proliferation, and antigen presentation to cognate T cells (Akkaya et al., 2018b; Hong et al., 2018). Furthermore, deletion of *Myd88* in activated B cells utilizing Aicda-cre had a lesser effect than deletion of *Myd88* with Mb1-cre prior to immunization, indicating that TLR/MyD88 signaling during the early phase of the response is important in the response to CpG-containing VLPs (Tian et al., 2018). This observation bolsters the idea that dual BCR and TLR9 signaling in naïve B cells provides a selective advantage that is maintained days later in the GC response. Thus, the difference in numbers and percentage of GC B cells could be a result of differences in early activation, though our gene expression data indicates that there are persistent MyD88-signaling events that are maintained during the GC, at least through day 14.

Both BCR and co-signaling through TLRs and αCD40 have been implicated in the metabolic reprogramming of activated B cells. Studies of early activation of B cells in vitro by BCR stimulation, TLR4 stimulation with LPS, or αCD40 + IL-4 stimulation to mimic helper T cell action have implicated increased glycolytic flux and increased oxidative/phosphorylation as critical metabolic shifts during the initial activation of naïve cells and for antibody production in vitro (Caro-Maldonado et al., 2014; Waters et al., 2018). Interestingly, B cells that receive a BCR-mediated signal alone undergo toxic mitochondrial reprogramming, leading to apoptosis unless a secondary signal such as TLR stimulation or CD40-mediated signaling rescues this metabolic dysfunction (Akkaya et al., 2018b). Thus, activation signals in naïve B cells directly reprogram the mitochondria and necessitate co-signaling events for survival, however the metabolic reprograming that occurs in GC B cells remains largely unknown. As discussed above, it is clear that Tfh cell help induces mTORC1 signaling and c-Myc expression (Calado et al., 2012; Dominguez-Sola et al., 2012; Ersching et al., 2017), two mediators of metabolism and cell cycle regulation. Previous studies have implicated a synergy between BCR stimulation and αCD40

mediated Tfh help to induce mTORC1(Luo et al., 2018), and our ex vivo stimulation data supports the idea that cosignaling of BCR and TLR9/MyD88 induce mTORC1. In addition, we found that TLR9/MyD88 signaling in GC B cells enhanced expression of genes involved in oxidative phosphorylation and mitochondrial function (Fig. 3.1B, S3.2, Table 3.2).

This work adds to our basic understanding of the molecular pathways within the GC B cell by which TLR recognition promotes their response and has shown that this involves activation of mTORC1 and increased c-Myc transcriptional activity, two critical events also resulting from antigen-presentation to Tfh cells. Such understanding may facilitate efforts to improve current vaccines or create new effective vaccines by rational approaches. The tight association of a CpG oligonucleotide to a protein antigen is in most circumstances sufficient to promote an increased humoral immunity and could serve as a strategy for vaccination as can the use of virus-like particles containing nucleic acid ligands for TLR9 or TLR7. Such immunogens likely mimic to some degree the nature of virus particles and engage an evolutionarily-derived mechanism to defend against viral infections. Utilizing endosomal TLR adjuvants to shape the humoral response and provide an increased number of GC B cells could be beneficial in anti-viral vaccine development.

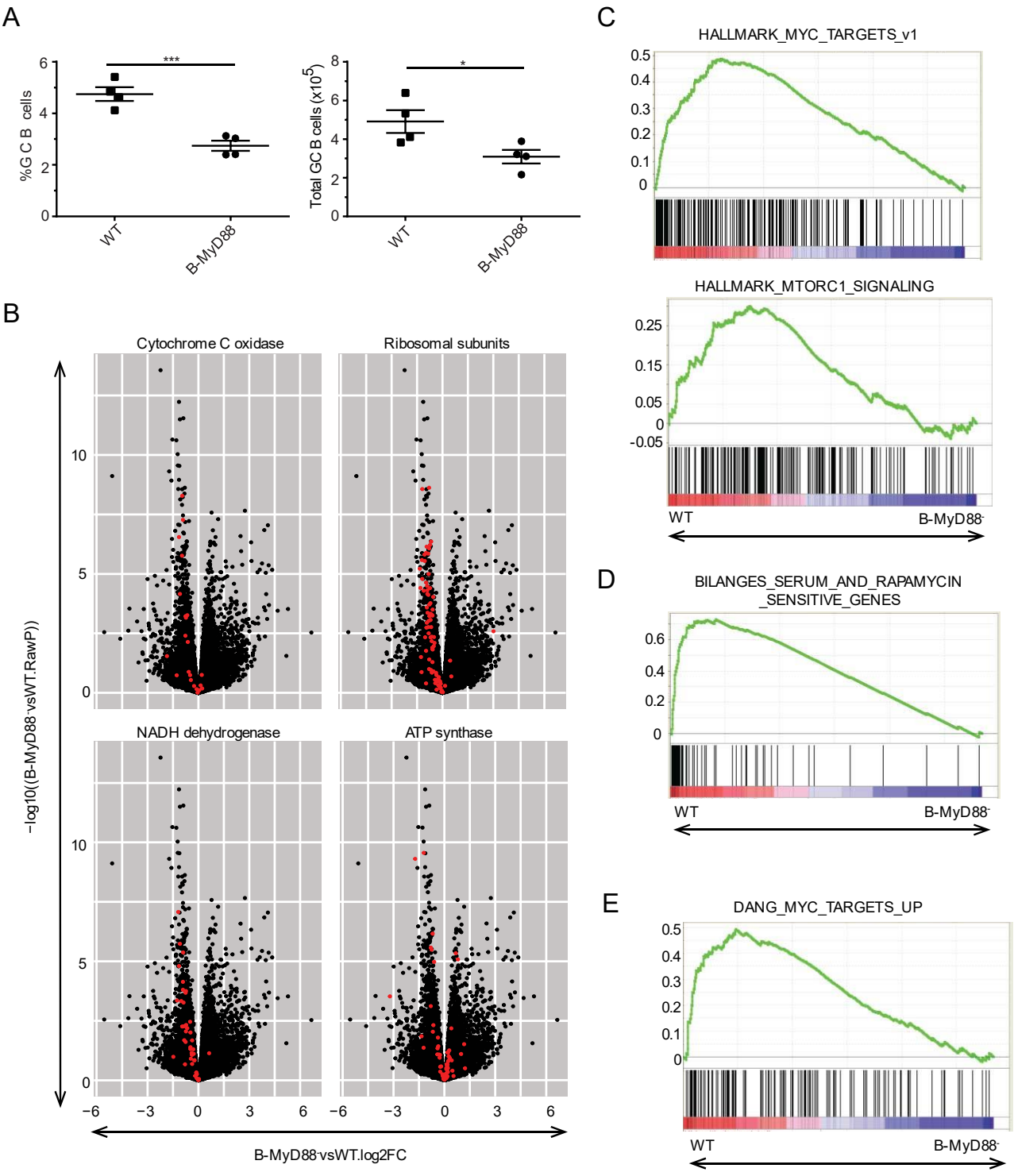
A
%G C B cells
***
WT
B-MyD88-
Total GC B cells (x10^5)
*
WT
B-MyD88-
B
Cytochrome C oxidase
Ribosomal subunits
NADH dehydrogenase
ATP synthase
−log10((B-MyD88-vsWT.RawP))
B-MyD88-vsWT.log2FC
C
HALLMARK_MYC_TARGETS_v1
HALLMARK_MTORC1_SIGNALING
WT
B-MyD88-
D
BILANGES_SERUM_AND_RAPAMYCIN_SENSITIVE_GENES
WT
B-MyD88-
E
DANG_MYC_TARGETS_UP
WT
B-MyD88-

Figure 3.1: mRNA-seq analysis of WT and B-MYD88$^-$ NP+ GC B cells shows increased c-Myc and mTORC1 gene expression signatures

A Enumeration of GC B cell percentages and total cell numbers from draining lymph nodes of WT and B-MYD88$^-$ animals at D14 post immunization. Shown is a representative of 4 independent experiments with at least 3 mice per group. B Volcano plots comparing gene expression fold changes to p value for all genes expressed in at least one sample after DESeq2 analysis. Red dots in each panel indicated genes associated with the given metabolic/synthetic complex listed. **C** GSEA plots for Hallmark gene sets for mTORC and c-Myc gene signatures enriched in WT transcriptional data. **D** GSEA plot from curated gene sets showing enrichment of rapamycin and serum sensitive genes in WT samples. **E** GSEA plot from curated gene sets showing enrichment of c-Myc target genes in WT samples.

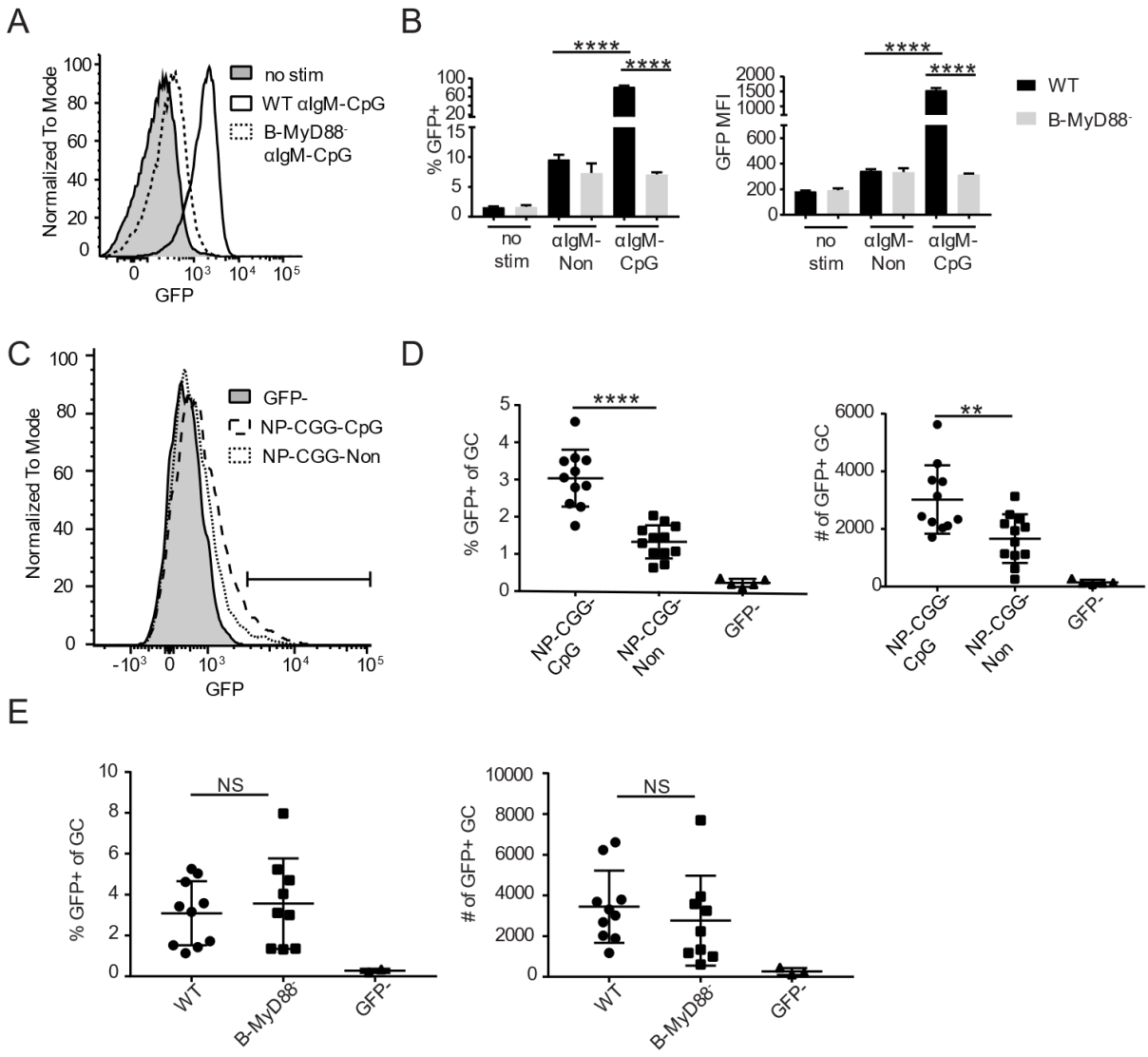

Figure 3.2: Dual BCR/TLR9 Signaling positively regulates c-Myc expression in naïve and GC B cells.

A Overlay of representative histograms showing c-Myc-GFP expression in response to αIgM-CpG stimulation for 24hs of WT c-Myc-GFP and B-MYD88^{-} c-Myc-GFP naïve B cells. **B** Enumeration of %GFP positive and MFI of cells in A (shown is a single experiment representative of 3 independent experiments). **C** Overlay of representative histograms showing GFP fluorescence gating on live, singlet, CD19^{+}, Fas^{+}, IgD^{lo}, GL7^{+} GC cells of c-Myc-GFP$^{+/+}$ mice immunized with NP-CGG-CpG or NP-CGG-Non D14 post immunization. **D** Enumeration of percent and number of GFP+ GC B cells from NP-CGG-CpG and NP-CGG-Non immunized c-Myc-GFP$^{+/+}$ mice (three combined experiments with at least 3 mice per group). **E** Enumeration of percent and number GFP positive cells from NP-CGG-CpG immunized B-MYD88^{-} and WT mice D14 (representative experiment of 3 independent experiments). **= $p<0.005$, ****= $p<0.0001$, NS = $p>0.05$ by one-way ANOVA and Holm-Sidak's multiple comparison test

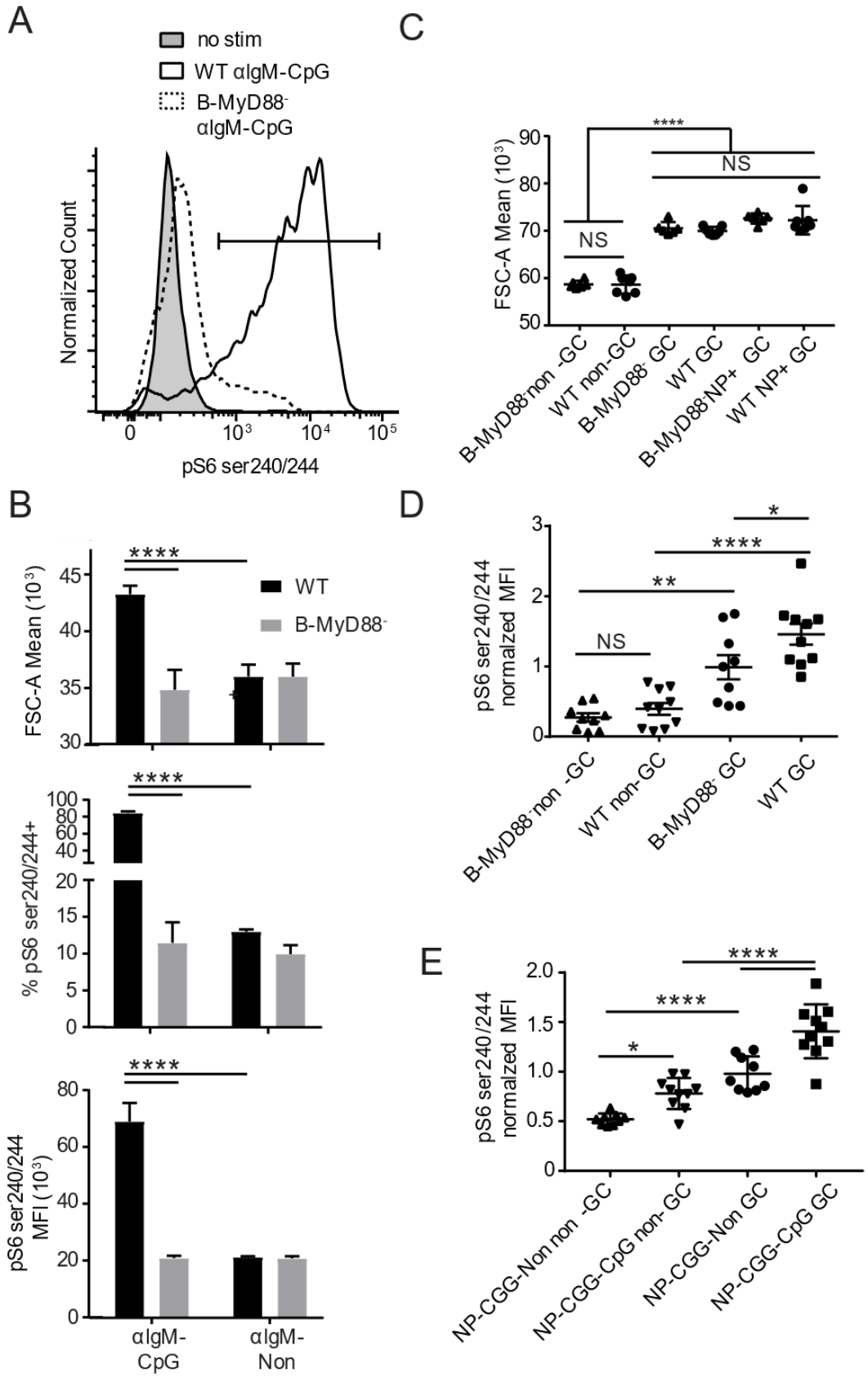
A
no stim
WT αIgM-CpG
B-MyD88-
αIgM-CpG
Normalized Count
0
10^3
10^4
10^5
pS6 ser240/244
B
WT
B-MyD88-
FSC-A Mean (10^3)
****
% pS6 ser240/244+
pS6 ser240/244
MFI (10^3)
αIgM-
CpG
αIgM-
Non
C
FSC-A Mean (10^3)
****
NS
NS
B-MyD88-non -GC
WT non-GC
B-MyD88- GC
WT GC
B-MyD88-NP+ GC
WT NP+ GC
D
pS6 ser240/244
normalzed MFI
*
****
**
NS
B-MyD88-non -GC
WT non-GC
B-MyD88- GC
WT GC
E
pS6 ser240/244
normalzed MFI
****
****
*
NP-CGG-Non non -GC
NP-CGG-CpG non-GC
NP-CGG-Non GC
NP-CGG-CpG GC

Figure 3.3: Dual BCR/TLR9 Signaling positively regulates mTORC1 activity measured by ribosomal protein S6 phosphorylation in naïve and GC B cells.
A Overlay of representative histograms showing pS6 ser240/244 levels in response to αIgM-CpG for 24 hr.in WT and B-MYD88- naïve B cells. **B** Enumeration of cell size by forward light scatter (FSC-A), % pS6 ser240/244 +, and MFI of those cells gated positively for pS6 ser240/244 cells for WT and B-MYD88^{-} naïve B cells stimulated with αIgM-CpG. **C** Enumeration of cell size from D14 NP-CGG-CpG immunized B-MYD88^{-} and WT non-GC and GC B cells (representative of 4 independent experiments). **D** phospho-flow MFI of mTORC1 downstream target pS6 ser240/244 D14 NP-CGG-CpG immunized B-MYD88^{-} and WT B cells normalized to mean of B-MYD88^{-} GC MFI (data are combined from 3 experiments with at least 3 mice per group) **E** phospho-flow MFI of mTORC1 downstream target pS6 ser240/244 D14 NP-CGG-CpG and NP-CGG-Non immunized mice normalized to mean MFI of NP-CGG-Non MFI (combined from 2 independent experiments with at least 4 mice per condition). ****= $p<0.0001$, NS = $p>0.05$ by one-way ANOVA and Holm-Sidak's multiple comparison test.

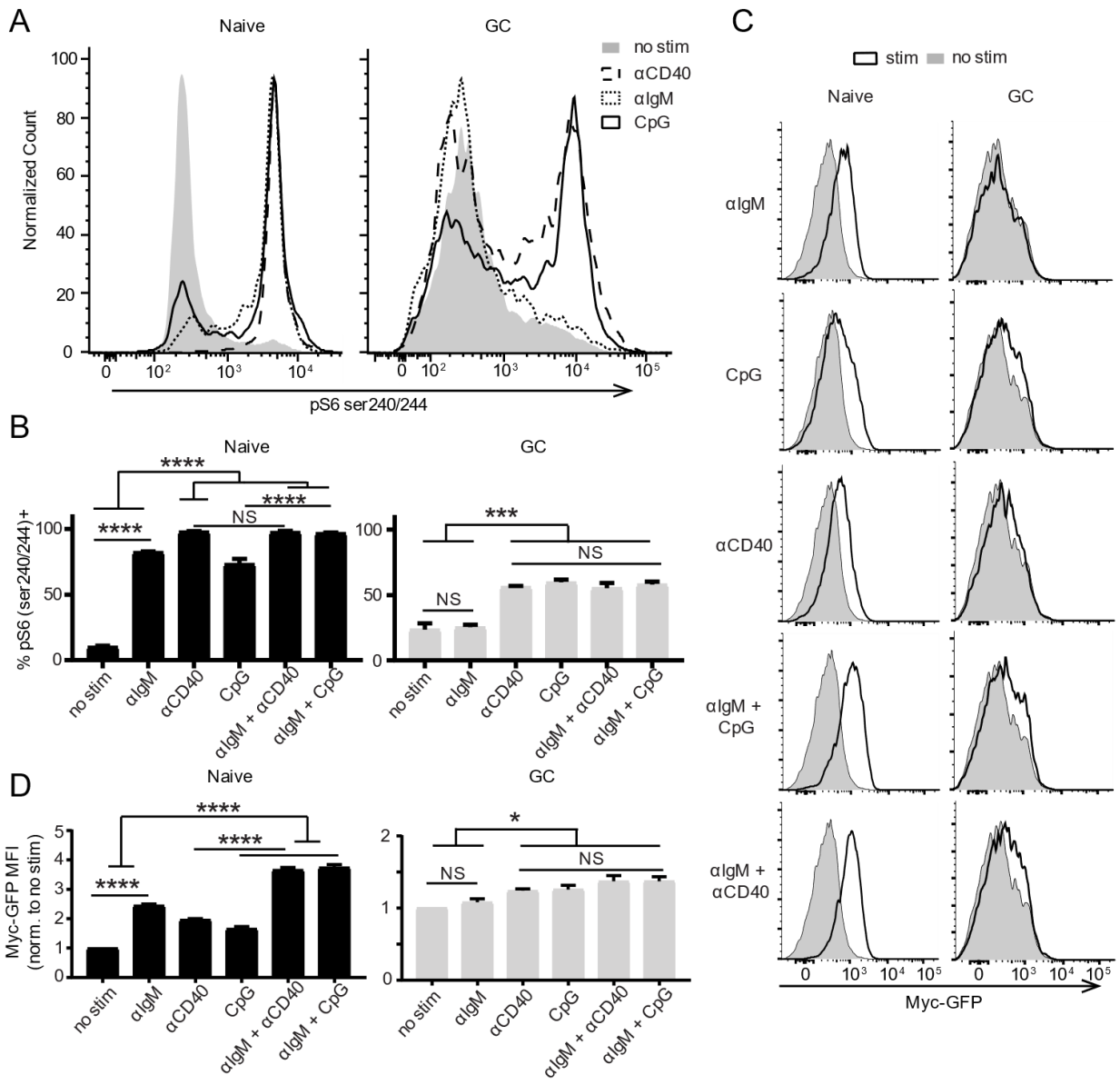

Figure 3.4: CpG Stimulation of GC B cells ex vivo increases mTORC1 signaling to similar levels as αCD40 stimulation.

A Representative histograms comparing phosphoflow pS6 ser240/244 staining of 4 hour ex vivo stimulated naïve and GC B cells isolated from i.p. NP-CGG alum immunized mouse spleens at D12-D14 (3 mice per experiment performed in 3 separate experiments). **B** Enumeration of experiments from A showing level of pS6 ser240/244 expression in Naive and GC B cells from A. **C** Overlays of c-Myc-GFP expression comparing no stimulation to the respective stimulation in Naïve and GC B cells after 4 hours. **D** Enumeration of the relative c-Myc-GFP MFI increase normalized to no stimulation of the samples in C (representative of 3 independent experiments with at least 3 mice per experiment). *= $p<0.05$, ****= $p<0.0001$, and NS = $p>0.05$ by one-way ANOVA and Tukey's multiple comparison test.

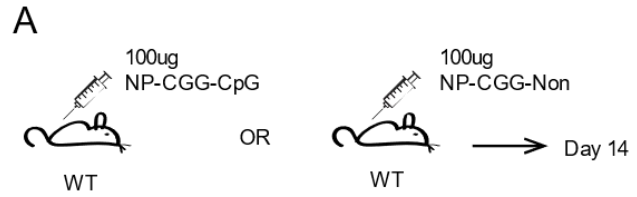
A
100ug
NP-CGG-CpG
WT
OR
100ug
NP-CGG-Non
WT
Day 14

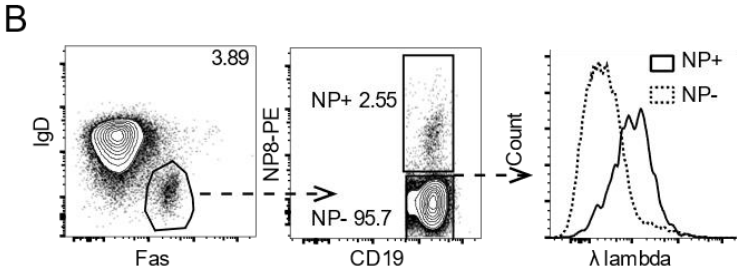
B
3.89
IgD
Fas
NP8-PE
NP+ 2.55
NP- 95.7
CD19
Count
NP+
NP-
λ lambda

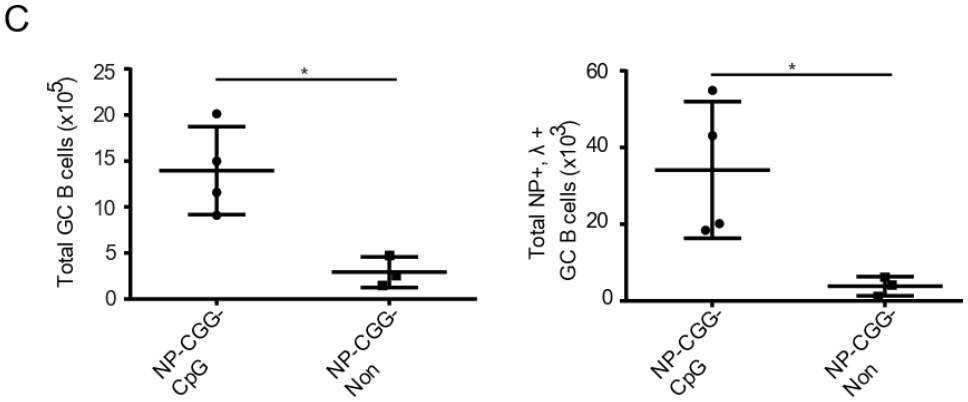
C
Total GC B cells (x10^5)
25
20
15
10
5
0
*
NP-CGG-CpG
NP-CGG-Non
Total NP+, λ + GC B cells (x10^3)
60
40
20
0
*
NP-CGG-CpG
NP-CGG-Non

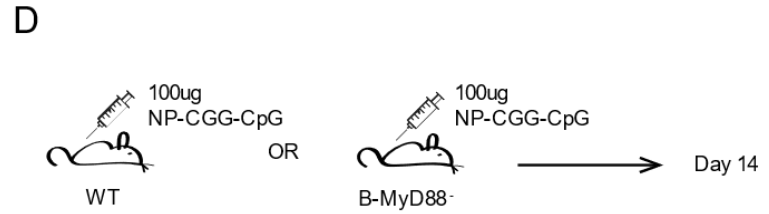
D
100ug
NP-CGG-CpG
WT
OR
100ug
NP-CGG-CpG
B-MyD88-
Day 14

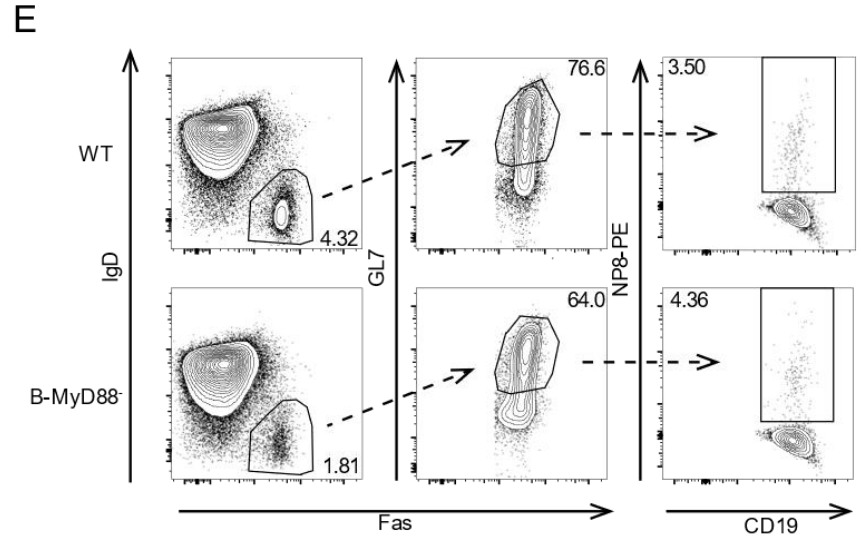
E
WT
B-MyD88-
IgD
4.32
1.81
GL7
76.6
64.0
NP8-PE
3.50
4.36
Fas
CD19

Supplemental Figure 3.1: Chemical and Genetic approach to studying TLR9 agonist in the GC. A Experimental design for immunizing C57BL/6J mice with complex NP-CGG-CpG and NP-CGG-Non antigen. **B** Example flow cytometry plot showing gating strategy from live, singlet, dump , CD19+ cells using Fas+, IgDlo followed by NP(8-14)-PE and λ light chain positive. **C** Enumeration of the number of GC and NP+, λ+ GC cells in immunized mice at D14. *= $p<0.05$ by Student's t test. **D** Experimental design for immunizing WT or B-MyD88- mice with complex NP-CGG-CpG antigen. **E** Gating strategy comparing WT and B-MYD88- live, singlet, dump-, CD19+ GC (Fas+, IgDlo, GL7+) cells and the resulting NP+ and negative populations. Large variability in NP-binding led to no significant difference in the NP+, λ+ population GC B cells (data not shown).

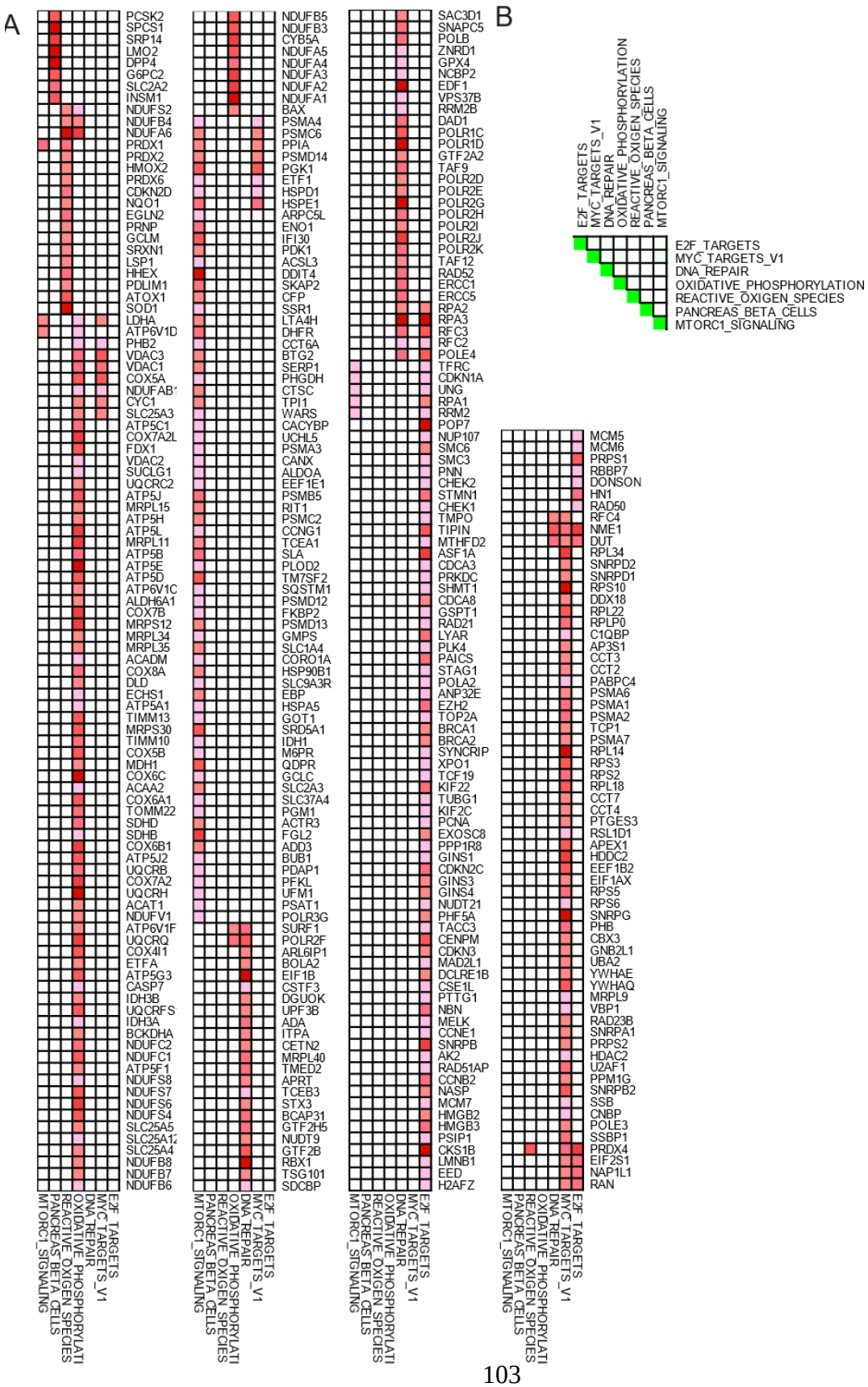
A
B
PCSK2
SPCS1
SRP14
LMO2
DPP4
G6PC2
SLC2A2
INSM1
NDUFS2
NDUFB4
NDUFA6
PRDX1
PRDX2
HMOX2
PRDX6
CDKN2D
NQO1
EGLN2
PRNP
GCLM
SRXN1
LSP1
HHEX
PDLIM1
ATOX1
SOD1
LDHA
ATP6V1D
PHB2
VDAC3
VDAC1
COX5A
NDUFAB1
CYC1
SLC25A3
ATP5C1
COX7A2L
FDX1
VDAC2
SUCLG1
UQCRC2
ATP5J
MRPL15
ATP5H
ATP5L
MRPL11
ATP5B
ATP5E
ATP5D
ATP6V1C
ALDH6A1
COX7B
MRPS12
MRPL34
MRPL35
ACADM
COX8A
DLD
ECHS1
ATP5A1
TIMM13
MRPS30
TIMM10
COX5B
MDH1
COX6C
ACAA2
COX6A1
TOMM22
SDHD
SDHB
COX6B1
ATP5J2
UQCRB
COX7A2
UQCRH
ACAT1
NDUFV1
ATP6V1F
UQCRQ
COX4I1
ETFA
ATP5G3
CASP7
IDH3B
UQCRFS
IDH3A
BCKDHA
NDUFC2
NDUFC1
ATP5F1
NDUFS8
NDUFS7
NDUFS6
NDUFS4
SLC25A5
SLC25A12
SLC25A4
NDUFB8
NDUFB7
NDUFB6
NDUFB5
NDUFB3
CYB5A
NDUFA5
NDUFA4
NDUFA3
NDUFA2
NDUFA1
BAX
PSMA4
PSMC6
PPIA
PSMD14
PGK1
ETF1
HSPD1
HSPE1
ARPC5L
ENO1
IFI30
PDK1
ACSL3
DDIT4
SKAP2
CFP
SSR1
LTA4H
DHFR
CCT6A
BTG2
SERP1
PHGDH
CTSC
TPI1
WARS
CACYBP
UCHL5
PSMA3
CANX
ALDOA
EEF1E1
PSMB5
RIT1
PSMC2
CCNG1
TCEA1
SLA
PLOD2
TM7SF2
SQSTM1
PSMD12
FKBP2
PSMD13
GMPS
SLC1A4
CORO1A
HSP90B1
SLC9A3R
EBP
HSPA5
GOT1
SRD5A1
IDH1
M6PR
QDPR
GCLC
SLC2A3
SLC37A4
PGM1
ACTR3
FGL2
ADD3
BUB1
PDAP1
PFKL
UFM1
PSAT1
POLR3G
SURF1
POLR2F
ARL6IP1
BOLA2
EIF1B
CSTF3
DGUOK
UPF3B
ADA
ITPA
CETN2
MRPL40
TMED2
APRT
TCEB3
STX3
BCAP31
GTF2H5
NUDT9
GTF2B
RBX1
TSG101
SDCBP
SAC3D1
SNAPC5
POLB
ZNRD1
GPX4
NCBP2
EDF1
VPS37B
RRM2B
DAD1
POLR1C
POLR1D
GTF2A2
TAF9
POLR2D
POLR2E
POLR2G
POLR2H
POLR2I
POLR2J
POLR2K
TAF12
RAD52
ERCC1
ERCC5
RPA2
RPA3
RFC3
RFC2
POLE4
TFRC
CDKN1A
UNG
RPA1
RRM2
POP7
NUP107
SMC6
SMC3
PNN
CHEK2
STMN1
CHEK1
TMPO
TIPIN
MTHFD2
ASF1A
CDCA3
PRKDC
SHMT1
CDCA8
GSPT1
RAD21
LYAR
PLK4
PAICS
STAG1
POLA2
ANP32E
EZH2
TOP2A
BRCA1
BRCA2
SYNCRIP
XPO1
TCF19
KIF22
TUBG1
KIF2C
PCNA
EXOSC8
PPP1R8
GINS1
CDKN2C
GINS3
GINS4
NUDT21
PHF5A
TACC3
CENPM
CDKN3
MAD2L1
DCLRE1B
CSE1L
PTTG1
NBN
MELK
CCNE1
SNRPB
AK2
RAD51AP
CCNB2
NASP
MCM7
HMGB2
HMGB3
PSIP1
CKS1B
LMNB1
EED
H2AFZ
MCM5
MCM6
PRPS1
RBBP7
DONSON
HN1
RAD50
RFC4
NME1
DUT
RPL34
SNRPD2
SNRPD1
RPS10
DDX18
RPL22
RPLP0
C1QBP
AP3S1
CCT3
CCT2
PABPC4
PSMA6
PSMA1
PSMA2
TCP1
PSMA7
RPL14
RPS3
RPS2
RPL18
CCT7
CCT4
PTGES3
RSL1D1
APEX1
HDDC2
EEF1B2
EIF1AX
RPS5
RPS6
SNRPG
PHB
CBX3
GNB2L1
UBA2
YWHAE
YWHAQ
MRPL9
VBP1
RAD23B
SNRPA1
PRPS2
HDAC2
U2AF1
PPM1G
SNRPB2
SSB
CNBP
POLE3
SSBP1
PRDX4
EIF2S1
NAP1L1
RAN
E2F_TARGETS
MYC_TARGETS_V1
DNA_REPAIR
OXIDATIVE_PHOSPHORYLATION
REACTIVE_OXIGEN_SPECIES
PANCREAS_BETA_CELLS
MTORC1_SIGNALING

Supplemental Figure. 2: Leading edge analysis of 7 Hallmark gene sets found to be upregulated in WT compared to B-MYD88- GC B cells. A Each gene listed is in at least one of the 7 data sets. Color from white to red shows relative level of mRNA expression. **B** Color from white showing no overlap to dark green demonstrating complete overlap for the 7 gene sets.

A

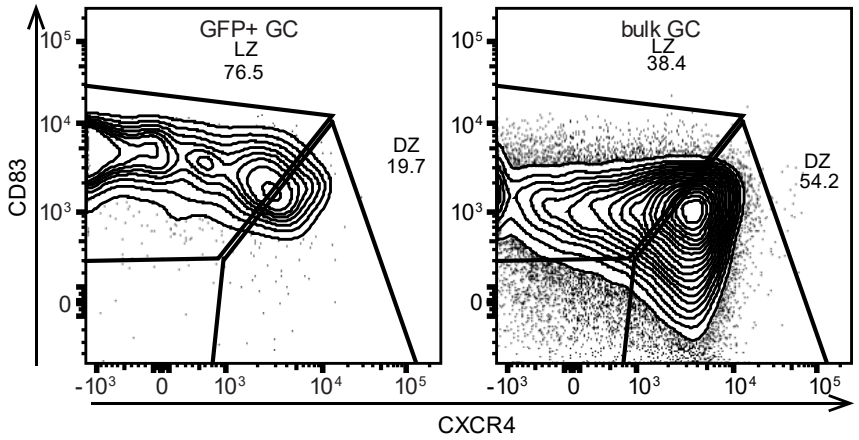
GFP+ GC
LZ
76.5
DZ
19.7
bulk GC
LZ
38.4
DZ
54.2
CD83
CXCR4

B

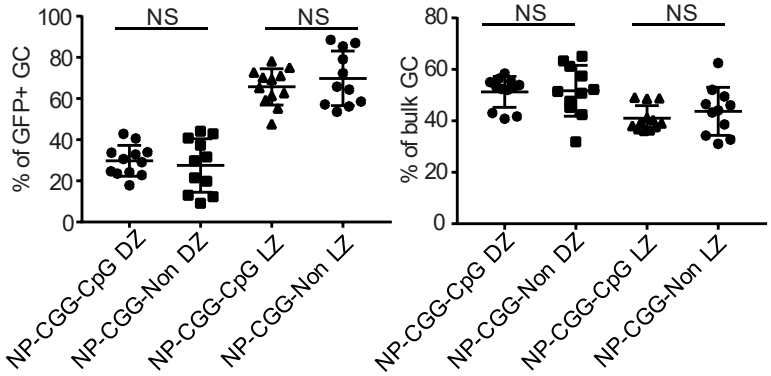
% of GFP+ GC
% of bulk GC
NS
NP-CGG-CpG DZ
NP-CGG-Non DZ
NP-CGG-CpG LZ
NP-CGG-Non LZ

C

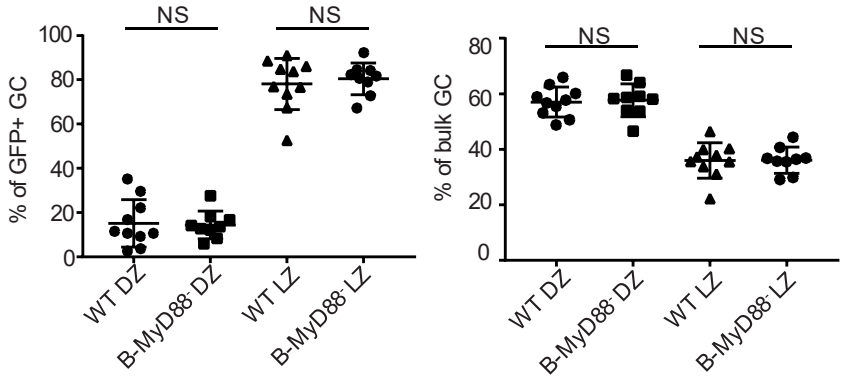
% of GFP+ GC
% of bulk GC
NS
WT DZ
B-MyD88- DZ
WT LZ
B-MyD88- LZ

D

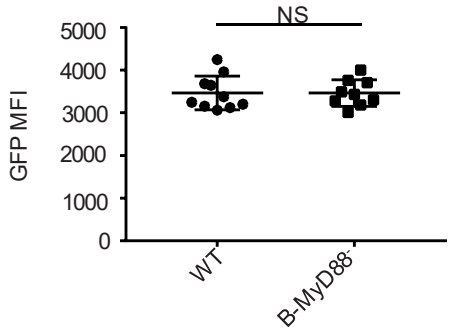
GFP MFI
NS
WT
B-MyD88-

Supplementary Figure 3.3: Gating strategy for DZ and LZ populations in the GC and numeration of these populations using both experimental strategies. A DZ and LZ gating strategy for GFP+ and bulk GC B cells. **B** Enumeration of DZ and LZ breakdown of GFP positive and bulk GC populations in NP-CGG-CpG and NP-CGG-Non immunized mice at D14 (3 combined experiments with at least 3 mice in each group). **C** Enumeration of DZ and LZ distribution of GFP positive and bulk GC populations in B-MYD88- and WT mice immunized with NP-CGG-CpG at D14 (3 combined experiments with at least 3 mice in each group). **D** MFI of GFP positive GC cells from C. NS = $p>0.05$ by student's t test.

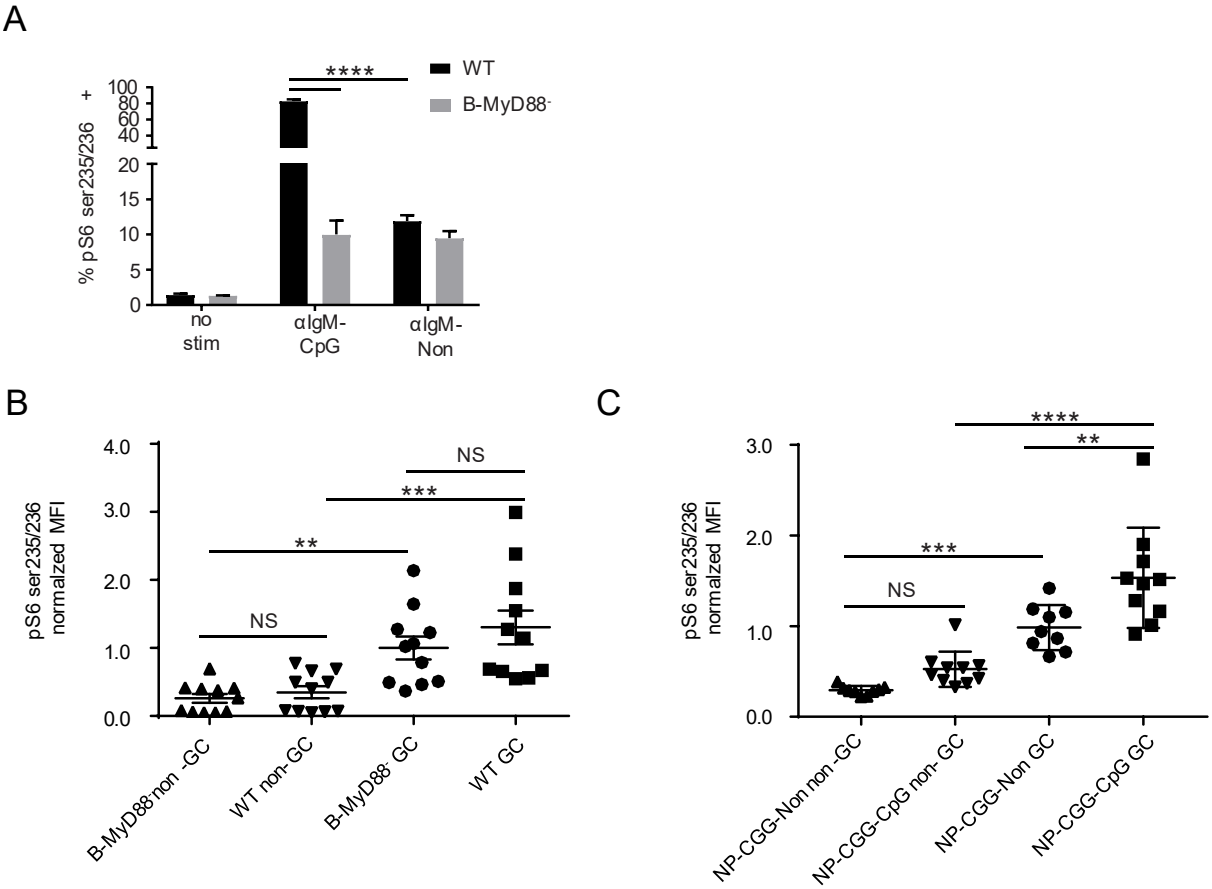

Supplementary Figure 3.4: Complimentary analysis for pS6 ser235/236 for in vitro complex antigen stimulation and in vivo immunizations.

A Enumeration of % pS6 ser235/236 +, for WT and B-MYD88 - naïve B cells stimulated in vitro with αIgM -CpG and αIgM-Non for 24 h ours. ****= p<0 .001 by Student's t test.

B phospho-flow MFI of mTORC1 downstream target pS6 ser235/236 of D14 NP-CGG -CpG immunized B-MYD88 - and WT B cells normalized to mean of B-MYD88 - GC MFI (3 combined experiments with at least 3 mice per group)**. C** phospho-flow MFI of mTORC1 downstream target pS6 ser235/236 of D14 NP-CGG-CpG and NP-CGG-Non immunized m ice normalized to mean NP-CGG-Non MFI . **= p<0.0 05, ** * = p<0.0005, ****= p<0.00 01, NS = p>0.05 by one-way ANOVA and Holm-Sidak's multiple comparison test.

Table 3.1: B Cell Activation, CSR, and Cell Fate Gene Expression

Gene	Log2(KO/WT)	Raw p value	FDR value
Ighg2c	-0.931278014	2.63E-06	0.000742214
Fas	0.141497226	0.364147352	0.93944051
Cxcr4	0.364550474	0.115060865	0.6353624
Cd86	-0.155604203	0.313582804	0.90908692
Cd80	-0.247780304	0.381587211	0.93944051
Aicda	-0.516289592	0.002956723	0.08882857
Prdm1	-1.091192869	0.003046472	0.08996182
Tlr9	0.115035034	0.502823401	0.97633773
Myd88	-1.7156157	2.80E-05	**0.00412237**
Bcl6	0.39066445	0.000556044	**0.03277441**
Bcl2	-1.081316005	0.000697559	**0.03849734**

Table 3.2: GSEA shows enrichment for mTORC1 and Myc signatures

NAME	SIZE	ES	NES	NOM p-val	FDR q-val
HALLMARK_OXIDATIVE_PHOSPHORYLATION	186	0.593	2.91	>1E-04	>1E-04
HALLMARK_MYC_TARGETS_V1	191	0.487	2.38	>1E-04	>1E-04
HALLMARK_REACTIVE_OXYGEN_SPECIES_PATHWAY	45	0.517	1.96	>1E-04	4.17E-04
HALLMARK_PANCREAS_BETA_CELLS	24	0.537	1.76	8.65E-03	8.19E-03
HALLMARK_DNA_REPAIR	134	0.360	1.71	>1E-04	1.01E-02
HALLMARK_E2F_TARGETS	191	0.327	1.60	>1E-04	2.10E-02
HALLMARK_UNFOLDED_PROTEINRESPONSE	104	0.332	1.49	1.59E-02	4.61E-02
HALLMARK_MTORC1_SIGNALING	189	0.299	1.46	4.77E-03	5.65E-02
DANG_MYC_TARGETS_UP	129	0.493	2.29	>1E-04	>1E-04
KEGG_RIBOSOME	72	0.819	3.45	>1E-04	>1E-04
BILANGES_SERUM_AND_RAPAMYCIN_SENSITIVE_GENES	59	0.727	2.95	>1E-04	>1E-04

Supplemental Table 3.1: Differential Genes from RNA-seq of B-MyD88-(KO) vs WT NP+, GC B cells

Gene	*KOvsWT .log2FC*	*KOvsWT.RawP*	*KOvsWT.FDR*
1110038F14Rik	-1.0765	1.653E-04	0.014651942
1700017B05Rik	0.8342	1.900E-06	0.000583898
1700039E15Rik	3.6174	6.640E-06	0.001400288
1810058I24Rik	-1.2067	1.330E-06	0.000451313
2010107E04Rik	-1.1014	1.430E-05	0.002481323
2210406O10Rik	6.9776	2.710E-05	0.004033915
2310022B05Rik	1.1578	6.068E-04	0.034464025
2610507I01Rik	-1.8086	4.383E-04	0.028623241
2700094K13Rik	-0.8576	9.553E-04	0.047603974
4930404N11Rik	-2.5629	1.200E-05	0.002171875
4930565N06Rik	1.6401	5.040E-06	0.001138243
4931414P19Rik	1.9676	6.790E-04	0.037829611
8430429K09Rik	-0.9238	4.729E-04	0.029544915
A4galt	3.1500	8.751E-04	0.045405681
Abca3	0.4743	5.136E-04	0.031213796
Abcc1	0.6749	2.129E-04	0.017295532
Abhd14b	1.7158	1.018E-03	0.049739221
Abracl	-0.9999	7.220E-04	0.039290757
Acp5	-0.9287	1.060E-05	0.001968641
Actl6b	-8.8456	5.764E-04	0.033549234
Adat1	0.8209	5.120E-05	0.006467641
Ago2	0.3623	9.774E-04	0.048445584
Aldh2	-0.7381	8.080E-07	0.000320533
Alg3	0.8949	4.787E-04	0.029790242
Amotl1	2.4874	2.590E-07	0.000144311
Anapc13	-1.4889	9.820E-07	0.000370441
Ankmy1	4.1605	2.051E-04	0.016838252
Arel1	0.4228	2.367E-04	0.018773841
Arid1a	0.4329	2.745E-04	0.021058997
Armc2	-8.6723	2.500E-06	0.000722975
Arpc3	-0.5500	3.158E-04	0.02294815
Arpp21	6.8774	4.578E-04	0.029094005
Asf1a	-0.5709	1.601E-04	0.014316035
Asnsd1	-1.3092	5.170E-06	0.001151389
Atcay	2.1018	2.610E-05	0.003916278
Atg16l1	0.5043	3.529E-04	0.024872335
Atg5	-0.6688	7.923E-04	0.042231252
Atp5c1	-0.6045	1.070E-05	0.001968641
Atp5d	-0.7971	7.644E-04	0.041214432

Gene	*KOvsWT .log2FC*	*KOvsWT.RawP*	*KOvsWT.FDR*
Atp5e	-1.2132	2.780E-10	6.74E-07
Atp5g3	-0.7529	3.240E-06	0.000824676
Atp5j	-0.6899	6.870E-07	0.000281867
Atp5j2	-0.8049	2.670E-06	0.000744799
Atp5k	-1.7238	4.920E-10	1.05E-06
Atp5sl	0.7965	8.300E-06	0.001673692
Atp6ap1	0.6728	4.560E-06	0.001055953
Atp7b	-3.2165	2.981E-04	0.022097454
Atxn2	0.6083	8.820E-06	0.001720336
Bace1	0.5842	1.494E-04	0.013929904
Bank1	-0.5621	2.459E-04	0.019376971
Bcl2	-1.0813	6.976E-04	0.03849734
Bcl6	0.3907	5.560E-04	0.032774406
Bhlhe41	-0.8016	8.482E-04	0.04455924
Blvrb	-0.5208	4.401E-04	0.028623241
Bora	0.4773	4.587E-04	0.029094005
Brk1	-0.8303	9.600E-07	0.000368208
Btg1	-0.6675	7.835E-04	0.041953654
C530005A16Rik	1.6945	1.250E-05	0.00223014
C78197	8.7523	6.390E-08	4.82E-05
Camkmt	-2.0795	1.920E-05	0.003000426
Cand2	0.7249	1.584E-04	0.014316035
Ccdc12	-1.1649	7.070E-05	0.008073327
Ccdc150	6.2158	9.947E-04	0.048798368
Ccdc181	-0.6987	1.476E-04	0.013818668
Cd36	-1.0168	7.600E-05	0.008472882
Cd52	-0.9132	3.240E-06	0.000824676
Cd72	-0.9570	1.572E-04	0.014316035
Cd8a	2.6972	2.012E-04	0.016578196
Cend1	6.9094	3.825E-04	0.026111812
Cenph	-0.5172	3.765E-04	0.025834217
Chchd1	-1.3564	1.210E-05	0.002178688
Chchd10	-0.8921	2.860E-12	1.87E-08
Chchd2	-0.9520	7.206E-04	0.039290757
Chchd4	-0.8634	3.754E-04	0.025834217
Cib1	-0.8042	5.306E-04	0.031836845
Cks1b	-0.6931	4.780E-05	0.006289102
Clcn6	0.6734	8.323E-04	0.043961925
Cnppd1	0.9037	5.135E-04	0.031213796
Col27a1	2.1316	1.541E-04	0.014308277
Col2a1	-6.0805	1.826E-04	0.015822329
Cox4i1	-0.7508	5.956E-04	0.034157962

Gene	*KOvsWT .log2FC*	*KOvsWT.RawP*	*KOvsWT.FDR*
Cox5b	-0.7359	6.912E-04	0.038329416
Cox6a1	-0.6589	5.444E-04	0.032249318
Cox6b1	-0.9579	5.230E-09	6.44E-06
Cox6c	-1.1395	2.830E-07	0.000151328
Cox7a2	-1.0844	6.990E-05	0.008058411
Cox7a2l	-0.9066	5.390E-08	4.35E-05
Cox7b	-0.9642	1.710E-06	0.00054866
Crip1	-1.2932	2.430E-11	9.49E-08
Cript	-0.5869	2.701E-04	0.020794843
Crocc	1.0387	1.082E-04	0.011198418
Csf3r	6.5603	3.316E-04	0.023874915
Csrp1	0.5208	4.832E-04	0.029992006
Cuta	-0.6388	3.837E-04	0.026111812
Cxcr3	-1.1198	2.880E-10	6.74E-07
Cxxc5	0.6463	3.722E-04	0.025834217
Cyb5a	-1.0595	5.290E-06	0.001168061
Cyba	-0.9666	5.980E-06	0.001283323
D430018E03Rik	2.8182	8.493E-04	0.04455924
D7Ertd715e	0.8068	5.908E-04	0.034006058
D830044I16Rik	4.6222	6.616E-04	0.036969625
Dbi	-0.8166	1.020E-06	0.00037766
Ddias	0.8861	3.556E-04	0.024911011
Ddit4	-1.4781	3.110E-06	0.000808821
Decr2	1.2238	8.420E-05	0.009255164
Dhx35	0.6081	8.628E-04	0.044964952
Dnaic2	3.8653	2.359E-04	0.018773841
Dnajc8	-0.4318	1.603E-04	0.014316035
Dock3	6.8496	1.219E-04	0.01219086
Dock9	0.6013	3.670E-06	0.000914093
Dtnbp1	-0.7108	3.670E-05	0.005241212
Edf1	-0.7876	3.740E-05	0.005271163
Eef1b2	-0.6445	3.438E-04	0.024381385
Efhc2	7.0358	1.923E-04	0.016183437
Eif1b	-1.0850	3.524E-04	0.024872335
Eif3k	-0.5966	4.650E-04	0.029405901
Elof1	-1.0343	9.410E-05	0.01019215
Eno1	-0.4554	8.891E-04	0.045884852
Entpd1	-1.8762	6.910E-06	0.001421219
Epha2	7.0624	3.012E-04	0.022195652
Evc	2.0085	5.060E-06	0.001138243
Eya1	1.0107	2.850E-07	0.000151328
Faim3	-0.5191	4.916E-04	0.030350114

Gene	*KOvsWT .log2FC*	*KOvsWT.RawP*	*KOvsWT.FDR*
Fam101a	1.6361	2.903E-04	0.021916498
Fam162a	-0.8300	4.419E-04	0.028623241
Fam65a	0.5877	7.239E-04	0.039300855
Fam96b	-1.5495	3.380E-07	0.000175758
Farsa	0.9069	1.180E-04	0.012004012
Fastk	0.7726	2.640E-08	2.47E-05
Fat1	3.9772	8.980E-06	0.001736816
Fgl2	-0.8424	9.800E-05	0.010379162
Fnta	-0.7390	1.439E-04	0.013698763
Foxk1	0.5517	6.390E-05	0.007550317
Foxred2	0.9637	1.900E-05	0.002979471
Fth1	-0.9710	1.260E-08	1.34E-05
Fundc2	-0.6213	5.989E-04	0.034182077
Gab1	-8.7409	8.166E-04	0.043329649
Gab2	4.9689	2.460E-06	0.000720777
Gas5	-0.4274	5.778E-04	0.033549234
Gimap7	-0.9184	5.980E-09	6.99E-06
Gm10524	0.8719	8.855E-04	0.045840909
Gm11510	2.1744	2.957E-04	0.022034196
Gm11831	4.0517	7.803E-04	0.041878732
Gm12158	0.8238	6.868E-04	0.038172829
Gm12917	4.6249	8.319E-04	0.043961925
Gm13351	1.5329	2.002E-04	0.016552299
Gm13873	-8.1103	2.415E-04	0.01909405
Gm15367	6.6092	9.048E-04	0.046226851
Gm15551	2.5991	9.086E-04	0.046321776
Gm15780	7.6744	3.880E-05	0.00543332
Gm15832	3.8695	2.546E-04	0.019925951
Gm15842	2.2579	1.404E-04	0.013629926
Gm15932	6.5219	9.917E-04	0.048798368
Gm16853	3.6628	4.690E-05	0.006205008
Gm17275	0.6879	6.300E-07	0.000263141
Gm21982	6.6941	1.945E-04	0.016193537
Gm23639	-4.3364	9.570E-05	0.010267533
Gm24636	5.1848	5.915E-04	0.034006058
Gm26049	1.4432	3.300E-05	0.0047633
Gm26518	1.5181	6.541E-04	0.036703527
Gm26847	3.5100	6.939E-04	0.038383653
Gm26917	0.8068	9.557E-04	0.047603974
Gm6225	2.9477	7.886E-04	0.042131632
Gm7741	-2.4921	5.597E-04	0.032909031
Gm8428	3.1306	4.999E-04	0.030621805

Gene	*KOvsWT .log2FC*	*KOvsWT.RawP*	*KOvsWT.FDR*
Gmnn	-0.5509	7.107E-04	0.038945758
Gng5	-0.8278	4.418E-04	0.028623241
Gon4l	0.5649	8.902E-04	0.045884852
Gorab	1.2249	1.640E-05	0.002637094
Gpx1	-0.6137	7.364E-04	0.039842021
Grhl1	1.2723	2.916E-04	0.021942221
Gtf2h4	-0.8898	1.300E-04	0.012940479
H2afv	-0.7579	1.958E-04	0.016246527
H2afy3	2.7394	1.922E-04	0.016183437
H6pd	2.2192	5.590E-05	0.006808762
Hbb-bt	-1.5492	1.950E-06	0.000591425
Hdac6	0.7128	4.019E-04	0.026960996
Hddc2	-0.8466	1.349E-04	0.013188907
Helz2	0.4356	3.691E-04	0.025708041
Hint1	-1.0847	1.360E-05	0.002387967
Hip1	1.3434	8.590E-06	0.001689613
Hlx	-7.9635	3.750E-04	0.025834217
Hmga1	0.5971	5.500E-05	0.006732969
Hscb	-0.8079	4.284E-04	0.028315653
Ier3ip1	-1.0133	4.178E-04	0.027775111
Ifitm2	7.4695	8.790E-05	0.009612004
Ift20	-0.6938	1.590E-05	0.002608299
Ighg2c	-0.9313	2.630E-06	0.000742214
Ighj3	-1.2035	9.300E-06	0.001784636
Ighv1-36	-8.7122	3.820E-11	1.28E-07
Ighv1-81	-2.6671	1.749E-04	0.01538845
Igkv1-117	-2.5787	3.649E-04	0.025490643
Igkv2-137	-5.0789	7.700E-10	1.50E-06
Igkv3-5	-4.0583	2.898E-04	0.021916498
Igkv4-56	-5.0126	9.199E-04	0.046692079
Igkv4-92	-9.1221	2.060E-04	0.016850441
Igkv5-45	-6.0949	2.180E-08	2.13E-05
Igkv8-19	-3.6130	9.942E-04	0.048798368
Igkv9-124	-2.9947	1.660E-05	0.002638288
Igkv9-129	-5.8406	3.937E-04	0.026622873
Iglc2	-0.9531	6.126E-04	0.034709
Iglv1	-0.9056	3.500E-08	3.15E-05
Il10ra	-1.0473	4.021E-04	0.026960996
Il18r1	3.1269	2.890E-06	0.000783828
Il1r2	6.5531	4.403E-04	0.028623241
Il2rb	0.9049	4.760E-07	0.000218413
Inf2	0.7756	4.137E-04	0.027583108

Gene	*KOvsWT .log2FC*	*KOvsWT.RawP*	*KOvsWT.FDR*
Ing2	-0.6442	9.537E-04	0.047603974
Ipo4	0.6788	2.910E-06	0.000783828
Iqcg	3.8828	1.430E-07	9.28E-05
Itga4	-0.5058	2.606E-04	0.020232397
Itpkb	0.6644	4.940E-05	0.006387711
Jtb	-0.8271	7.200E-05	0.008142611
Kat7	0.5510	3.049E-04	0.022294947
Kif18b	0.7108	4.950E-07	0.000222938
Klf11	1.4374	1.650E-05	0.002637094
Lifr	-2.4426	8.578E-04	0.044803716
Lmln	1.9443	1.942E-04	0.016193537
Lmo2	-0.6469	1.353E-04	0.013188907
Lmo7	0.4499	1.453E-04	0.013698763
Lrrc61	0.7846	2.954E-04	0.022034196
Lrrn3	2.3693	4.517E-04	0.029037179
Lsm3	-0.7128	1.181E-04	0.012004012
Lsm4	-0.8247	5.360E-05	0.006638948
Ltbp3	4.3012	6.620E-04	0.036969625
Ly6a	-1.1402	5.910E-13	6.91E-09
Ly6k	-6.9868	3.470E-07	0.000176538
Ly86	-0.6502	1.122E-04	0.011553694
Lyrm4	-1.2520	2.040E-06	0.000611303
Lyz1	7.4062	5.230E-05	0.006515547
Malsu1	-1.0333	2.270E-06	0.000672253
Mapk7	0.6069	2.272E-04	0.018197719
Mfsd6	0.7817	4.546E-04	0.029094005
Mif	-0.7683	4.735E-04	0.029544915
Minos1	-1.1133	8.830E-08	5.98E-05
Mir378b	1.8067	7.743E-04	0.04165293
Mov10	0.6664	1.194E-04	0.012039275
Mrgpre	-0.7557	2.279E-04	0.018197719
Mrpl11	-0.9142	1.557E-04	0.014316035
Mrpl18	-0.5489	4.180E-06	0.001007875
Mrpl37	0.5029	9.582E-04	0.047603974
Mrpl41	-1.2250	5.800E-05	0.007030782
Mrpl52	-0.9241	4.670E-04	0.029456446
Mrpl57	-0.7498	1.593E-04	0.014316035
Mrps14	-1.2231	9.280E-11	2.71E-07
Mrps28	-0.9644	5.423E-04	0.032208661
Ms4a4c	-0.8284	1.414E-04	0.013646282
Msh4	5.6446	6.980E-05	0.008058411
Mtfp1	-2.2271	9.314E-04	0.047094098

Gene	*KOvsWT .log2FC*	*KOvsWT.RawP*	*KOvsWT.FDR*
Myd88	-1.7156	2.800E-05	0.004122366
Myeov2	-1.5296	2.260E-11	9.49E-08
Myom1	-2.4360	3.050E-05	0.00445408
Mzb1	-0.6029	4.450E-05	0.005982602
N6amt1	0.8526	1.480E-07	9.33E-05
Naa40	0.5983	1.924E-04	0.016183437
Nab2	0.7146	1.440E-04	0.013698763
Naprt	-1.3595	9.318E-04	0.047094098
Ndufa1	-1.0844	1.850E-06	0.00058173
Ndufa11	-1.1860	8.440E-08	5.98E-05
Ndufa13	-0.8980	4.230E-06	0.001010246
Ndufa2	-0.9127	1.578E-04	0.014316035
Ndufa3	-0.9147	7.280E-05	0.008187189
Ndufa6	-1.0083	4.720E-04	0.029544915
Ndufb5	-0.7293	1.782E-04	0.015619555
Ndufb9	-0.8765	5.416E-04	0.032208661
Ndufc1	-1.2590	4.409E-04	0.028623241
Ndufs4	-0.7539	2.101E-04	0.017126599
Ndufs6	-1.1416	1.590E-05	0.002608299
Nedd8	-0.9852	1.860E-06	0.00058173
Nnat	4.0976	8.940E-08	5.98E-05
Noc2l	0.7132	1.586E-04	0.014316035
Nop10	-1.1869	1.380E-05	0.002415011
Nploc4	0.4202	5.285E-04	0.031791045
Nr1d1	6.5400	9.551E-04	0.047603974
Nsfl1c	-0.5622	5.772E-04	0.033549234
Nsmce1	-0.8671	1.590E-05	0.002608299
Nsmce2	-0.5926	5.559E-04	0.032774406
Nsun6	-0.8160	4.576E-04	0.029094005
Nudt7	1.3019	1.004E-04	0.01058553
Oas3	1.6097	2.960E-06	0.000786414
Ost4	-0.7516	7.372E-04	0.039842021
Pak6	4.0709	4.530E-05	0.006044397
Papln	1.3124	8.420E-06	0.0016832
Pard6a	-2.2654	9.047E-04	0.046226851
Parp12	4.8174	5.910E-04	0.034006058
Pcdhgb7	7.3292	9.470E-05	0.010211046
Pcdhgb8	7.6552	5.020E-06	0.001138243
Pdcd4	-0.9480	2.280E-05	0.003537589
Pdrg1	-0.8280	7.140E-05	0.008110238
Per1	0.5855	1.080E-06	0.000388467
Pfdn5	-0.9342	4.860E-05	0.006355132

Gene	*KOvsWT .log2FC*	*KOvsWT.RawP*	*KOvsWT.FDR*
Pglyrp1	-1.3727	2.211E-04	0.017777615
Phc2	0.7720	1.860E-05	0.002944154
Phf1	0.8978	3.839E-04	0.026111812
Pigo	0.6128	5.170E-05	0.006475261
Pigt	0.5337	6.920E-06	0.001421219
Pim1	1.0014	6.010E-07	0.000258235
Pip4k2b	0.7778	2.440E-05	0.003706705
Pithd1	-0.8423	3.480E-05	0.004990462
Plac8	-1.2200	3.016E-04	0.022195652
Plcd1	6.7731	4.588E-04	0.029094005
Plec	0.6529	5.767E-04	0.033549234
Pmf1	-0.6670	2.510E-05	0.003785935
Polr1d	-0.8250	4.230E-09	5.50E-06
Polr2g	-0.8581	1.210E-06	0.000421191
Pon2	-0.5908	6.170E-05	0.00740491
Ppa2	-1.1284	1.651E-04	0.014651942
Ppdpf	-0.8993	1.203E-04	0.012077273
Ppp1r13l	1.9110	2.198E-04	0.017732791
Prdx5	-1.1248	6.670E-05	0.007805941
Prkch	5.7893	1.040E-06	0.000380619
Prmt2	7.6606	2.300E-05	0.003537589
Prpf4	0.5918	9.690E-05	0.010303263
Psma1	-0.5857	2.758E-04	0.021094337
Psma2	-0.4918	9.670E-05	0.010303263
Psmb1	-0.6629	1.490E-05	0.002537713
Psmb10	-0.8905	1.830E-07	0.000109906
Psmb8	-0.5571	6.020E-08	4.69E-05
Psme2	-0.7814	6.590E-08	4.82E-05
Ptger1	1.0496	1.350E-05	0.002387967
Ptges3l	3.4863	8.590E-06	0.001689613
Ptpn3	3.9362	3.412E-04	0.024265385
Ptprcap	-0.8669	1.600E-06	0.000519161
Puf60	-0.5827	8.156E-04	0.043329649
Qtrtd1	0.7433	1.801E-04	0.015727098
Rabac1	-1.3877	4.948E-04	0.030386385
Rad51c	0.5694	1.579E-04	0.014316035
Rag1	-8.3703	6.460E-05	0.007598937
Rasal3	0.4516	4.550E-05	0.006044397
Rbm38	0.4478	1.458E-04	0.013698763
Rbm44	-2.2297	2.720E-14	6.36E-10
Rbms2	0.6455	1.326E-04	0.013063631
Rbx1	-0.7696	2.768E-04	0.021101396

Gene	*KOvsWT .log2FC*	*KOvsWT.RawP*	*KOvsWT.FDR*
Rcc1	0.4691	1.423E-04	0.013646282
Retsat	2.5250	1.120E-06	0.000395938
Rfc3	-0.4219	8.364E-04	0.044081825
Rgs7	4.3554	6.790E-06	0.001418467
Rilpl2	-1.3288	1.451E-04	0.013698763
Rnf213	0.4807	9.571E-04	0.047603974
Rnf219	-0.6905	4.300E-07	0.000211301
RP23-102B12.2	1.7814	4.428E-04	0.028623241
RP23-264E23.1	6.9990	5.891E-04	0.034006058
RP23-323E20.2	2.2708	5.016E-04	0.030646583
RP23-328J8.3	0.6053	7.073E-04	0.038850306
RP23-395G18.1	6.5192	3.250E-04	0.023472429
RP23-456B9.18	2.5842	4.130E-06	0.001006441
RP23-98F21.12	6.7000	1.813E-04	0.015772248
RP24-271M20.4	0.8163	1.500E-05	0.002537713
RP24-337A16.2	3.1043	4.720E-07	0.000218413
RP24-338G10.1	0.9055	5.260E-07	0.000232157
RP24-490B17.7	3.7508	3.660E-06	0.000914093
RP24-546N2.2	0.8876	5.080E-05	0.00646751
RP24-74O18.2	1.1618	5.050E-08	4.22E-05
RP24-87I22.4	6.4477	4.195E-04	0.027808794
RP24-88B13.5	1.9255	1.061E-04	0.011029589
RP24-92E18.2	6.5864	5.239E-04	0.031680477
RP24-93F24.2	4.1442	4.340E-06	0.001024702
Rpa3	-0.9530	3.133E-04	0.022837157
Rpl13a	-0.9367	7.160E-07	0.000288717
Rpl14	-1.0443	2.880E-06	0.000783828
Rpl18	-0.7698	1.925E-04	0.016183437
Rpl18a	-1.0521	1.550E-06	0.00050972
Rpl22	-0.7930	8.380E-07	0.000326826
Rpl23	-0.9741	1.310E-06	0.00044925
Rpl26	-0.8778	4.322E-04	0.02848664
Rpl29	-0.9042	3.230E-05	0.004696993
Rpl29-ps1	4.6712	3.540E-04	0.024872335
Rpl32	-0.7027	4.686E-04	0.029479146
Rpl34	-0.9658	2.310E-05	0.003537589
Rpl35a	-0.8442	1.400E-06	0.000466495
Rpl37	-1.3331	6.030E-06	0.001283323
Rpl37a	-0.9193	2.575E-04	0.020081536
Rpl39	-1.3013	3.900E-05	0.005434638
Rpl41	-0.8306	7.550E-05	0.008448902
Rpl8	-0.7389	6.070E-07	0.000258235

Gene	*KOvsWT .log2FC*	*KOvsWT.RawP*	*KOvsWT.FDR*
Rplp0	-0.5916	5.702E-04	0.033437458
Rplp1	-1.1920	1.610E-05	0.002608299
Rplp2	-0.7706	5.972E-04	0.034167518
Rps10	-1.1858	2.730E-09	3.80E-06
Rps11	-0.7032	8.664E-04	0.045054292
Rps15	-0.6246	5.233E-04	0.031680477
Rps15a	-0.7338	3.930E-05	0.005445758
Rps18	-0.5429	9.310E-05	0.01013161
Rps19	-0.7958	2.370E-09	3.69E-06
Rps20	-0.8948	4.890E-05	0.006361927
Rps25	-0.8144	1.010E-05	0.001924218
Rps26	-1.2162	2.630E-06	0.000742214
Rps28	-1.0982	5.140E-05	0.006467641
Rps3	-0.6728	4.420E-07	0.000211301
Rps3a1	-0.8900	6.920E-05	0.008051088
Rps4x	-0.7095	1.714E-04	0.015134516
Rps5	-0.5833	3.185E-04	0.023075185
Rps6ka1	0.4278	9.793E-04	0.048445584
Rps6kb2	0.6940	3.920E-06	0.000965421
Rps8	-0.8121	9.432E-04	0.047565342
Rtp4	2.7631	3.330E-04	0.023899449
Sdc4	-1.3695	1.550E-07	9.53E-05
Sec11c	-0.3822	8.995E-04	0.046156686
Sec14l1	0.6263	8.240E-05	0.009094634
Sec61b	-1.1638	1.600E-05	0.002608299
Sema7a	0.3681	5.335E-04	0.031897477
Serpinc1	5.2825	2.984E-04	0.022097454
Shfm1	-1.0192	4.160E-05	0.005728064
Sipa1l3	0.6365	9.833E-04	0.048540178
Skap2	-0.6163	4.410E-05	0.005982602
Slc12a3	1.3302	5.070E-05	0.00646751
Slc22a23	2.4067	4.442E-04	0.028633884
Slc25a3	-0.3671	6.280E-05	0.007460177
Slc30a4	0.8651	4.857E-04	0.030067093
Slc39a13	0.7242	1.858E-04	0.015983646
Slc6a6	0.7102	4.390E-07	0.000211301
Slc9a8	0.4852	6.250E-05	0.007460177
Smdt1	-0.7615	2.543E-04	0.019925951
Snrpb2	-0.7427	3.100E-06	0.000808821
Snrpg	-1.1458	1.420E-04	0.013646282
Snx3	-0.6313	8.010E-05	0.008882859
Sod1	-1.0827	3.190E-12	1.87E-08

Gene	*KOvsWT .log2FC*	*KOvsWT.RawP*	*KOvsWT.FDR*
Sptb	6.8808	3.362E-04	0.023983793
Srp19	-0.4994	1.869E-04	0.016023916
Srsf9	-0.7185	7.450E-06	0.001515866
Stk16	-0.7760	1.070E-05	0.001968641
Stk35	0.5204	8.939E-04	0.045973334
Stpg1	6.5747	6.148E-04	0.034749528
Stra13	-1.0078	5.760E-06	0.001259633
Strn4	0.7164	6.010E-06	0.001283323
Sub1	-1.5856	1.190E-09	1.99E-06
Sv2b	-4.1621	2.530E-07	0.000144311
Sync	6.7751	9.179E-04	0.046692079
Syngr2	0.6606	2.760E-05	0.004082412
Tbc1d4	1.3563	4.934E-04	0.030385557
Tbca	-1.0437	5.900E-05	0.007119252
Tbrg4	0.5565	1.930E-04	0.016183437
Tceb1	-0.6888	2.148E-04	0.017389765
Tcf7	1.5659	1.460E-05	0.002514129
Tcp11	6.7363	6.375E-04	0.03594709
Tet3	0.3712	1.185E-04	0.012004012
Tmed9	-0.4972	3.911E-04	0.026523908
Tmem120b	1.9406	1.306E-04	0.012951588
Tmem136	4.3659	2.882E-04	0.02189904
Tmem14c	-0.8568	2.010E-07	0.000117315
Tmem259	0.5680	2.939E-04	0.022034196
Tmsb4x	-0.8788	3.752E-04	0.025834217
Tnk2os	7.4300	1.190E-05	0.002169958
Tomm7	-1.1319	2.611E-04	0.020232397
Traf4	0.8896	3.730E-05	0.005271163
Trappc1	-0.7412	5.090E-05	0.00646751
Trbc2	1.8712	2.702E-04	0.020794843
Trbv13-2	6.6686	9.983E-04	0.048871902
Trp53i13	1.8640	4.045E-04	0.027046227
Trpm4	2.2614	1.921E-04	0.016183437
Tstd3	-0.7534	5.344E-04	0.031897477
Ttbk1	7.5687	5.440E-05	0.006695136
Ttc26	6.5280	5.254E-04	0.031686164
Txn1	-0.7871	4.490E-06	0.001049821
Ubr4	0.4378	1.510E-05	0.002547635
Uqcr10	-0.7589	1.036E-04	0.010823153
Uqcrh	-1.0670	7.380E-09	8.22E-06
Uqcrq	-1.1135	1.329E-04	0.013063631
Use1	-0.9520	2.760E-09	3.80E-06

Gene	*KOvsWT .log2FC*	*KOvsWT.RawP*	*KOvsWT.FDR*
Usp19	0.4495	9.471E-04	0.047603974
Usp30	0.8678	6.038E-04	0.034376873
Utrn	1.0442	1.018E-04	0.010679699
Vasp	-0.6681	4.450E-05	0.005982602
Vpreb3	-1.1381	1.100E-09	1.98E-06
Vsig10l	2.6839	4.014E-04	0.026960996
Wdr31	3.9940	7.050E-05	0.008073327
Wrnip1	-0.7507	6.435E-04	0.036199004
Xdh	4.5193	1.578E-04	0.014316035
Xlr3b	-2.6180	3.045E-04	0.022294947
Xpo6	0.3132	7.159E-04	0.039140118
Ywhaq	-0.7769	3.343E-04	0.023925901
Zc3h12c	-1.9522	8.523E-04	0.044617056
Zeb2	-1.0680	1.126E-04	0.011553694
Zfp180	0.5798	4.260E-05	0.005832368
Zfp365	2.7412	2.190E-08	2.13E-05
Zfp366	7.6177	1.832E-04	0.015822329
Zfp704	7.5681	1.040E-05	0.001968641
Zfp951	1.9242	7.069E-04	0.038850306

References

Akira, S., and K. Takeda. 2004. Toll-like receptor signalling. *Nat Rev Immunol* 4:499-511.

Akkaya, M., B. Akkaya, A.S. Kim, P. Miozzo, H. Sohn, M. Pena, A.S. Roesler, B.P. Theall, T. Henke, J. Kabat, J. Lu, D.W. Dorward, E. Dahlstrom, J. Skinner, L.H. Miller, and S.K. Pierce. 2018a. Toll-like receptor 9 antagonizes antibody affinity maturation. *Nat Immunol* 19:255-266.

Akkaya, M., B. Akkaya, P.W. Sheehan, P. Miozzo, M. Pena, C.F. Qi, J. Manzella-Lapeira, S. Bolland, and S.K. Pierce. 2017. T cell-dependent antigen adjuvanted with DOTAP-CpG-B but not DOTAP-CpG-A induces robust germinal center responses and high affinity antibodies in mice. *Eur J Immunol* 47:1890-1899.

Akkaya, M., J. Traba, A.S. Roesler, P. Miozzo, B. Akkaya, B.P. Theall, H. Sohn, M. Pena, M. Smelkinson, J. Kabat, E. Dahlstrom, D.W. Dorward, J. Skinner, M.N. Sack, and S.K. Pierce. 2018b. Second signals rescue B cells from activation-induced mitochondrial dysfunction and death. *Nat Immunol* 19:871-884.

Arunkumar, N., C. Liu, H. Hang, and W. Song. 2013. Toll-like receptor agonists induce apoptosis in mouse B-cell lymphoma cells by altering NF-kappaB activation. *Cell Mol Immunol* 10:360-372.

Azulay-Debby, H., E. Edry, and D. Melamed. 2007. CpG DNA stimulates autoreactive immature B cells in the bone marrow. *Eur J Immunol* 37:1463-1475.

Bilanges, B., R. Argonza-Barrett, M. Kolesnichenko, C. Skinner, M. Nair, M. Chen, and D. Stokoe. 2007. Tuberous sclerosis complex proteins 1 and 2 control serum-dependent translation in a TOP-dependent and -independent manner. *Mol Cell Biol* 27:5746-5764.

Blasius, A.L., and B. Beutler. 2010. Intracellular toll-like receptors. *Immunity* 32:305-315.

Calado, D.P., Y. Sasaki, S.A. Godinho, A. Pellerin, K. Kochert, B.P. Sleckman, I.M. de Alboran, M. Janz, S. Rodig, and K. Rajewsky. 2012. The cell-cycle regulator c-Myc is essential for the formation and maintenance of germinal centers. *Nature Immunology* 13:1092-1100.

Caro-Maldonado, A., R. Wang, A.G. Nichols, M. Kuraoka, S. Milasta, L.D. Sun, A.L. Gavin, E.D. Abel, G. Kelsoe, D.R. Green, and J.C. Rathmell. 2014. Metabolic reprogramming is required for antibody production that is suppressed in anergic but exaggerated in chronically BAFF-exposed B cells. *J Immunol* 192:3626-3636.

Cato, M.H., I.W. Yau, and R.C. Rickert. 2011. Magnetic-based purification of untouched mouse germinal center B cells for ex vivo manipulation and biochemical analysis. *Nat Protoc* 6:953-960.

Chaturvedi, A., D. Dorward, and S.K. Pierce. 2008. The B cell receptor governs the subcellular location of Toll-like receptor 9 leading to hyperresponses to DNA-containing antigens. *Immunity* 28:799-809.

Chiu, H., L.V. Jackson, K.I. Oh, A. Mai, Z.A. Ronai, D. Ruggero, and D.A. Fruman. 2019. The mTORC1/4E-BP/eIF4E Axis Promotes Antibody Class Switching in B Lymphocytes. *J Immunol* 202:579-590.

Clingan, J.M., and M. Matloubian. 2013. B Cell-intrinsic TLR7 signaling is required for optimal B cell responses during chronic viral infection. *J Immunol* 191:810-818.

Conacci-Sorrell, M., L. McFerrin, and R.N. Eisenman. 2014. An overview of MYC and its interactome. *Cold Spring Harb Perspect Med* 4:a014357.

DeFranco, A.L., D.C. Rookhuizen, and B. Hou. 2012. Contribution of Toll-like receptor signaling to germinal center antibody responses. *Immunol Rev* 247:64-72.

Dominguez-Sola, D., G.D. Victora, C.Y. Ying, R.T. Phan, M. Saito, M.C. Nussenzweig, and R. Dalla-Favera. 2012. The proto-oncogene MYC is required for selection in the germinal center and cyclic reentry. *Nat Immunol* 13:1083-1091.

Eckl-Dorna, J., and F.D. Batista. 2009. BCR-mediated uptake of antigen linked to TLR9 ligand stimulates B-cell proliferation and antigen-specific plasma cell formation. *Blood* 113:3969-3977.

Ersching, J., A. Efeyan, L. Mesin, J.T. Jacobsen, G. Pasqual, B.C. Grabiner, D. Dominguez-Sola, D.M. Sabatini, and G.D. Victora. 2017. Germinal Center Selection and Affinity Maturation Require Dynamic Regulation of mTORC1 Kinase. *Immunity* 46:1045-1058 e1046.

Gavin, A.L., K. Hoebe, B. Duong, T. Ota, C. Martin, B. Beutler, and D. Nemazee. 2006. Adjuvant-enhanced antibody responses in the absence of toll-like receptor signaling. *Science* 314:1936-1938.

Giles, J.R., A.T. Neves, A. Marshak-Rothstein, and M.J. Shlomchik. 2017. Autoreactive helper T cells alleviate the need for intrinsic TLR signaling in autoreactive B cell activation. *JCI Insight* 2:e90870.

Hong, S., Z. Zhang, H. Liu, M. Tian, X. Zhu, Z. Zhang, W. Wang, X. Zhou, F. Zhang, Q. Ge, B. Zhu, H. Tang, Z. Hua, and B. Hou. 2018. B Cells Are the Dominant Antigen-Presenting Cells that Activate Naive CD4(+) T Cells upon Immunization with a Virus-Derived Nanoparticle Antigen. *Immunity* 49:695-708 e694.

Hou, B., P. Saudan, G. Ott, M.L. Wheeler, M. Ji, L. Kuzmich, L.M. Lee, R.L. Coffman, M.F. Bachmann, and A.L. DeFranco. 2011. Selective utilization of Toll-like receptor and MyD88 signaling in B cells for enhancement of the antiviral germinal center response. *Immunity* 34:375-384.

Huang, C.Y., A.L. Bredemeyer, L.M. Walker, C.H. Bassing, and B.P. Sleckman. 2008. Dynamic regulation of c-Myc proto-oncogene expression during lymphocyte development revealed by a GFP-c-Myc knock-in mouse. *Eur J Immunol* 38:342-349.

Iwasaki, A., and R. Medzhitov. 2004. Toll-like receptor control of the adaptive immune responses. *Nat Immunol* 5:987-995.

Jegerlehner, A., P. Maurer, J. Bessa, H.J. Hinton, M. Kopf, and M.F. Bachmann. 2007. TLR9 signaling in B cells determines class switch recombination to IgG2a. *J Immunol* 178:2415-2420.

Jones, D.D., B.T. Gaudette, J.R. Wilmore, I. Chernova, A. Bortnick, B.M. Weiss, and D. Allman. 2016. mTOR has distinct functions in generating versus sustaining humoral immunity. *J Clin Invest* 126:4250-4261.

Lee, S.H., L.L. Hu, J. Gonzalez-Navajas, G.S. Seo, C. Shen, J. Brick, S. Herdman, N. Varki, M. Corr, J. Lee, and E. Raz. 2010. ERK activation drives intestinal tumorigenesis in Apc(min/+) mice. *Nat Med* 16:665-670.

Luo, W., F. Weisel, and M.J. Shlomchik. 2018. B Cell Receptor and CD40 Signaling Are Rewired for Synergistic Induction of the c-Myc Transcription Factor in Germinal Center B Cells. *Immunity* 48:313-326 e315.

MacLeod, M.K., A.S. McKee, A. David, J. Wang, R. Mason, J.W. Kappler, and P. Marrack. 2011. Vaccine adjuvants aluminum and monophosphoryl lipid A provide distinct signals to generate protective cytotoxic memory CD8 T cells. *Proc Natl Acad Sci U S A* 108:7914-7919.

Mayer, C.T., A. Gazumyan, E.E. Kara, A.D. Gitlin, J. Golijanin, C. Viant, J. Pai, T.Y. Oliveira, Q. Wang, A. Escolano, M. Medina-Ramirez, R.W. Sanders, and M.C. Nussenzweig. 2017.

The microanatomic segregation of selection by apoptosis in the germinal center. *Science* 358:

McKee, A.S., and P. Marrack. 2017. Old and new adjuvants. *Curr Opin Immunol* 47:44-51.

O'Neill, S.K., M.L. Veselits, M. Zhang, C. Labno, Y. Cao, A. Finnegan, M. Uccellini, M.L. Alegre, J.C. Cambier, and M.R. Clark. 2009. Endocytic sequestration of the B cell antigen receptor and toll-like receptor 9 in anergic cells. *Proc Natl Acad Sci U S A* 106:6262-6267.

Pasare, C., and R. Medzhitov. 2005. Control of B-cell responses by Toll-like receptors. *Nature* 438:364-368.

Pua, H.H., D.F. Steiner, S. Patel, J.R. Gonzalez, J.F. Ortiz-Carpena, R. Kageyama, N.T. Chiou, A. Gallman, D. de Kouchkovsky, L.T. Jeker, M.T. McManus, D.J. Erle, and K.M. Ansel. 2016. MicroRNAs 24 and 27 Suppress Allergic Inflammation and Target a Network of Regulators of T Helper 2 Cell-Associated Cytokine Production. *Immunity* 44:821-832.

Rawlings, D.J., G. Metzler, M. Wray-Dutra, and S.W. Jackson. 2017. Altered B cell signalling in autoimmunity. *Nat Rev Immunol* 17:421-436.

Raybuck, A.L., S.H. Cho, J. Li, M.C. Rogers, K. Lee, C.L. Williams, M. Shlomchik, J.W. Thomas, J. Chen, J.V. Williams, and M.R. Boothby. 2018. B Cell-Intrinsic mTORC1 Promotes Germinal Center-Defining Transcription Factor Gene Expression, Somatic Hypermutation, and Memory B Cell Generation in Humoral Immunity. *J Immunol* 200:2627-2639.

Rookhuizen, D.C., and A.L. DeFranco. 2014. Toll-like receptor 9 signaling acts on multiple elements of the germinal center to enhance antibody responses. *Proc Natl Acad Sci U S A* 111:E3224-3233.

Schmitz, F., A. Heit, S. Dreher, K. Eisenacher, J. Mages, T. Haas, A. Krug, K.P. Janssen, C.J. Kirschning, and H. Wagner. 2008. Mammalian target of rapamycin (mTOR) orchestrates the defense program of innate immune cells. *Eur J Immunol* 38:2981-2992.

Sindhava, V.J., M.A. Oropallo, K. Moody, M. Naradikian, L.E. Higdon, L. Zhou, A. Myles, N. Green, K. Nundel, W. Stohl, A.M. Schmidt, W. Cao, S. Dorta-Estremera, T. Kambayashi, A. Marshak-Rothstein, and M.P. Cancro. 2017. A TLR9-dependent checkpoint governs B cell responses to DNA-containing antigens. *J Clin Invest* 127:1651-1663.

Subramanian, A., P. Tamayo, V.K. Mootha, S. Mukherjee, B.L. Ebert, M.A. Gillette, A. Paulovich, S.L. Pomeroy, T.R. Golub, E.S. Lander, and J.P. Mesirov. 2005. Gene set enrichment analysis: a knowledge-based approach for interpreting genome-wide expression profiles. *Proc Natl Acad Sci U S A* 102:15545-15550.

Tian, M., Z. Hua, S. Hong, Z. Zhang, C. Liu, L. Lin, J. Chen, W. Zhang, X. Zhou, F. Zhang, A.L. DeFranco, and B. Hou. 2018. B Cell-Intrinsic MyD88 Signaling Promotes Initial Cell Proliferation and Differentiation To Enhance the Germinal Center Response to a Virus-like Particle. *J Immunol* 200:937-948.

Victora, G.D., D. Dominguez-Sola, A.B. Holmes, S. Deroubaix, R. Dalla-Favera, and M.C. Nussenzweig. 2012. Identification of human germinal center light and dark zone cells and their relationship to human B-cell lymphomas. *Blood* 120:2240-2248.

Victora, G.D., T.A. Schwickert, D.R. Fooksman, A.O. Kamphorst, M. Meyer-Hermann, M.L. Dustin, and M.C. Nussenzweig. 2010. Germinal center dynamics revealed by multiphoton microscopy with a photoactivatable fluorescent reporter. *Cell* 143:592-605.

Wang, X., M. Cunningham, X. Zhang, S. Tokarz, B. Laraway, M. Troxell, and R.C. Sears. 2011. Phosphorylation regulates c-Myc's oncogenic activity in the mammary gland. *Cancer Res* 71:925-936.

Waters, L.R., F.M. Ahsan, D.M. Wolf, O. Shirihai, and M.A. Teitell. 2018. Initial B Cell Activation Induces Metabolic Reprogramming and Mitochondrial Remodeling. *iScience* 5:99-109.

Wigton, E.J., A.L. DeFranco, and K.M. Ansel. 2019. Antigen Complexed with a TLR9 Agonist Bolsters c-Myc and mTORC1 Activity in Germinal Center B Lymphocytes. *Immunohorizons* 3:389-401.

Zeller, K.I., A.G. Jegga, B.J. Aronow, K.A. O'Donnell, and C.V. Dang. 2003. An integrated database of genes responsive to the Myc oncogenic transcription factor: identification of direct genomic targets. *Genome Biol* 4:R69.

Zhang, S., M. Pruitt, D. Tran, W. Du Bois, K. Zhang, R. Patel, S. Hoover, R.M. Simpson, J. Simmons, J. Gary, C.M. Snapper, R. Casellas, and B.A. Mock. 2013. B cell-specific deficiencies in mTOR limit humoral immune responses. *J Immunol* 191:1692-1703.

Publishing Agreement

It is the policy of the University to encourage open access and broad distribution of all theses, dissertations, and manuscripts. The Graduate Division will facilitate the distribution of UCSF theses, dissertations, and manuscripts to the UCSF Library for open access and distribution. UCSF will make such theses, dissertations, and manuscripts accessible to the public and will take reasonable steps to preserve these works in perpetuity.

I hereby grant the non-exclusive, perpetual right to The Regents of the University of California to reproduce, publicly display, distribute, preserve, and publish copies of my thesis, dissertation, or manuscript in any form or media, now existing or later derived, including access online for teaching, research, and public service purposes.

DocuSigned by:
58DF859285EB481...
Author Signature

5/31/2020
Date